eScholarship@UMassChan

Conformational Lability in MHC II Proteins: A Dissertation

Item Type	Doctoral Dissertation
Authors	Painter, Corrie A.
DOI	10.13028/j2sf-cm12
Publisher	University of Massachusetts Medical School
Rights	Copyright is held by the author, with all rights reserved.
Download date	2025-06-18 09:35:29
Link to Item	https://hdl.handle.net/20.500.14038/31878

CONFORMATIONAL LABILITY IN MHC II PROTEINS

A Dissertation Presented

By

Corrie A. Painter

Submitted to the faculty of the
University of Massachusetts Graduate School of Biomedical Sciences, Worcester
In partial fulfillment of the requirements for the degree of

DOCTOR OF PHILOSOPHY

DEDICATION

This work is dedicated to my beautiful children, Charly Elizabeth Painter,

Madelyn Blanca Painter and Robert Martin Painter. I love you more than the

universe.

CONFORMATIONAL LABILITY IN MHC II PROTEINS
A Dissertation Presented By
Corrie A. Painter

The signatures of the Dissertation Defense Committee signifies completion and
approval as to style and content of the Dissertation

_____
Lawrence J. Stern, Ph.D., Thesis Advisor

_____
Mary Munson, Ph.D., Member of Committee

_____
Scot A. Wolfe, Ph.D., Member of Committee

_____
William Royer, Ph.D., Member of Committee

_____
Elizabeth D. Mellins, M.D., External Member of Committee

The signature of the Chair of the Committee signifies that the written dissertation
meets the requirements of the Dissertation Committee

_____
Allan Jacobson, Ph.D., Chair of Committee

The signature of the Dean of the Graduate School of Biomedical Sciences
signifies that the student has met all graduation requirements of the school

_____
Anthony Carruthers, Ph.D.
Dean of the Graduate School of Biomedical Sciences

Program in Biochemistry & Molecular Pharmacology

ACKNOWLEDGEMENTS

the world! I would also like to thank Robby's afro which brings a smile to my face even as I format this thesis.

All of my friends have been tremendously supportive throughout my graduate studies; in particular, I'd like to thank Jennifer Christianson for mental telepathy and Bring Ba Ba. I would also like to thank Lauren Ryan for having the courage to start a support group for angiosarcoma, without which, I would be lost.

My family has been amazingly supportive and I'd like to thank each member for their love, and endless support. My Mom, Karen Sanders, who dropped everything to live with us in the most selfless loving manner as I battled cancer, my Dad, Morton Perlroth, who would move the world to a different orbit if he though it'd help, my brothers Glen and Howard Perlroth for their love.

THESIS ABSTRACT

MHC II proteins are heterodimeric glycoproteins that form complexes with antigenic peptides in order to elicit a $CD4^+$ adaptive immune response. Even though there have been numerous MHC II-peptide crystal structures solved, there is little insight into the dynamic process of peptide loading. Through biochemical and biophysical studies, it has been shown that MHC II adopt multiple conformations throughout the peptide loading process. At least one of these conformations is stabilized by the MHC II-like homologue, HLA-DM. The main focus of this thesis is to elucidate alternate conformers of MHC II in an effort to better understand the structural features that enable HLA-DM catalyzed peptide loading. In this thesis, two altered conformations of HLA-DR were investigated, one modeled in the absence of peptide using molecular dynamics, and one stabilized by the mutation αF54C.

The model for the peptide-free form of HLA-DR1 was derived from a molecular dynamics simulation. In this model, part of the alpha-subunit extended-strand region proximal to the peptide binding groove is folded into the peptide-binding groove such that the architecture of the critical peptide binding pocket, P1, as well as the invariant hydrogen bonding network were maintained. Biochemical studies aimed at validating the predicted structural changes were consistent with the model generated from the simulations.

Next, structural studies were carried out on an MHC II mutant, αF54C, which was shown to have unique peptide binding characteristics as well as enhanced susceptibility to HLA-DM. Although this mutation did not affect the affinity for peptide, there was a striking increase in the rate of intrinsic peptide release. Both αF54C and αF54A were over 100-fold more susceptible to HLA-DM catalyzed peptide release than wild type as well as other mutants introduced along the peptide binding groove. In addition, mutation of the αF54 position results in a higher affinity for HLA-DM, which, unlike wild type, is detectable by surface plasmon resonance. Crystallographic studies resulted in a 2.3 Å resolution structure for the αF54C-Clip complex. There were two molecules in the asymmetric unit, one of which had no obvious deviations from other MHC II-pep complexes and one which had a conformational change as a result of a crystal contact on the αF51 residue, a residue which has been shown to be involved in the HLA-DM/HLA-DR binding interface. The crystal structure of wild type HLA-DR1-Clip was also solved, but did not have the altered conformation even though there was a similar crystal contact at the αF51. These data suggest the altered conformation seen in the mutant structure, results from increased lability in the extended stand region due to the αF54C mutation. As a result of this work, we have developed a new mechanistic model for how structural features of MHC II influence DM mediated peptide release.

TABLE OF CONTENTS

Chapter IV

LIST OF TABLES

LIST OF FIGURES

PREFACE

The work presented in this thesis is aimed at describing conformational changes that occur in MHC II proteins.

Chapter I contains background relevant to our understanding of the MHC II structure and highlights what is known about MHC II-peptide interactions, MHC II structural variability, and MHC II–peptide loading mediated by the accessory molecule HLA-DM.

Chapter II describes a hypothetical model for the peptide free state of HLA-DR1, a common MHC II allele. In collaboration with the University of Puerto Rico, a molecular dynamics simulation was carried out using the coordinates of a MHC II-peptide structure, with the peptide removed. The results from this simulation suggest that in the peptide free state, the alpha 50-57 strand region is capable of dynamic conformational changes such that it could engage the peptide binding groove in an extended conformation much like the canonical peptide structure in the bound crystal structure. The most striking feature of this model is that the alpha F54 was positioned into the large hydrophobic P1 pocket, much like the peptide tyrosine in the bound crystal structure. The model was evaluated using biological probes that have been mapped to regions within the MHC II that were predicted to undergo small, moderate or large conformational differences. The binding of the probes was in agreement with the conformational changes predicted by the model.

Chapter III describes a HLA-DR1 mutant, αF54C, which is dramatically susceptible to HLA-DM mediated peptide exchange, and has a higher affinity for HLA-DM as compared to wild type HLA-DR1. The αF54C substitution results in a weakening of the N-terminal hydrogen bonds, which were mapped using a hydrogen deuterium exchange assay coupled with a novel electron transfer dissociation-based mass spectrometry approach. Crystal structure analysis of the αF54C in complex with CLIP peptide revealed a conformational change in the alpha 3_{10} helical region and adjacent strand region proximal to the P1 pocket. The conformational change was seen in only one molecule of the asymmetric unit and was induced by a crystal contact at the αF51 position, a residue known to be critical for HLA-DM interaction. The αF54C substitution increases conformational lability within the extended strand region, such that contact at the HLA-DM binding site induces concerted movements along the entire alpha 3_{10} helical region. These results thus provide a structural context for how HLA-DM may induce conformational changes within MHC II proteins.

Chapter IV summarizes the work done in this thesis and describes future directions that might extend the work presented here.

Appendix 1 provides an analysis of structural variability in HLA-DQ alleles

List of publications and manuscripts in progress

1) Painter CA, Stern LJ. Structural insights into MHC II conformational variability. Review in preparation for Current Topics in Biochemical Research. (Chapter I/Appendix 1)

2) Painter CA, Cruz A, Lopez GE, Stern LJ, Zavala-Ruiz Z. PLoS One. 2008 Jun 11;3(6)e2403. (Chapter II) I am co-first author of this work and performed analysis of the molecular dynamics simulation as well as biochemical assays to test the model.

3) Painter CA, Negroni MP, Kellersberger K, Stern LJ. The Class II 3_{10} helix and adjacent strand region are key structural determinants for HLA-DM interaction and peptide exchange. (Chapter III) The work done for this paper was carried out primarily by myself. Larry Stern and Jim Evans developed the concepts for the HDx and ETD data, and Katherine Kellersburger helped perform the ETD. Manuscript in preparation for Nature Structural biology

4) De Wall, SL, Painter C, Stone JD, Bandaranayake R, Wiley DC, Mitchison TJ, Stern LJ, DeDecker BS. Nat Chem Biol. 2006 Apr;2(4): 197-201. I contributed to this work by testing a panel of monoclonal antibodies for differential binding to a cisplatin induced conformation of HLA-DR1. (data not included in this thesis)

CHAPTER I

INTRODUCTION

ABSTRACT

Antigen presentation by class II MHC proteins (MHC II) is a critical component of the adaptive immune response to foreign pathogens. Our understanding of how antigens are presented has been greatly enhanced by crystallographic studies of MHC II-peptide complexes, which have shown a canonical extended conformation of peptide antigens within the peptide-binding domain of MHC II. However, a detailed understanding of the peptide loading process, which is mediated by the accessory molecule HLA-DM (DM), remains unresolved. MHC II proteins appear to undergo conformational changes during the peptide loading/exchange process that have not been clearly described in a structural context. In the absence of a crystal structure for the DM-MHC II complex, mutational studies have provided a low resolution understanding as to how these molecules interact. This introduction will focus on structural and biochemical studies of the MHC II-peptide interaction, and on studies of the DM-MHC II interaction, with an emphasis on identifying structural features important for the mechanism of DM mediated peptide catalysis.

Formation of the MHC II-peptide complex

MHC II proteins are ~50 kD heterodimeric transmembrane glycoproteins that are assembled in the endoplasmic reticulum (Cresswell 1994). The nascent complex as expressed in the endoplasmic reticulum is comprised of three alpha-beta MHC II proteins in complex with the invariant chain (Ii) trimer (Roche, Marks et al. 1991; Lamb and Cresswell 1992). The invariant chain has been proposed to carry out a dual function to both direct the MHC II to endosomal compartments as well as to block the peptide binding groove of the MHC II (Bakke and Dobberstein 1990; Roche and Cresswell 1990). In endosomal compartments, regions of the Ii that are not protected by the MHC II are proteolyzed by cysteine proteases (Morton, Zacheis et al. 1995). This results in an MHC II protected peptide fragment, *CL*ass II *I*nvariant chain *P*eptide (CLIP), which remains bound to the MHC II in the antigen binding site (Riberdy, Newcomb et al. 1992). In order for antigen presentation to occur, CLIP must be exchanged with endosomal peptides, a process which is catalyzed by the MHC II homologue HLA-DM (Sloan, Cameron et al. 1995). There is evidence that HLA-DM has a dual function to both stabilize an empty conformation of MHC II (Kropshofer, Arndt et al. 1997), as well as catalyze peptide exchange (Sherman, Weber et al. 1995), as discussed below. Although the involvement of HLA-DM in promoting peptide exchange has been definitively described, the mechanism of this process is poorly understood (Ferrante and Gorski ; Weber, Evavold et al. 1996; Zarutskie,

Busch et al. 2001; Stratikos, Wiley et al. 2004; Narayan, Chou et al. 2007; Ferrante, Anderson et al. 2008; Narayan, Su et al. 2009; Zhou, Callaway et al. 2009).

MHC II structure

Prior to the first solved MHC II crystal structure, a hypothetical model of the MHC II was developed based on the MHC I structure (Brown, Jardetzky et al. 1988). Genetic analysis had revealed that class I and II molecules shared similar domain and genomic organization (Kaufman, Auffray et al. 1984). It was therefore predicted that the MHC II structure would reveal one membrane distal peptide binding site that would be comprised of regions with high residue polymorphisms (Kaufman, Auffray et al. 1984). In 1993, a 3.3Å structure of the extracellular portion of HLA-DR1 in complex with a mixture of peptides isolated from B-cells provided a detailed molecular model describing the fold of the MHC II as well as the architecture of the peptide binding groove (Brown, Jardetzky et al. 1993). The crystal structure revealed a peptide binding groove that is formed by the α1 and β1 domains (Fig. 1.1). The binding groove has a beta sheet floor flanked by two alpha helices formed by both the alpha and beta chains. Ig domains comprise the membrane proximal portion from both the α2 and β2 regions (Fig. 1.1). Although the structures were obtained from soluble ectodomains of the protein, there are also alpha and beta chain transmembrane domains as well as short cytoplasmic tails that have been implicated in signal

FIGURE 1.1
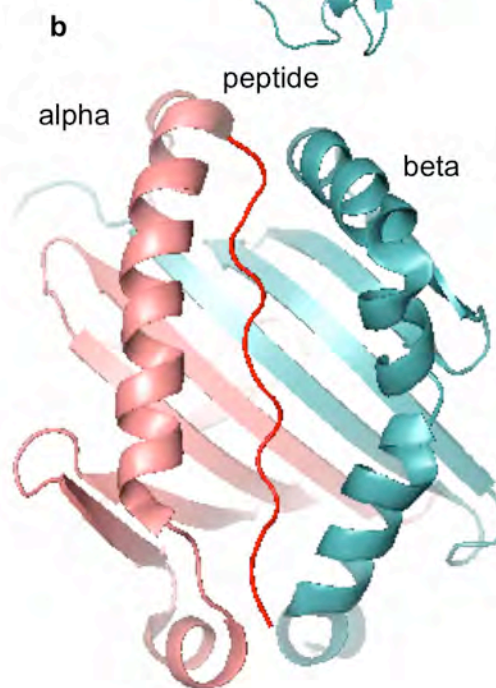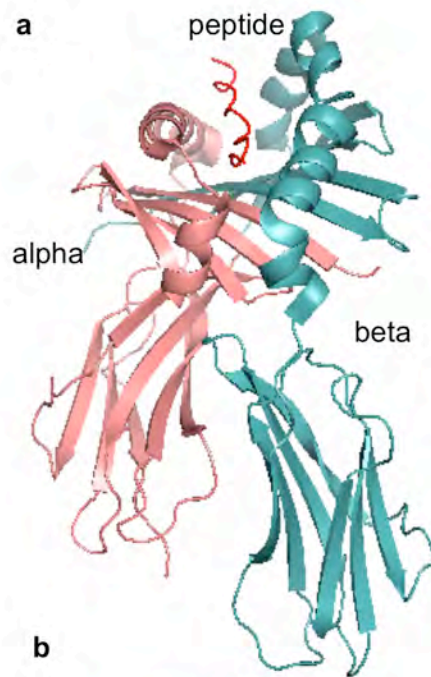
FIGURE 1.1. Crystal structure of MHC II. (a) Cartoon representation of an HLA-DR1 peptide complex (1DHL). The alpha chain is shown in salmon, the beta chain in teal and the peptide in red. (b) 90° rotation showing the top of the peptide binding groove.

transduction (Nabavi, Freeman et al. 1992). This first structure of an MHC II

peptide complex revealed that peptides bind in an extended conformation. In

contrast to the MHC I peptide structures, the MHC II structure showed that the

peptide binding groove is open ended at both the N and C-terminus of the

peptide suggesting that peptides of variable length could bind into the groove

(Brown, Jardetzky et al. 1993). Subsequently, it has been demonstrated that

MHC II proteins can bind peptides with lengths ranging from 2-4 residues (Sato,

Zarutskie et al. 2000) all the way to unfolded intact proteins (Lindner and Unanue

1996).

In 1994, the crystal structure of HLA-DR1 with a single defined peptide, an

immunodominant fragment from Heamaglutinin (HA), was solved and the

molecular details of the peptide MHC II interaction were described (Stern, Brown

et al. 1994). The peptide bound in an extended conformation corresponding to a

type II polyproline twist, in which 35% was solvent exposed and therefore

theoretically able to interact with CD4+ T-cells. This structure showed pockets in

the overall peptide binding groove that accommodated five of the thirteen side

chains from the peptide. In addition, a hydrogen-bonding network was clearly

defined in this structure, with twelve hydrogen bonds involving the main chain of

the peptide and conserved residues in the MHC II (Fig. 1.2). Further evidence

that the hydrogen bond network was a common motif in MHC II–peptide

interactions was revealed by another MHC II structure bound to a mixture of

FIGURE 1.2
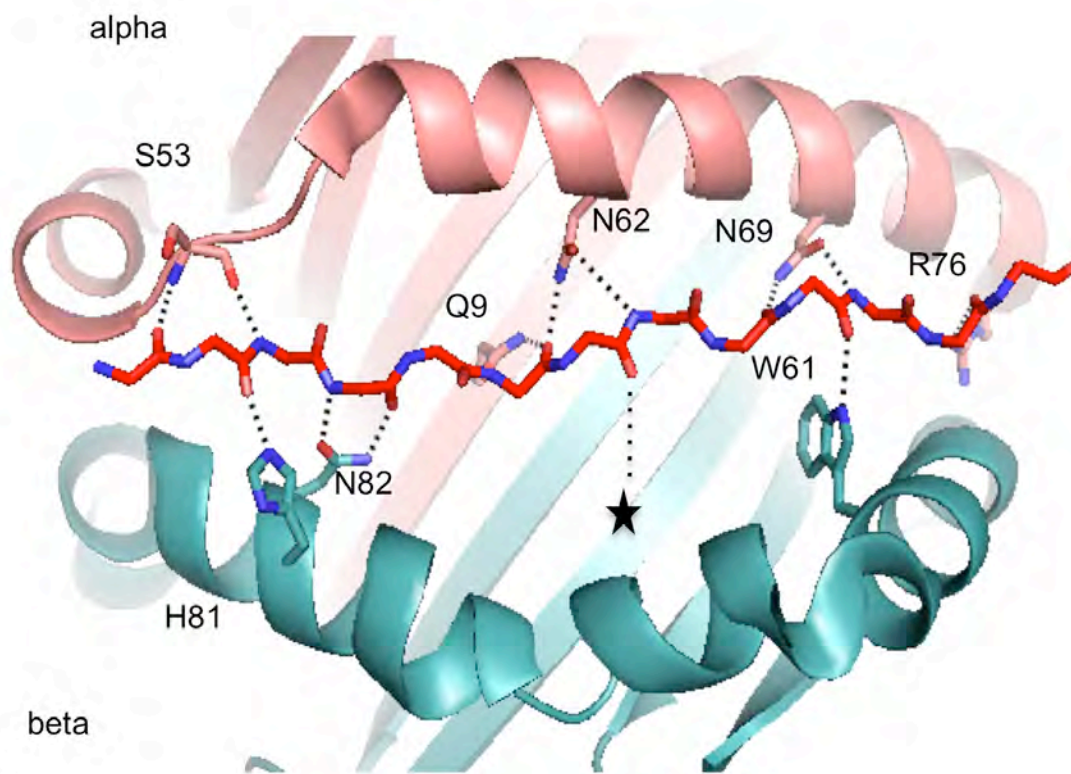
FIGURE 1.2. Conserved hydrogen bond network of MHC II. Cartoon

representation of peptide binding groove, alpha chain in salmon, beta chain in

teal, peptide in red stick with amine groups colored blue, and carboxyl groups

colored pink. Conserved residues in MHC II are shown in stick with dashed lines

representing hydrogen bonds to the peptide backbone. Note that bonds are

formed between conserved side chains in the MHC II except for the S53, where

the bonds are mediated by the main chain atoms in the MHC II. The beta 71

position, represented by a star, is polymorphic. In most HLA-DR alleles, there is

an h-bond formed between this reside and the carbonyl of the peptide backbone,

shown as a dashed line, however, in the HLA-DQ, HLA-DP, IA alleles, there is no

h-bond formed at this position.

endogenous peptides determined at higher resolution by co-crystallization

with a bacterial superantigen, which showed the peptide conformation to be

constrained by the pattern of side-chain binding pockets as well as by the

hydrogen bonds that extended from the backbone of the peptide to conserved

asparagine and glutamine residues on the MHC II (Jardetzky, Brown et al. 1996).

Through these structural studies, it became evident that there are two

different aspects of the peptide MHC II interaction. One is mediated through a

hydrogen bond network that is formed by the peptide backbone and both main

chain and side chain atoms of the MHC II, and the other mediated by peptide

side chain interactions with binding groove pockets (Fig 1.2; Fig 1.3).

MHC II variation and peptide binding interactions

There are four main binding pockets present in all MHC II structures

determined to date, called P1, P4, P6 and P9 that accommodate peptide side

chains.   These pockets are highly polymorphic and therefore diverse in the

shape and charge specificity between different MHC II proteins (Fig 1.3). HLA-

DR1 has been extensively studied and numerous structures show a large P1

hydrophobic binding pocket (Fig 1.4) (Stern, Brown et al. 1994; Jardetzky, Brown

et al. 1996). This pocket is the most important determinant of binding specificity

for HLA-DR1 (Jardetzky, Gorga et al. 1990; Sato, Zarutskie et al. 2000) However,

there is sequence variation for residues lining the P1 pocket of the MHC II

proteins, which affects the charge and shape of the pocket, ultimately leading to

FIGURE 1.3

a

1DLH (HLA-DR1-HA peptide)

b

3LQZ (HLA-DP2-self peptide)

c

2NNA (HLA-DQ8-gluten peptide)

d

1A6A (HLA-DR3-CLIP peptide)
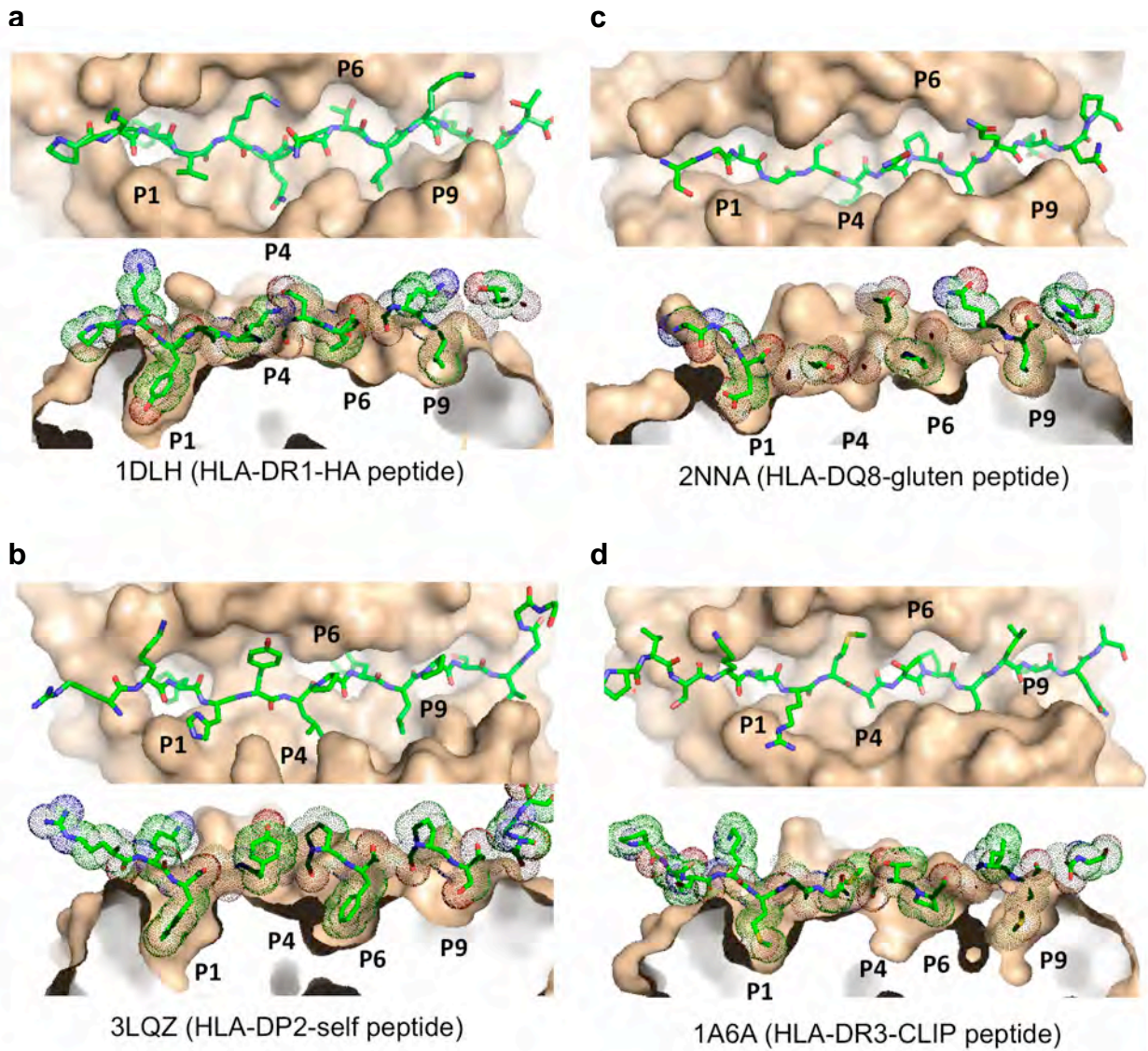
FIGURE 1.3. Peptide binding grooves of multiple MHC II show differences in peptide side chain specificity pockets. (a) HLA-DR1 (PDB ID: 1DLH) Surface representation of the top of the peptide binding groove, with peptide shown in stick. Main anchoring specificity pockets P1, P4, P6 and P9 are designated below. (bottom) 90° rotation showing side of peptide binding groove with peptide side chains lodged into specificity pockets, peptide shown in stck and dots. (b) HLA-DP2 (PDB ID: 3LQZ) shown as in same orientation as (a). (c) HLA-DQ8 (PDB ID: 2NNA) shown as in same orientation as (a). (d) HLA-DR3 (PDB ID: 1A6A) shown as in same orientation as (a).

differences in what side chains can be accommodated at this position (Fig. 1.4). Indeed, the sequence variations within the peptide binding domain of the MHC II proteins cause differences in specificity for the anchor residues all along the peptide binding groove (see below) (Fig. 1.3).

After the first HLA-DR1 structures were solved, the residues forming the anchor pockets were defined. Subsequent structures of different MHC II variants allowed a detailed look into the effect of polymorphisms and sequence variations on the size, shape and specificities of the different pockets. Numerous crystal structures for MHC II alleles of HLA-DR, HLA-DP and HLA-DQ have helped to refine our understanding of the peptide MHC II interaction (Table 1.1). In addition, crystal structures for I-E the mouse MHC II homologue of the human HLA-DR, as well as I-A, the homologue for the human HLA-DQ, have been solved (Table 1.1). To date, there are 81 MHC II structures deposited in the PDB, encompassing over 15 different allelic variants of the five human and murine class II MHC proteins (Table 1.1). Although this is a narrow view into the thousands of documented MHC II alleles (Robinson, Waller et al. 2009), these structures are strikingly similar in overall fold with polymorphic differences concentrated in the binding groove.

An example of how MHC II sequence variation can alter the size, shape and specificity of the key anchoring pockets was described by Fremont et. al. after the crystal structure of the mouse HLA-DR homologue, I-E^k, was solved

FIGURE 1.4

a
HLA-DR1 (tyrosine P1)

b
HLA-DQ0602 (Leucine P1)

c
IE$_k$ (isoleucine P1)

Glycine beta 86

Phenylalanine beta 87

Phenylalanine beta 86
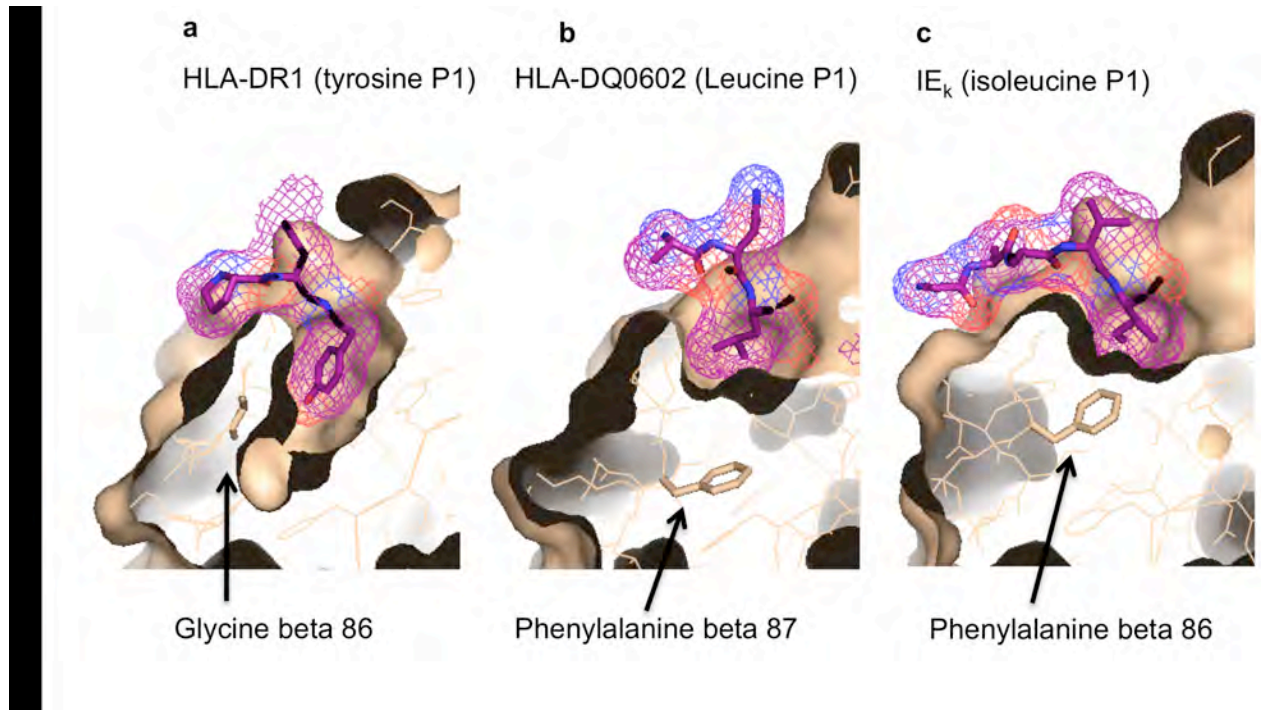
FIGURE 1.4. Diversity of size and shape of the P1 pocket. Changes in beta 86/87 contribute to alterations in the size and shape of the P1 pocket. Each of the structures are represented in both surface and lines with the beta 86 or 87 residue shown in stick. The peptide is in purple stick and mesh with the P1 residue indicated above. (a) HLA-DR1 (PDB ID# 1DLH) has a glycine at beta 86, which allows a large hydrophobic pocket at the P1. (b) the HLA-DQ0602 structure (PDB ID# 1UV6) has a phenylalanine at the beta 87 residue. (c) the IE_k (PDB ID# 1IEA) has a phenylalanine at the beta 86 position.

TABLE 1.2 Current list of MHC II structures in the PDB

PBD ID	Allele	Peptide	Res.	Citation
3LQZ	HLA-DP2 (A1*0103/B1*0201)	self DRa	3.25	(2010) Proc.Natl.Acad.Sci
1UVQ	HLA-DQ6 (A1*0102/B1*0602)	hypocretin	1.80	(2004) Proc.Natl.Acad.Sci.
3PL6	HLA-DQ1 (A1*0102/B1*0502)	MBP	2.55	(2011) J.Exp.Med.
1S9V	HLA-DQ2 (A1*0501/B1*0201)	Deaminated Gliadin	2.20	(2004) Proc.Natl.Acad.Sci.
2NNA	HLA-DQ8 (A1*0301/B1*0302)	Deaminated Gluten	2.10	(2007) Immunity
1JK8	HLA-DQ8 (A1*0301/B1*0302)	human Insulin	2.40	(2001) Nat.Immunol.
1H15	HLA-DR 01/05	EBV	3.10	(2002) Nat.Immunol.
1KLU	HLA-DR1	TPI	1.93	(2002) J.Mol.Biol.
3PDO	HLA-DR1	CLIP (102-120)	1.95	(2010) Proc.Natl.Acad.Sci.
2G9H	HLA-DR1	HA	2.00	(2006) J.Biol.Chem.
1PYW	HLA-DR1	HA variant	2.10	(2003) J.Biol.Chem.
3L6F	HLA-DR1	MART-1	2.10	(2010) J.Mol.Biol.
1SJH	HLA-DR1	HIV 13mer	2.25	(2004) Proc.Natl.Acad.Sci.Usa
1JWU	HLA-DR1	HA	2.30	(2003) Structure
2IPK	HLA-DR1	HA variant Fluor	2.30	(2007) Nat.Chem.Biol
1KLG	HLA-DR1	TPI	2.40	(2002) J.Mol.Biol.
1T5W	HLA-DR1	synthetic peptide	2.40	(2004) Chem.Biol.
2ICW	HLA-DR1	HA	2.41	(2007) Nat.Struct.Mol.Biol.
1AQD	HLA-DR1	endogenous	2.45	(1997) Structure
1SJE	HLA-DR1	HIV 16mer	2.45	(2004) Proc.Natl.Acad.Sci.
1TX5	HLA-DR1	synthetic peptide	2.50	(2004) Chem.Biol.
1FYT	HLA-DR1	HA	2.60	(2000) EMBO J.
1HXY	HLA-DR1	HA	2.60	(2001) Embo J.
1JWS	HLA-DR1	HA	2.60	(2003) Structure
1R5I	HLA-DR1	MAM	2.60	(2004) Structure
1KGO	HLA-DR1	EBV	2.65	(2002) Mol.Cell
3PGC	HLA-DR1	CLIP (Flipped)	2.66	(2010) Proc.Natl.Acad.Sci.
1JWM	HLA-DR1	HA	2.70	(2003) Structure
1SEB	HLA-DR1	endogenous	2.70	(1994) Nature
3PGD	HLA-DR1	CLIP (102-120)	2.72	(2010) Proc.Natl.Acad.Sci.
1DLH	HLA-DR1	HA	2.80	(1994) Nature 368
2IAM	HLA-DR1	TPI	2.80	(2007) Nat.Immunol.
2IAN	HLA-DR1	TPI	2.80	(2007) Nat.Immunol.
2OJE	HLA-DR1	HA	3.00	(2007) J.Biol.Chem.
2WBJ	HLA-DR1	ENGA	3.00	TBP*
2FSE	HLA-DR1	Collagen II	3.10	(2006) J.Immunol.
1LO5	HLA-DR1	HA	3.20	(2002) Structure
1FV1	HLA-DR2	MBP	1.90	(2000) J.Mol.Biol.
1BX2	HLA-DR2	MBP	2.60	(1998) J.Exp.Med.
1ZGL	HLA-DR2a	MBP	2.80	(2005) Embo J.
1HQR	HLA-DR2a	MBP	3.20	(2001) Immunity

PBD ID	Allele	Peptide	Res.	Citation
1YMM	HLA-DR2b	MBP	3.50	(2005) Nat. Immunol.
1A6A	HLA-DR3	CLIP	2.75	(1995) Nature
1D5M	HLA-DR4	pep mimetic	2.00	(2000) J.Med.Chem.
1D5Z	HLA-DR4	pep mimetic	2.00	(2000) J.Med.Chem.
2XN9	HLA-DR4	HA	2.30	(2010) Nat.Commun.
1J8H	HLA-DR4	HA	2.40	(2002) J.Exp.Med.
1D5X	HLA-DR4	pep mimetic	2.45	(2000) J.Med.Chem.
1D6E	HLA-DR4	pep mimetic	2.45	(2000) J.Med.Chem.
2SEB	HLA-DR4	Collagen II	2.50	(1997) Immunity
3O6F	HLA-DR4	MBP	2.80	(2011) Embo J.
2Q6W	HLA-DR52a	platelet integrin	2.25	(2007) J.Mol.Biol.
3C5J	HLA-DR52c	UNP	1.80	(2008) Proc.Natl.Acad.Sci.
1ES0	I-Ag7	Gad65	2.6	(2000) Science
3MBE	I-Ag7	HEL	2.89	(2010) J.Clin.Invest.
3CUP	I-Ag7	GAD	3.09	TBP*
1F3J	I-Ag7	HEL	3.10	(2000) Immunity
1FNE	I-eK	HB	1.90	(2001) J.Immunol.
1FNG	I-eK	HB	1.90	(2001) J.Immunol.
1MUJ	IA-b	CLIP	2.15	(2003) J.Mol.Biol.
1LNU	IA-b	EALPHA3K	2.50	(2002) Proc.Natl.Acad.Sci.
3C5Z	IA-B	3K	2.55	(2008) Immunity
3C60	IA-B	3K	3.05	(2008) Immunity
3C6L	IA-B	3K	3.40	(2008) Immunity
1IAO	IA-d	Ova	1.60	(1998) Immunity
2IAD	IA-d	HA	2.40	(1998) Immunity
1IAK	IA-k	HEL	1.90	(1998) Immunity
1D9K	IA-k	Conalbumin	3.20	(1999) Science
1JL4	IA-k	Ovotransferrin	4.30	(2001) Proc.Natl.Acad.Sci.
2P24	IA-u	MBP	2.15	(2008) J.Mol.Biol.
1K2D	IA-U	MBP	2.20	(2002) Immunity
2PXY	IA-u	MBP	2.23	(2007) Nat.Immunol.
1U3H	IA-u	MBP	2.42	(2005) Immunity
2Z31	IA-u	MBP	2.70	(2007) Nat.Immunol.
1IEA	IE-k	HB	2.30	(1996) Science
1I3R	IE-k	Hemoglobin Beta2	2.40	(2001) Immunity
1KTD	IE-k	Pigeon Cyto C	2.40	(2002) J.Exp.Med.
1R5V	IE-k	artificial peptide	2.50	(2003) Mol.Cell
1IEB	IE-k	HSP70	2.70	(1996) Science
1KT2	IE-k	Moth Cyto C	2.80	(2002) J.Exp.Med.
1R5W	IE-k	artificial peptide	2.90	(2003) Mol.Cell

* To be published

(PDB ID: 1IEA) (Fremont, Hendrickson et al. 1996). This structure shows that polymorphisms in the beta chain give rise to differences along the binding pockets. The P1 pocket is smaller in I-E^k due to a phenylalanine at the beta86 position, which in DR1 is a glycine (Fig 1.4). The beta 86 position forms the side of the P1 pocket, so larger residues at this position decrease the volume of the pocket, which restricts binding to smaller residues. In I-E^k, the largest pocket is the P4. Unlike HLA-DR1, this allows a large hydrophobic residue to be engaged in the middle of peptide (Fremont, Hendrickson et al. 1996).

The beta 86 position also contributes to alterations in the shape of HLA-DR alleles. For instance, in some HLA-DR alleles, there is a valine at this position instead of the glycine found in HLA-DR1. This dimorphism allows discrimination between allelic variants of HLA-DR based on the amino acid sequence at a single position within a peptide (Newton-Nash and Eckels 1993). Other polymorphisms within HLA-DR variants alter structural properties of the P4 and P6 pockets. For example, differences in charge for residues lining the P4 pocket in HLA-DR alleles play a role in susceptibility to rheumatoid arthritis (RA) (Taneja and David), such that a positive residue at beta71 in HLA-DRB1*0401 and HLA-DRB1*0101 is linked to RA, but a negative residue as found in HLA-DRB1*0402 confers a non-RA associated phenotype. In addition, polymorphic differences extend to the P6 position of HLA-DRB1*0101 which prefers small, polar or neutral residues, whereas the DRB1*0401 can accommodate Thr, Asn, and Ser (Bolin, Swain et al. 2000).

Structures of other MHC II variants have highlighted the diversity in size, shape, specificities, and general architecture of the peptide binding groove. The mouse HLA-DQ homologue is I-A. One major structural difference between the I-A/HLA-DQ and the I-E /HLA-DR proteins is due to an alpha 9 glycine insertion which contributes to a beta-bulge in the floor of the peptide-binding groove (Fig. 1.5 b) (Fremont, Monnaie et al. 1998; Scott, Peterson et al. 1998; Zhu, Rudensky et al. 2003). Intriguingly, this bulge precludes large anchor residues from engaging anchor pockets within the core of the peptide binding groove, while at the same time, it draws the peptide deeper into the groove because of additional hydrogen bonds that form between the peptide and the main chain atoms of the beta bulge residues (Scott, Peterson et al. 1998). Ultimately, these effects allow tight binding to peptides that are not anchored by side chain specificity pockets within the core of the peptide binding domain (Scott, Peterson et al. 1998).

HLA-DP2 is the only HLA-DP allele for which a structure has been solved. It has a similar charge and shape as HLA-DR1 for the P1 pocket, which can accommodate large hydrophobic anchor side chains (Dai, Murphy et al.) (Fig. 1.3). However, unlike other HLA-DR alleles, this structure shows that the P6 pocket is equal in size to the P1 and can also act as a major anchoring site (Dai, Murphy et al.). One of the interesting features from this structure is that there is a solvent exposed acidic pocket between the peptide backbone and the β-chain α-helix that is believed to be responsible for the linkage of this allele with Chronic beryllium disease (Richeldi, Sorrentino et al. 1993), a T-cell mediated

FIGURE 1.5

DR1 (1DLH)
DR1 (1SEB)
DR52a (2Q6W)
DR52c (3C5J)
DR2 (1FV1)
DR3 (1A6A)
DR4 (1DZ5)

DP2 (3LQZ)
IE(k) (1IEA)
IA(u) (1K2D)
IA(b) (1MUJ)
IA(k) (1IAK)
IA(g7) (1ES0)

DQ6 (1UVQ)
DQ2 (1SV9)
DQ8 (2NNA)
DQ1 (3PL6)
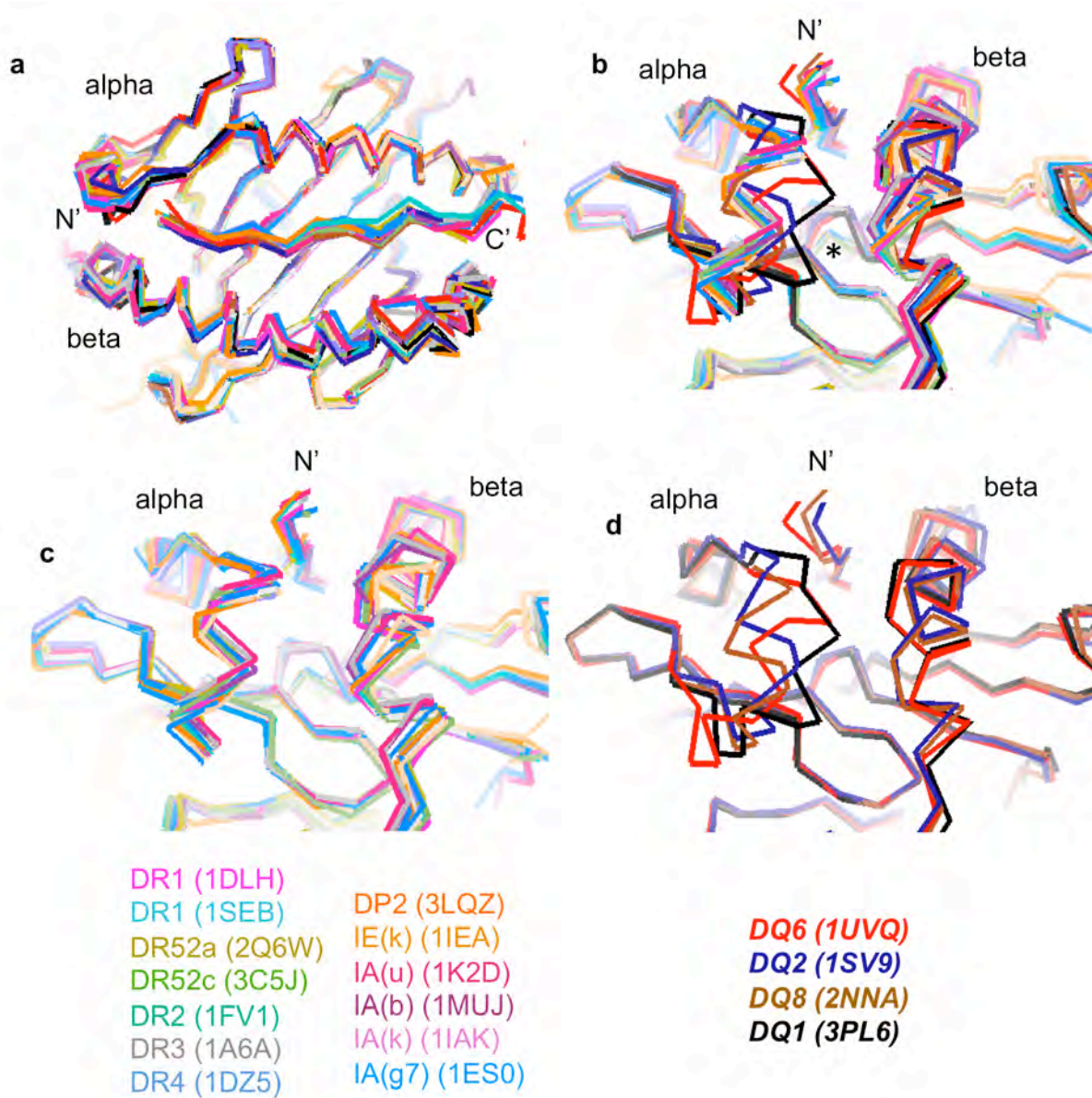
FIGURE 1.5. Structural alignment of MHC II protiens. Crystal structures for each of the MHC II proteins with representative alleles are shown aligned by residues alpha 4-80 and beta 4-90, which comprise the peptide binding groove. The alpha and beta chains are labeled for each panel, and the peptide is labeled N' for the N-terminus and C' for the C terminus. (a) Ribbon diagram of the top of the binding groove for each of the alleles (listed at the bottom by color). (b) Ribbon diagram of the N-terminal peptide binding region, asterisk designates beta bulge at alpha Gly9 in IA and DQ structures. (c) Same view as in (b) with the DQ alleles omitted. (d) same view as in (b) with only DQ alleles.

hypersensitivity to beryllium metal, oxides, and alloys {Fontenot, 2001 #767}.

Structures of other MHC II variants show yet even more diversity in the size and shape of the binding groove pockets. The HLA-DQ8 (A1*0301/B1*0302) structure (PDB ID: 2NNA), has a P1 pocket that is deep and highly charged. However, unlike HLA-DR1, there are deep pockets for the P4 position, which can accommodate large hydrophobic residues, and the P9 position, which is deep and charged. The P6 pocket is shallow and accommodates only minor anchor residues (Lee, Wucherpfennig et al. 2001; Henderson, Tye-Din et al. 2007).

The crystal structure for HLA-DQ06 (A1*0102/B1*0602), an allele which is linked to protection from type I diabetes (Barker 2006), shows significant main chain and side chain conformational differences for the alpha 46 to 55 region as well as the beta 85 to 91 region. The P1 pocket is shallow as compared to HLA-DR1, mostly due to a phenylalanine at the beta 87 position, which "fills" the P1, much like other alleles which have polymorphisms at the beta 86 position that alter the P1 size and shape (Fig. 1.4). This structure reveals fairly equivalent sizes and shape for the P4, P6 and P9 pockets (Siebold, Hansen et al. 2004).

The structure of HLA-DQ2 (A1*0501/B1*0201, PDB ID:1SV9) also deviates from the canonical MHC II structure with deviations in the tilt in the alpha 45-51 helical region toward the long alpha helical stretch of the alpha chain. In addition, the beta 85-91 region is tilted in toward the peptide binding domain relative to other MHC II structures. HLA-DQ2 (1SV9) has a region of positive electrostatic charge between the P4 and P6 pockets unlike the HLA-DQ8

(2NNA) structure, which has a neutral electrostatic potential in this region. The P9 can accommodate bulky hydrophobic residues (Kim, Quarsten et al. 2004). T

There is tremendous diversity within the peptide binding groove of MHC II proteins, which in turn allows peptide antigens with variable sequences to bind these proteins for presentation to CD 4+ T cells. With the exception of HLA-DR alleles (Belmares, Busch et al. 2002), the role that these pocket differences confer on the ability of DM to mediate peptide exchange has not been thoroughly explored (see below).

Hydrogen Bonding interactions between the peptide and MHC II

Even though there is great diversity of the residues lining the peptide binding groove, highly conserved residues across all MHC II alleles give rise to a canonical hydrogen bonding network which provides a peptide sequence independent type of interaction (Fig. 1.2, 1.6). There are however a couple of deviations from the canonical network. Notably, the HLA-DQ06 (1UVQ), has a rotamer change for the βH81 such that the imidazole group is positioned away from the peptide backbone and therefore unable to form a hydrogen bond at this position. This structural feature complicates efforts to assign specific functional attributes to conserved residues. Although particular residues may be highly conserved, positional changes may alter the functional group associated with that residue. The hypocretin peptide in this complex has a proline in the P2 position which may induce structural changes that propogate through the protein's

FIGURE 1.6
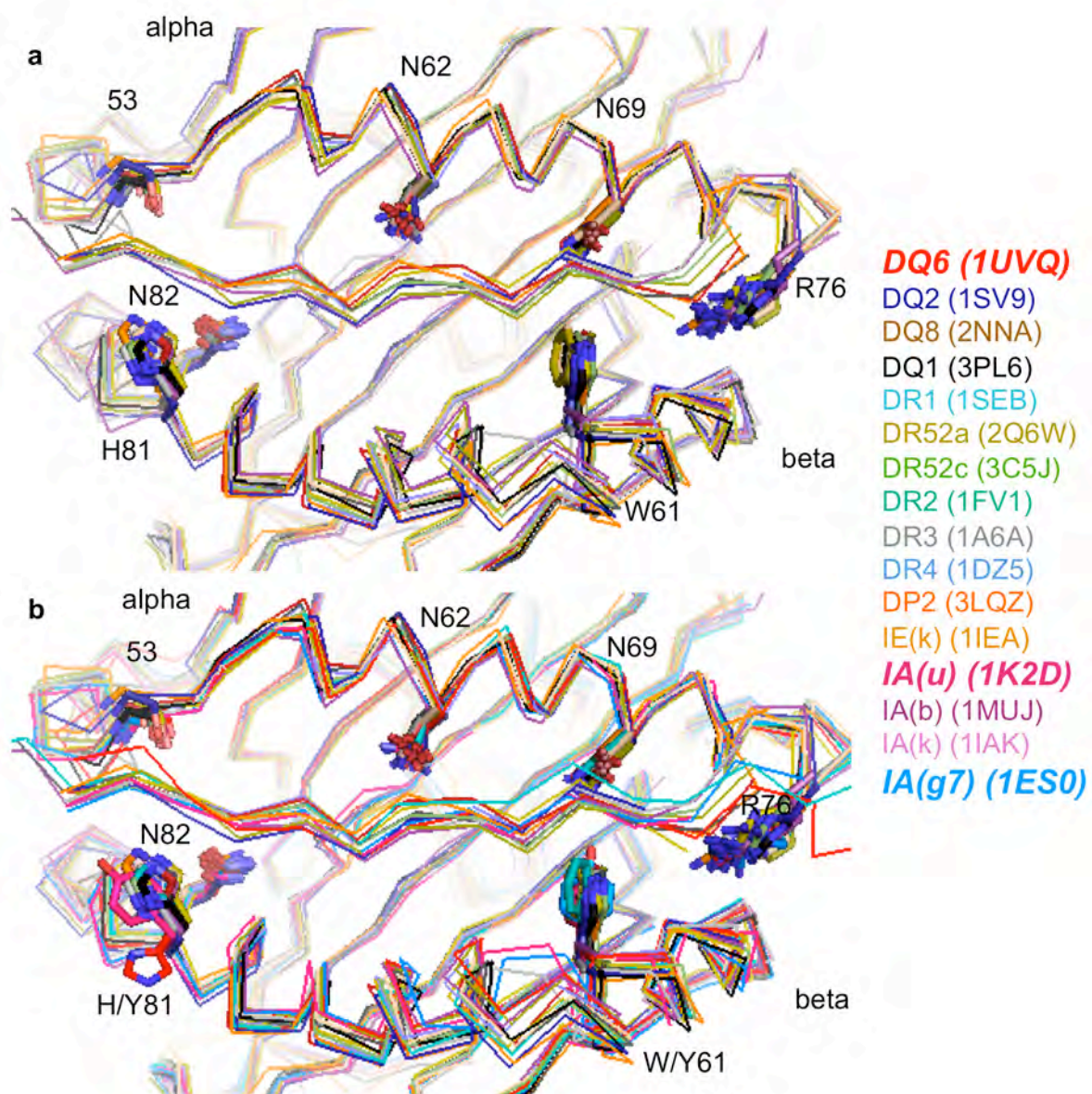
FIGURE 1.6. Conserved hydrogen bond network across multiple MHC II proteins. Representative structures from each of the MHC II proteins/alleles that have crystal structures were aligned by the alpha1/beta1 peptide binding domain. (a) Proteins invariant at positions considered to be part of the "canonical" hydrogen bonding network. (b) Proteins that have deviations in the hydrogen bond network are overlaid with the invariant alleles, shown as italicized and bold to the right. HLA-DQ6 (1UVQ) has a rotamer shift of the betaH81 away from the peptide backbone. The IA(u) has tyrosines at the $\beta81$ and the $\beta61$ and the and IA(g7) has a tyrosine at the $\beta61$ position.

secondary structure (discussed in appendix I). The βH81 position has been implicated in peptide binding stability and has been posited as a key residue involved in the function of DM mediated peptide exchange (Narayan, Chou et al. 2007; Bandyopadhyay, Arneson et al. 2008). However, the βH81 is not invariant, for example it is a tyrosine in I-A^u (Fig 1.6). Because the MHC II βH81 hydrogen currently is understood to be a major component of the MHC II peptide interaction, alleles that can bind peptides without forming this hydrogen bond should be more completely characterized.

Conformational changes in MHC II

Conformational changes have been reported for MHC II proteins (Germain and Hendrix 1991; Lee, Kay et al. 1992; Natarajan, Stern et al. 1999; Rotzschke, Falk et al. 1999; Schmitt, Boniface et al. 1999; Zarutskie, Sato et al. 1999; Verreck, Fargeas et al. 2001; Carven, Chitta et al. 2004; Carven and Stern 2005). Although direct structural analysis of MHC II peptide complexes suggest a highly stereotypic structure for these proteins, biochemical data does exist for alternate conformers under conditions that differ primarily in peptide occupancy and pH. Evidence for a peptide loading induced conformational change suggests that prior to peptide loading, empty MHC II exist in a "floppy" conformation (Germain and Hendrix 1991; Rotzschke, Falk et al. 1999). Peptide empty MHC II are less stable in SDS such that the subunits of the empty MHC II dissociate and migrate as individual chains, whereas MHC II in

25

complex with stably bound peptide migrates as an intact complex (Stern and Wiley 1992).

Peptide loading has been shown to alter the apparent molecular weight as assessed by gel filtration, which changes from 50kDa, for MHC II in complex with stable peptide to 60kDa, for empty MHC II (Zarutskie, Sato et al. 1999). Since the actual molecular weight of the peptide complex is larger than the empty protein, the larger apparent molecular weight for the empty protein implies that there is a difference in shape. In addition, a change in hydrodynamic radius from 37.4 Å for empty MHC II, to 31.8 Å for MHC II-peptide complex has been observed (Zarutskie, Sato et al. 1999). Studies using far-UV circular dichroism (CD) spectroscopy suggest that peptide empty MHC II exists in a conformation that has slightly less helical content (Rabanal, Ludevid et al. 1993; Zarutskie, Sato et al. 1999).

In addition to peptide-induced variations in MHC II structure, there is evidence that pH may play a role in MHC II conformational changes. The relevance of this pH change is likely due to the acidic environment of the endosome where peptide exchange occurs. The effect of pH on MHC II conformation has been partially attributed to increased peptide binding at low pH (Jensen 1990; Sadegh-Nasseri and Germain 1991). In endosomal compartments (pH ~5), exposure to peptides that can form stable MHC II peptide complexes decreased the floppy conformation, noted above, and promoted an SDS stable conformation of the complex (Sadegh-Nasseri and

Germain 1991). In addition, there are changes in the far-UV spectrum for MHC

II under acidic conditions as compared to spectra taken at neutral pH,

suggesting that there is loss of helicity for MHC II under acidic conditions (Lee,

Kay et al. 1992; Reich, Altman et al. 1997). A histidine at position alpha 33 has

also been implicated as a pH "trigger" for MHC II conformational changes

(Rotzschke, Lau et al. 2002). When the alpha His 33 is mutated to a tyrosine, a

relatively isosteric analogue that is unable to undergo protonation at endosomal

pH, the stability of the peptide-MHC II complex is unaffected by changes in pH

(Rotzschke, Lau et al. 2002).

Although the aforementioned studies suggest that MHC II can undergo

alterations in conformation as a result of peptide binding and/or changes in pH,

they do not reveal the regions of the MHC II that are involved. Studies designed

to better understand which regions of the MHC II participate in peptide induced

changes have subsequently been carried out and include epitope mapping of

antibodies specific for empty MHC (Carven, Chitta et al. 2004), differential

chemical modification due to peptide occupancy (Carven and Stern 2005), as

well as molecular dynamics simulations of the peptide free form of MHC II

(Painter, Cruz et al. 2008). These studies will be described below.

Using a panel of monoclonal antibodies raised against the denatured beta

chain of HLA-DR1 and screened for preferential reactivity against peptide-empty

vs. peptide-loaded HLA-DR1, Carven et al was able to map regions along the

beta chain of HLA-DR1 that had different activity when the MHC II complex was

empty or loaded with peptide. Antibodies that reacted differentially to empty and

peptide loaded HLA-DR1 were mapped to two distinct regions along the beta

chain. One set of antibodies mapped to the alpha helical region in the beta 1

domain from the 53-73 positions; notably, this region is kinked, with the L53

pointing down toward the peptide binding groove which is seen in structures of

HLA-DR peptide complexes. In order for there to be a recognizable epitope at the

L53, there presumably would have to be an alteration of this region that exposed

that residue. The other region that was recognized by the empty, but not peptide

loaded HLA-DR1 mapped to the membrane-proximal C-terminal region of the

beta chain and encompassed residues 186-189. The implications of having this

region differentially recognized is that the conformation of the empty protein must

have differences that propagate to regions far away from the peptide binding

domain (Carven, Chitta et al. 2004).

Carven et al continued to define differences in conformation between

empty and peptide loaded MHC II by probing for differential reactivity towards

selective chemical modifications between the bound and unbound complexes

(Carven and Stern 2005). Here, they determined differential reactivity for a

residue in the alpha chain proximal to the P1 pocket, Arg 50, as well as 2 other

residues, βR198 and βK98, which mapped to the same lateral face of HLA-DR1

that is predicted to be at the binding interface between MHC II and HLA-DM.   An

additional residue in the alpha chain, K67, was also observed to be differentially

reactive between the empty and peptide loaded structures (Carven and Stern 2005).

In addition to identifying regions and residues thought to be involved in the peptide induced conformational change for MHC II proteins, studies using molecular dynamics simulations, as well as normal mode analysis, of the peptide free MHC II, have been performed (Nojima, Takeda-Shitaka et al. 2003; Painter, Cruz et al. 2008; Yaneva, Springer et al. 2009). These studies have implicated the beta 57-67 residues, described as a region differentially recognized in empty MHC II by monoclonal antibodies above, as well as the short 3_{10} alpha helix and adjacent strand region of the alpha chain, which is proximal to the P1 pocket, as undergoing conformational changes during peptide loading. In chapter II of this thesis, a molecular dynamics study is presented which enabled the development of a model for the peptide free state of MHC II in which the alpha 50-59 region partially unwinds and engages the peptide binding groove, with the αF54 repositioning into the P1 pocket.

The conformational changes described in the aforementioned studies are based on HLA-DR alleles. However, an overlay of the structures for different MHC II alleles reveal that even in the peptide bound form there are regions that can adopt alternate conformations, some of which are beyond the side chain specificity pockets (Fig. 1.5). The beta chain helical region has a distinct kink, which has been implicated as a region that undergoes conformational changes based on peptide occupancy, as described above.

However, even in the peptide bound form, the position of this kink can move toward or away from the peptide binding groove (Fig. 1.5). In addition to this variable conformation on the beta chain, the alpha 3_{10} helical region can adopt alternate conformations in the HLA-DQ alleles (Fig. 1.5). Intriguingly, the HLA-DQ0602 structure (1UVQ; A1*0102/B1*0602) and the HLA-DQ1 (3PL6; A1*0102/B1*0502) have the same alpha chain, yet have alterations in the conformation of the alpha 3_{10} helix (Fig. 1.7). The HLA-DQ2 (1SVP; A1*0501/B1*0201) also deviates from the majority of MHC II structures in the 3_{10} helical region (Fig. 1.5). A comparative analysis of the differences between the HLA-DQ alleles as well as implications for the differences therein, are discussed in Appendix I.

HLA-DM

Human Leukocyte Antigen-DM (DM), H-2M in the mouse, is an MHC II-like alpha beta heterodimer that is structurally homologous to classical MHC II proteins (Fig. 1.8) (Mosyak, Zaller et al. 1998). The structure of DM revealed that it is comprised of two Ig membrane proximal domains, $\alpha l2/\beta 2$, and two membrane distal domains that contain two anti-parallel alpha helices that flank a beta sheet platform (Fremont, Crawford et al. 1998; Mosyak, Zaller et al. 1998). Although DM shares only 28% sequence identity with the MHC II allele, HLA-DR1, the structural similarities between the two molecules are striking. The crystal structure of DM has the same overall fold as DR1 with one obvious

FIGURE 1.7

31
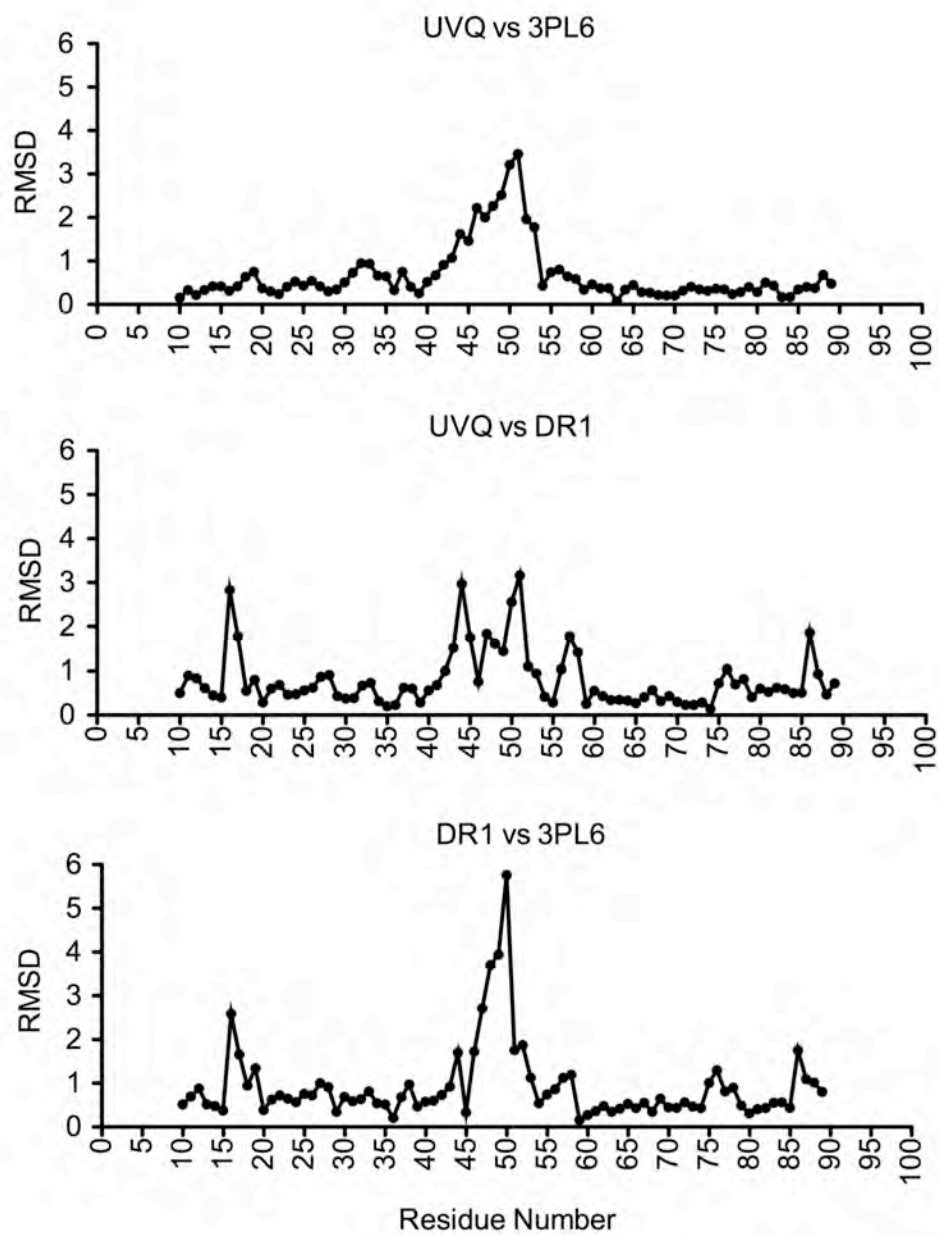
FIGURE 1.7. **The alpha 3_{10} helical region can adopt alternate conformations even in HLA-DQ alleles that contain the same alpha chain**. (top) LSQ alignment, between the HLA-DQ structures, 1UVQ and 3PL6 (both contain the same alpha chain), of the C-alpha atoms for residues in the 3_{10} alpha helix. (middle) The same alignment was performed for the HLA-DQ structure 1UVQ vs. the HLA-DR1 structure, 1DLH. (bottom) The same analysis is shown for the HLA-DR1 structure, 1DLH and the HLA-DQ structure 3PL6. In all cases, there is a deviation in RMSD in the 3_{10} helical region.

deviation, the region which constitutes the peptide binding domain of HLA-DR1 is partially collapsed, leaving only a vestigial P4 pocket, and is devoid of peptide (Fig 1.8) (Fremont, Crawford et al. 1998; Mosyak, Zaller et al. 1998)

HLA-DM is an endosomal resident that is necessary for proper antigen presentation by MCH II proteins (Morris, Shaman et al. 1994). As noted above, in the absence of DM, most MHC II remain occupied with CLIP indicating that the repertoire of peptides displayed at the cell surface requires the catalytic action of DM (Denzin, Robbins et al. 1994; Morris, Shaman et al. 1994). The individual crystal structures of DM and MHC II reveal no obvious docking site, although analysis of the DM structure did reveal a tryptophan rich hydrophobic cluster on one lateral face of DM that was proposed to be binding sites for either MHC II and/or HLA-DO, an inhibitor of DM catalyzed peptide exchange (Mosyak, Zaller et al. 1998). Several subsequent studies have aimed at identifying the DM-MHC II interface, as described below.

The mechanism through which DM mediates peptide catalysis remains to be elucidated. However, various functions of DM have been described. DM acts as a chaperone to protect peptide free MHC II from forming inactive aggregates (Stern and Wiley 1992; Denzin, Hammond et al. 1996; vogt, Moldenhauer et al. 1997). In addition, DM promotes peptide exchange from MHC II (Morris, Shaman et al. 1994; Vogt, Kropshofer et al. 1996; Weber, Evavold et al. 1996), and increases peptide binding to "empty" MHC II (Grotenbreg, Nicholson et al. 2007). Given the structural differences between

FIGURE 1.8
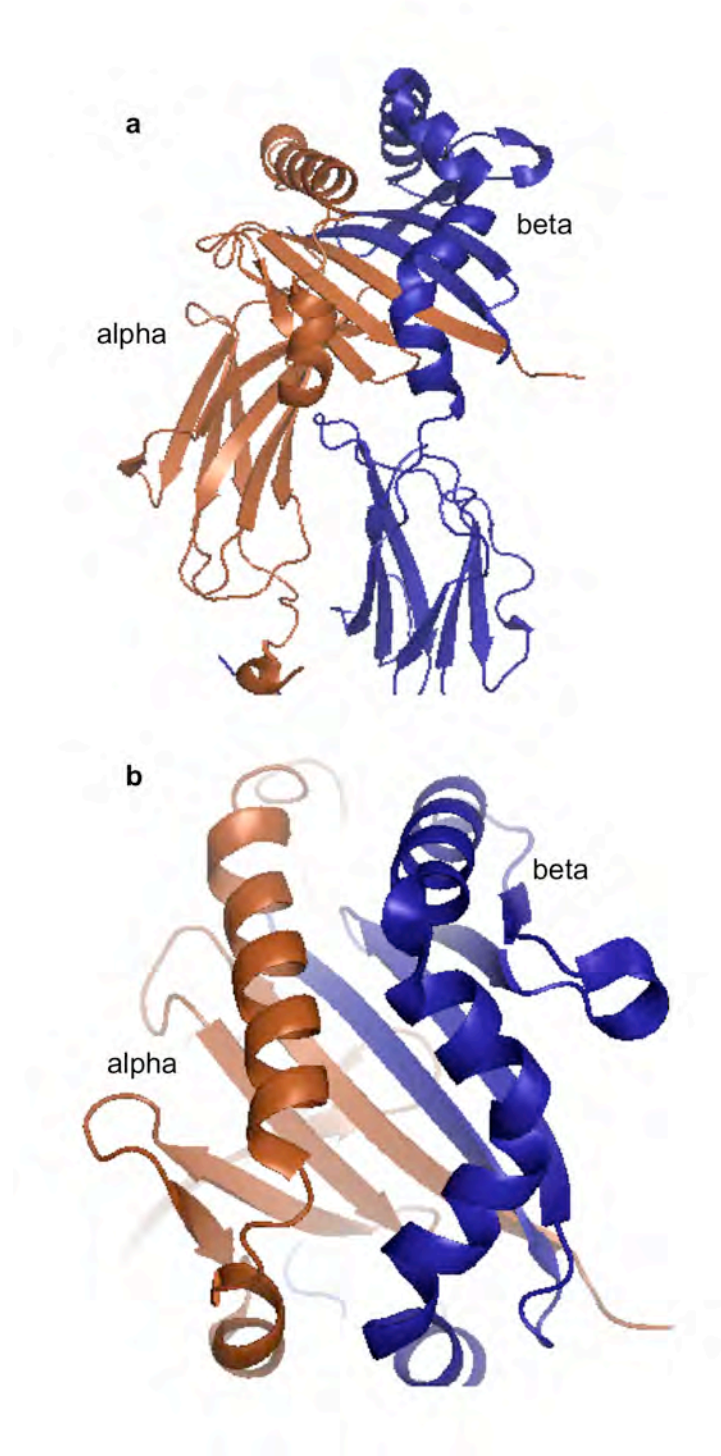
FIGURE 1.8. Crystal structure of HLA-DM. (a) Cartoon representation of HLA-DM (PDB ID# 2BC4). The alpha chain is shown in brown, the beta chain in blue. (b) 90° rotation showing the top of the closed groove that corresponds to the peptide binding groove in other MHC II proteins.

empty and loaded MHC II, and the roles for DM in promoting peptide exchange and stabilizing empty protein, one might expect that DM interacts specifically with particular conformations of MHC II.

.

Identification of the DM-MHC II interface

Given that there is no co-crystal of the DM-MHC II complex, nor structural information regarding the dynamic nature of this interaction, studies have focused on identification of key residues and regions involved in the DM-MHC II interaction in order to gain insight into the mechanism of peptide catalysis. Early work aimed at identifying interaction sites for DM on MCH II was presented by Doebele et al (Doebele, Busch et al. 2000), in which random mutagenesis of both chains of the MHC II allele, HLA-DR3, was performed in order to test which residues were important for the DM-MHC II interaction. Using a screening method for cell surface HLA-DR3 bound CLIP, in an DM deficient cell line, this group identified HLA-DR3 mutations that led to elevated cell surface expression of CLIP, and were therefore not able to undergo DM induced peptide exchange. The results implicated one lateral face of HLA-DR3, (Doebele, Busch et al. 2000) (Fig 1.9).

Looking at other regions of both MHC II and DM proteins, Weber et al investigated the role of the transmembrane and cytoplasmic domains of DM and MHC II which were determined to be of importance only in colocalization of

FIGURE 1.9

a

-N-terminal peptide H-bonds

-Alpha strand lability

-P1 pocket flexibility

-P1 pocket occupancy

alpha

beta

-Lateral face; leucine zippers, mutagenesis; tethered peptides

b

HLA-DM

alpha   beta

Putative Binding interface

HLA-DR

alpha   beta
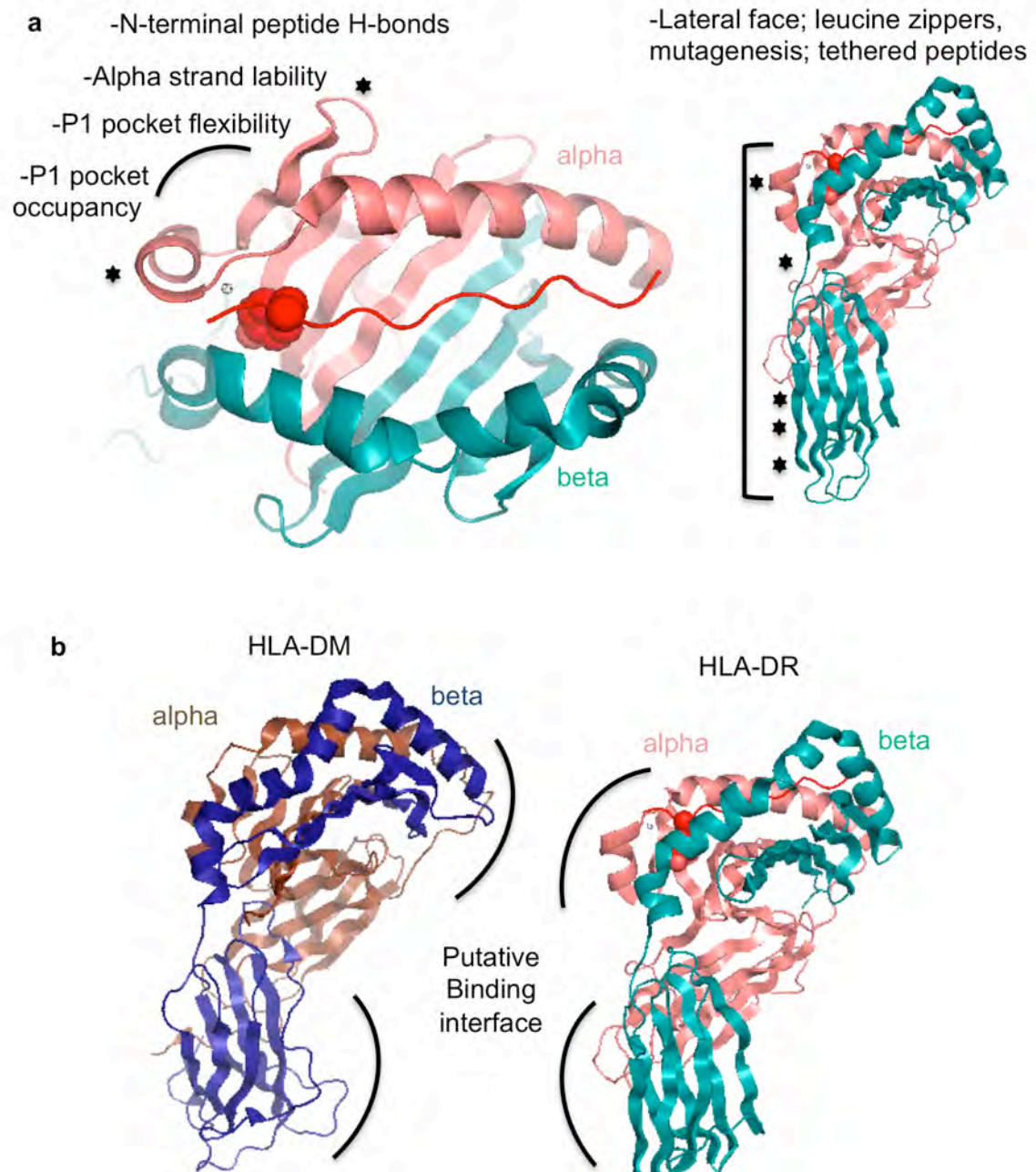
DM-MHC II interactions. (a left) Ribbon diagram of the top of the peptide binding domain of HLA-DR1 with the alpha chain in salmon, the beta chain in tela and the peptide in red. The P1 tyrosine of the peptide peptide in shown in spheres. Curve represents regions implicated in the DM-MHC II interaction, with brief descriptions noted. Stars represent residues found to be important in the DM-HLA-DR3 interaction. (a right) Side view of the HLA-DR1 peptide complex depicted on the left with residues important in the DM-HLA-DR3 interaction indicated as stars, bracket indicates the lateral face of HLA-DR thought to be at the interface with DM in the DM-MHC II complex. (b) Ribbon diagram depicting the putative DM HLA-DR binding interface

the two proteins within the same membrane, i.e. and not involved in the mechanism per se (Weber, Dao et al. 2001).

Due to the low affinity of soluble DM and MHC II (Busch, Reich et al. 1998), and the recent evidence that tethering to the membrane by both molecules was necessary for optimal DM mediated peptide catalysis, Busch et al (Busch, Pashine et al. 2002) devised a system whereby DM and HLA-DR could be tethered in parallel orientations that would differentially bring opposing lateral faces of the molecules in close proximity with each other (Busch, Pashine et al. 2002). This was accomplished by tethering leucine zippers to either alpha or beta chains of each protein with variable linker distances. This work further established that the lateral face implicated in earlier mutagenesis work to be at the interface between DM and MHC II. In addition, the orientation which leads to optimal DM mediated peptide catalysis suggested that the HLA-DR and DM beta chains were in closer proximity than either of the alpha chains (Fig. 1.9).

Further details regarding the orientation of DM and MHC II emerged from work carried out by Stratikos et al (Stratikos, Mosyak et al. 2002). This group tethered either the N- or C-termini of antigenic peptides to a free cysteine $\beta46$ on DM, and tested the ability of DM to "exchange" the tethered peptide on HLA-DR1. When the N-terminal peptide/DM complex was used, exchange rates were several orders of magnitude greater then when the C-terminal tethered peptide, or untethered peptide was used. This finding established the

N-terminal peptide binding region of the MHC II to be involved at the interface between these molecules, thus supporting work implicating this lateral face (Fig. 1.9).

Providing further information on the orientation of the DM-MHC II complex, another study used mutagenesis of DM residues to reveal that there was a lateral face on DM that contained residues important to the DM-MHC II interaction (Fig. 1.9) (Pashine, Busch et al. 2003). This work helped to unequivocally define the faces of DM and MHC II that were involved at the interface during peptide catalysis. However, taken together, the studies outlined here, establish only a low resolution structural model for the DM/ MHC II complex.

The P1 pocket MHC II has been implicated also as important in the DM-MHC II interaction. The flexibility of the P1 pocket has been postulated by Chou et al as a key structural determinant of DM susceptibility (Chou and Sadegh-Nasseri 2000). They proposed that when the P1 pocket is empty and/or flexible, DM can recognize the MHC II and induce a peptide receptive state. From this work, the flexibility rather then the stability of the complex was introduced as a determinant for DM action (Chou J. ex med 2000) (Fig. 1.9).

Using a panel of peptides that were unable to form various hydrogen bonds along the peptide backbone, Stratikos et al (Stratikos, Wiley et al. 2004) determined that hydrogen bonds that formed between the N-terminal region of the peptide and conserved residues of the MHC II, proximal to the P1 pocket,

were critical determinants of DM action. When these bonds were broken, DM catalysis of peptide release was augmented up to an order of magnitude (Stratikos, Wiley et al. 2004) (Fig. 1.9).

Recently, a new model has been proposed that suggests DM recognition of MHC II peptide complexes only occurs for MHC II that have a vacant P1 pocket as well as disrupted N-terminal hydrogen bonds (Anders, Call et al.). In this model, spontaneous protein motions in the N-terminal region of the peptide would eject the peptide from the P1 pocket, providing a novel MHC-pep complex that DM could recognize. Although this is the most recent model put forth for the mechanistic action of DM, by no means does it provide a complete understanding of the catalytic role of DM, which remains still unresolved.

The functional studies described above were limited to HLA-DR alleles, however there are conformational differences in regions of HLA-DQ alleles that lie at the presumptive DM-MHC II interface (Fig 1.5, Fig 1.9). It has been established that DM has different susceptibility for allelic variants of HLA-DR (Belmares, Busch et al. 2002), and there are hints that HLA-DQ structural differences may play a role in DM susceptibility (Fallang, Roh et al. 2008), however a thorough examination of HLA-DM susceptibility for non-HLA-DR MHC II proteins has not been fully explored and would be necessary for a comprehensive understanding into the nature of DM mediated peptide catalyses.

In summary, structural analysis of the individual molecules, mutagenesis studies, and biochemical characterization of the DM-MHC II interaction have elucidated key components of the DM-MHC II interaction, however, details that would enable a full understanding of the peptide exchange process remain elusive. In chapter III of this thesis, studies of an MHC II point mutant, αF54C HLA-DR1, show dramatic increases in DM susceptibility and affinity as well as a conformational change in the same regions as those seen in some of the HLA-DQ alleles (see appendix I). These studies have identified lability within the MHC II 3_{10} alpha helix and adjacent strand region as a key structural determinant for DM mediated peptide exchange.

CHAPTER II

MODEL FOR THE PEPTIDE-FREE CONFORMATION OF CLASS II MHC PROTEINS

Corrie A. Painter *[†], Anthony Cruz *[§], Gustavo E. López[§], Lawrence J. Stern [†‡‖],

Zarixia Zavala-Ruiz [§¶‖]

[†]Department of Biochemistry and Molecular Pharmacology, and [‡]Department of Pathology, University of Massachusetts Medical School, 55 Lake Ave North, Worcester, MA 01655; [§]Department of Chemistry, University of Puerto Rico, PO Box 00681, Mayagüez, 00681 [¶]Department of Chemistry, University of Puerto Rico, PO Box 23346, Río Piedras, PR 00931.

* These authors contributed equally to this work, Anthony Cruz performed the molecular dynamics simulations. I performed analysis on the simulation in addition to all the biochemical assays.

ABSTRACT

Major histocompatibility complex proteins are believed to undergo significant conformational changes concomitant with peptide binding, but structural characterization of these changes has remained elusive. Here we use molecular dynamics simulations and experimental probes of protein conformation to investigate the peptide-free state of class II MHC proteins. Upon computational removal of the bound peptide from HLA-DR1-peptide complex, the α50-59 region folded into the P1-P4 region of the peptide binding site, adopting the same conformation as a bound peptide. Strikingly, the structure of the hydrophobic P1 pocket is maintained by engagement of the side chain of Phe α54. In addition, conserved hydrogen bonds observed in crystal structures between the peptide backbone and numerous MHC side chains are maintained between the α51-55 region and the rest of the molecule. The model for the peptide-free conformation was evaluated using conformationally-sensitive antibody and superantigen probes predicted to show no change, moderate change, or dramatic changes in their interaction with peptide-free DR1 and peptide-loaded DR1. The binding observed for these probes is in agreement with the movements predicted by the model.

INTRODUCTION

Class II major histocompatibility complex (MHC) are heterodimeric proteins which bind antigenic peptides as part of the adaptive immune response to foreign pathogens. Upon binding peptides derived from endosomes or the extracellular milieu, the intact MHC II-peptide complex is displayed at the cell surface of antigen presenting cells (APC) for surveillance by CD4+ T-cells (Trombetta and Mellman 2005) Interaction between the APC and its cognate CD4+ T-cell leads to an effector response which then clears the body of the invading pathogen.

Peptides bind to the MHC II in an extended polyproline type II helix along a binding groove contributed to by both the alpha and beta subunits. Crystal studies of allelic variants bound to a variety of peptides has revealed a conserved hydrogen bonding network which exists between the peptide backbone and main chain residues along the helices of the alpha and beta binding domain (McFarland and Beeson 2002). Additionally, binding energy is created by the interaction of peptide side chains and pockets within the binding groove of the MHC II binding domain. Residues lining these pockets vary between alleles which thus lead to tremendous diversity within the peptide repertoire. Generally, these pockets accommodate residue side chains from the peptide at the P1, P4, P6 and P9 positions with smaller pockets or shelves in the binding site accommodating the P3 and P7 residues; these pockets are numbered along the peptide relative to a large usually hydrophobic pocket near the peptide binding

site. For HLA-DR1, DRB1*0101, (DR1), a common human class II MHC protein and the subject of this study, the P1 pocket shows a strong preference for large hydrophobic side chains (Trp, Tyr, Phe, Leu and Ile), the P6 pocket has a strong preference for smaller residues (Gly, Ala, Ser and Pro) and the P4 and P9 pockets have weaker preference for residues with some aliphatic character (Stern, Brown et al. 1994)

Although there is little structural variation observed among crystal structures determined for MHC II-peptide complexes, numerous studies have reported alternate conformations for particular MHC II-peptide complexes (Schmitt, Boniface et al. 1999; Kasson, Rabinowitz et al. 2000; Doebele, Pashine et al. 2003; Lovitch and Unanue 2005) and for peptide-free MHC II molecules (Zarutskie, Sato et al. 1999; Hansen, Lybarger et al. 2005). Peptide-free DR1 has been shown to have a larger hydrodynamic radius than the peptide loaded form (29 vs 35 Å), as well as a decrease in helicity as measured by circular dichroism (Zarutskie, Sato et al. 1999; Sato, Zarutskie et al. 2000). These differences are reversed upon binding peptide. Peptide binding and dissociation experiments have shown that peptide-free MHC II can adopt two interconverting forms, one receptive to and one averse to peptide loading (Rabinowitz, Vrljic et al. 1998; Natarajan, Assadi et al. 1999; Joshi, Zarutskie et al. 2000). The receptive state is able to bind peptide rapidly, but will convert to the peptide averse form within minutes if not stabilized by peptide or by association with the chaperone HLA-DM (DM). It has been proposed that DM mediates its function by shifting the

equilibrium of peptide averse to a peptide receptive state; however, the peptide loading process is still relatively undefined (Zarutskie, Busch et al. 2001; Grotenbreg, Nicholson et al. 2007). In order to gain a better understanding of this process, it is necessary to develop a more detailed understanding into the structural changes that exist based on peptide occupancy.

Previous work using conformationally sensitive monoclonal antibodies raised against the β chain of DR1 has revealed that a noncontiguous epitope in the peptide binding region (residues β53-67) and another in the lower Ig-like domain (residues β186-189) are accessible only in the peptide-free conformation (Carven, Chitta et al. 2004). Another study which used differential chemical modification found residues α50, 67, β98,189 were selectively modified in peptide-free but not peptide-loaded DR1 (Carven and Stern 2005). Although these studies helped to define regions within the structure that change upon the peptide occupancy state, there is not enough information to generate a working model of the peptide-free DR1. Molecular dynamics simulations have been used to gain insight into conformational changes relative to an experimentally defined structure (Zheng, Brooks et al. 2007; Laberge and Yonetani 2008). Combined with experimental support, models developed from this method can be substantiated. In this study, we performed molecular dynamics simulation of DR1 in both the peptide-free and peptide-loaded states. Several regions of DR1 were predicted by this analysis to change conformation substantially upon loss of bound peptide. Differential binding of conformationally-specific antibody and

superantigen probes to the peptide-free and peptide-loaded forms of DR1 provides experimental support for this model.

RESULTS

Modeling the structure of the peptide-free form of HLA-DR1 by molecular dynamics

A model for the peptide-free structure of DR1 was obtained by molecular dynamics simulation starting from the X-ray coordinates of a DR1-peptide complex (PDB Code: 1SJE, (Zavala-Ruiz, Strug et al. 2004)) from which peptide was removed before the start of the simulation. A parallel simulation was started from the same coordinates but without the removal of peptide. Simulations were carried out in a water-filled box at constant temperature and pressure using the GROMOS force field (Berdensen 1995) and 2 fs time steps. During the simulation, the total root mean square deviation, RMSD, from the starting coordinates was followed in various regions of the protein, Fig. 2.1a-1c. Large changes in RMSD were observed over the first 5-10ns, particularly in the a1b1 peptide binding domain and the lower b2 immunoglobulin-like domain, with much smaller fluctuations occurring thereafter. The models were investigated in detail at the 10ns time point, as described below.

RMS fluctuations during the first 10ns of the peptide-loaded and peptide-free simulations are shown in Fig. 2.1d and e as a function of residue number. A trajectory of the simulation is depicted in Fig. 2.1f for the peptide-free and in

FIGURE 2.1
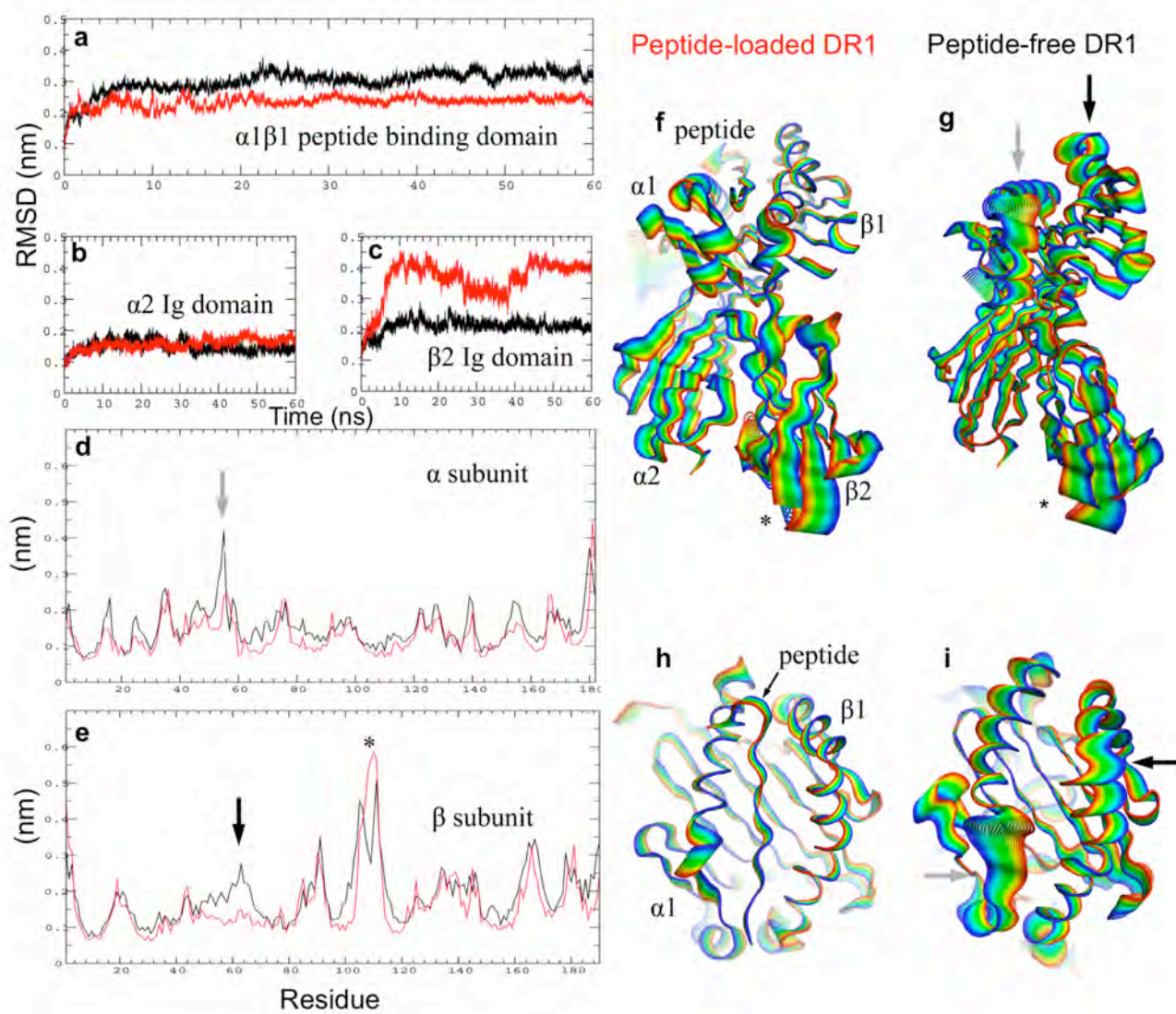
FIGURE 2.1 Molecular dynamics simulation of peptide-bound and peptide-free DR1. (a-c) RMS deviation over time for the peptide-loaded (red) and peptide-free (black) simulations, for the a1b1 peptide-binding domain (a), the Ig-like α2 domain (b), and the Ig-like β2 domain (c). (d-e) Root mean square (RMS) fluctuation during the simulation for each residue (all atoms included) for the α (d) and β (e) subunits. (f-i) Molecular dynamic trajectories for the peptide-loaded (f,h) and peptide-free (g,i) form of DR1. Initial states shown in blue, final states shown in red, with a linear interpolation of conformations between the initial and final structures shown in other colors. (f,g), Side view of entire protein, (h,i)Top view of peptide binding site only.

Fig. 2.1 g for the peptide-loaded dynamics runs. Panels h and i show a different view highlighting the peptide binding region. In the peptide-binding site, significant movements can be seen in the α-helices of the peptide-free form, as compared to those of the peptide-loaded form, which do not fluctuate or move as much. In the α subunit, the principle differences between the peptide-loaded and peptide-free simulations were in the region α34-60 (light arrows). This region, part of the peptide binding domain, corresponds to the last two strands of the beta sheet "floor" and the first half of the helical region forming one side of the peptide binding site. In the β subunit the largest RMS fluctuations were in the lower β2 immuoglobulin domain, residues β90 – 110, and were observed in both peptide-loaded and peptide-free simulations (Fig. 2.1c and e, asterisk). Different orientations of the β2 domain relative to the peptide binding domain already have been observed in different HLA-DR1 crystal structures, reflecting orientational flexibility in this domain (Fig. 2.2). Elsewhere in the β-subunit, large RMS fluctuations were observed for the region β50-70 in the peptide binding site. In this region larger deviations were observed in the peptide-free as compared to the peptide-loaded simulation (Fig. 2.1f-i). A difference distance matrix plot (Schneider 2000) calculated at 10ns highlights the regions that are different in this simulated peptide-loaded and peptide-free forms (Fig. 2.3).

FIGURE 2.2

Model	PDB ID	chain
1	1DLH	AB
2	1DLH	DE
3	1AQD	AB
4	1AQD	DE
5	1AQD	GH
6	1AQD	JK
7	1T5W	AB
8	1T5W	DE
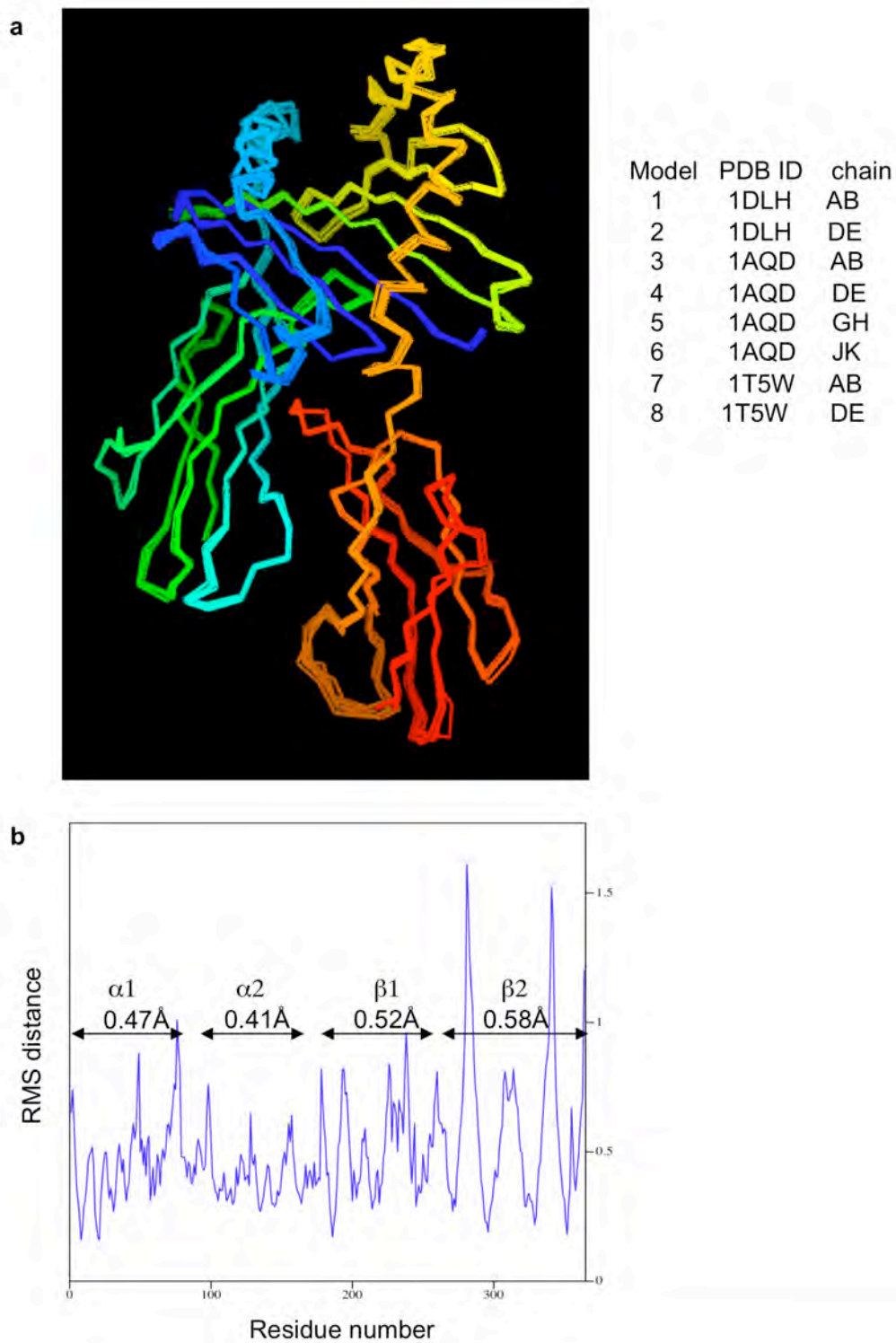
FIGURE 2.2. Conformational variation in DR1 crystal structures. (a) Overlay of crystallographically distinct αβ heterodimers from three crystal structures reported for DR1-peptide complexes solved in the absence of a protein that helps DR1 crystallize, superantigen. (b) RMS Cα distances for aligned αβ ˋheterodimers, with mean RMS in each domain indicated. Structures aligned using LSQMAN

FIGURE 2.3
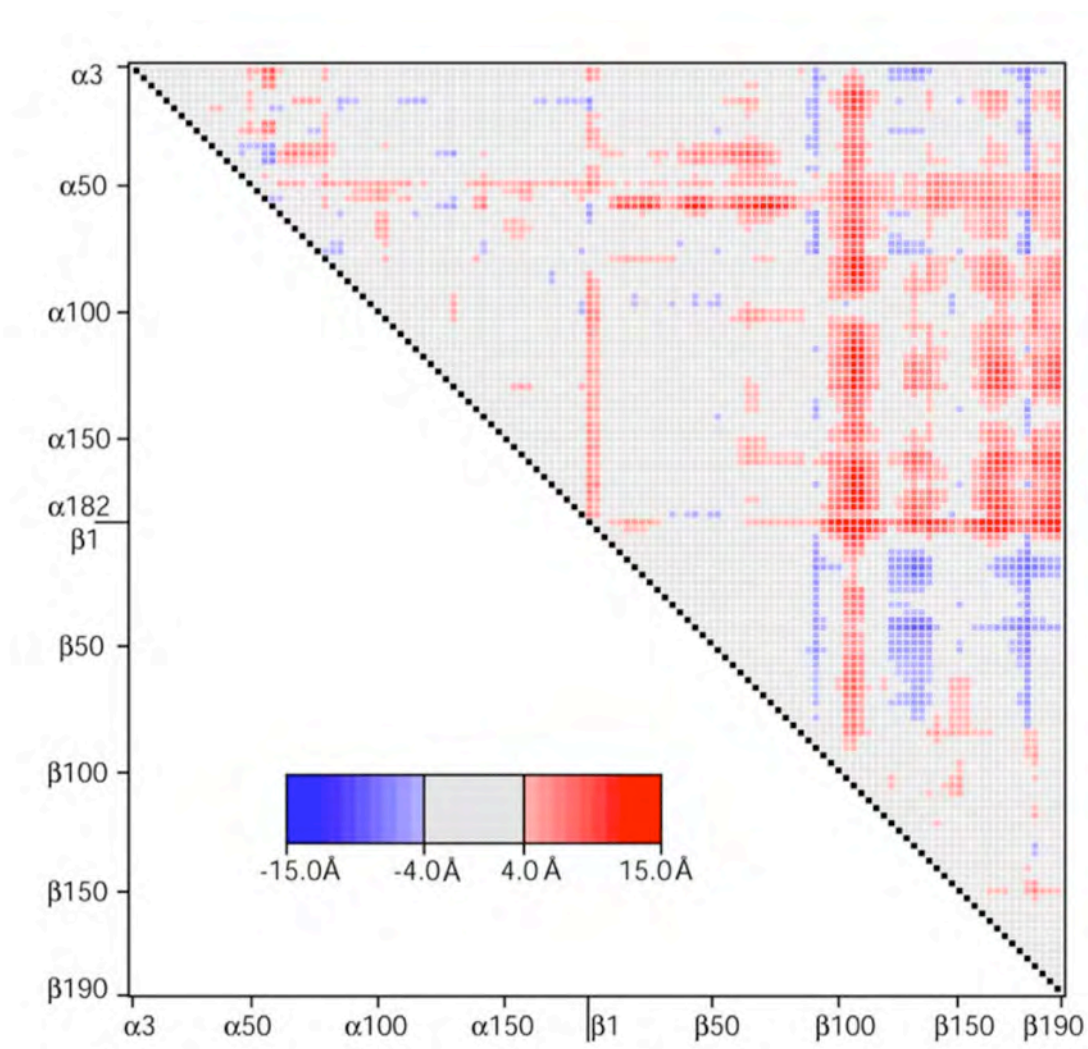
FIGURE 2.3. **Difference distance matrix between the peptide-loaded and peptide-free conformations of HLA-DR1.** The blue squares show areas in the protein that move away from each other in the peptide-free model when compared to the peptide-loaded conformation, with stronger blue intensity for the areas that are the further apart (15Å difference) and lighter blue for the areas that move away but not as much (4Å difference). The red squares show regions on the peptide-free form that move closer to other regions in the protein when compared to peptide-loaded HLA-DR1; intense red color are areas that move more. The gray squares are regions that do not change as much (0-3.99 Å).

Motion of the α50-59 region into the amino-terminal end of the peptide binding

site

The major conformational alteration observed during the simulations is a

narrowing of the N-terminal region of the peptide-binding site (Fig. 2.4 a). This

narrowing of the site occurred early during the dynamics simulations run in the

absence of peptide, and persisted throughout the entire 60ns time course. Such

narrowing was not observed during dynamics simulations of the peptide-loaded

form (Fig. 2.4 b), although at late time points (>15ns) the peptide-loaded

simulation occasionally sampled conformations having some characteristics of

the peptide-free form (not shown). In the model of the peptide-free form of DR1

derived by molecular dynamics simulation, the peptide binding site is dramatically

altered as compared to the highly stereotyped conformation observed in crystal

structures of the peptide-bound form. During the simulation, the α50-59 region of

DR1 moves to fill the amino-terminal end of the peptide-binding site occupying, in

part, the area where the antigenic peptide is usually found (Fig. 2.5).   The

amino-terminal region of the peptide-binding site of DR1 was previously

suggested to be more flexible upon peptide-removal in a normal mode analysis

(Nojima, Takeda-Shitaka et al. 2003) as well as in another molecular dynamics

calculation (Gupta, Hopner et al. 2008). In our model, a sharp kink forms at Gly

α58, allowing the region α50-59 to fold into the binding site, taking the place of

the bound peptide in the P1 to P4 region. Smaller changes but still significant

FIGURE 2.4
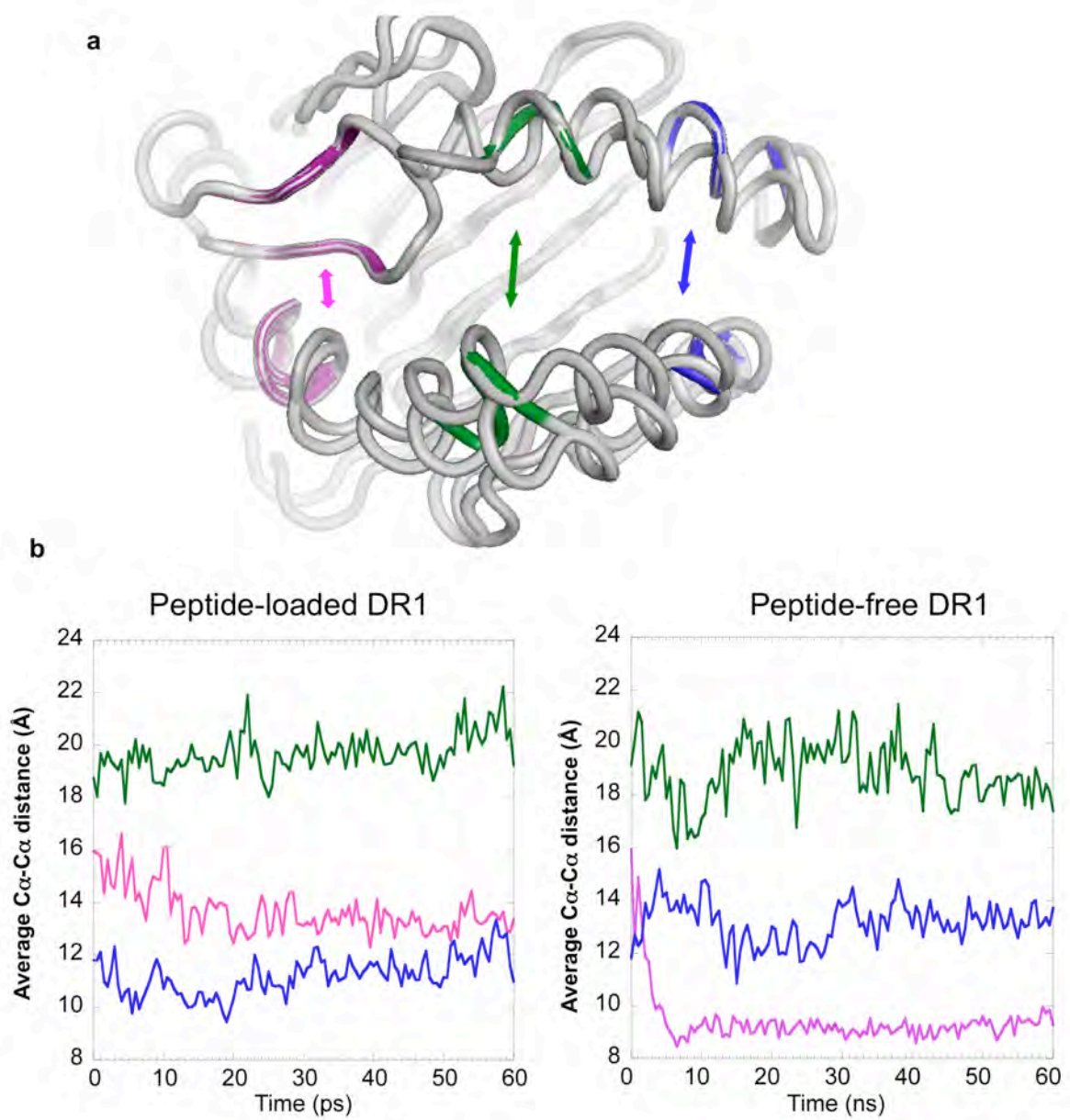
FIGURE 2.4 Motion of α50-59 into the peptide binding site during molecular dynamics in the absence of peptide (a), Ribbon diagram of peptide-free DR1 before and after molecular dynamics simulations, showing residues at N-terminal end (magenta, α52-57 and β79-83), central region (green, α62-66 and β65-69), or C-terminal end (blue, α71-75 and β58-62) of peptide binding site, used to calculate distances across the binding site (indicated by arrows). (b) Changes during molecular dynamics simulation of distances across the peptide binding site at three different locations, colored as indicated in panel (a).

FIGURE 2.5
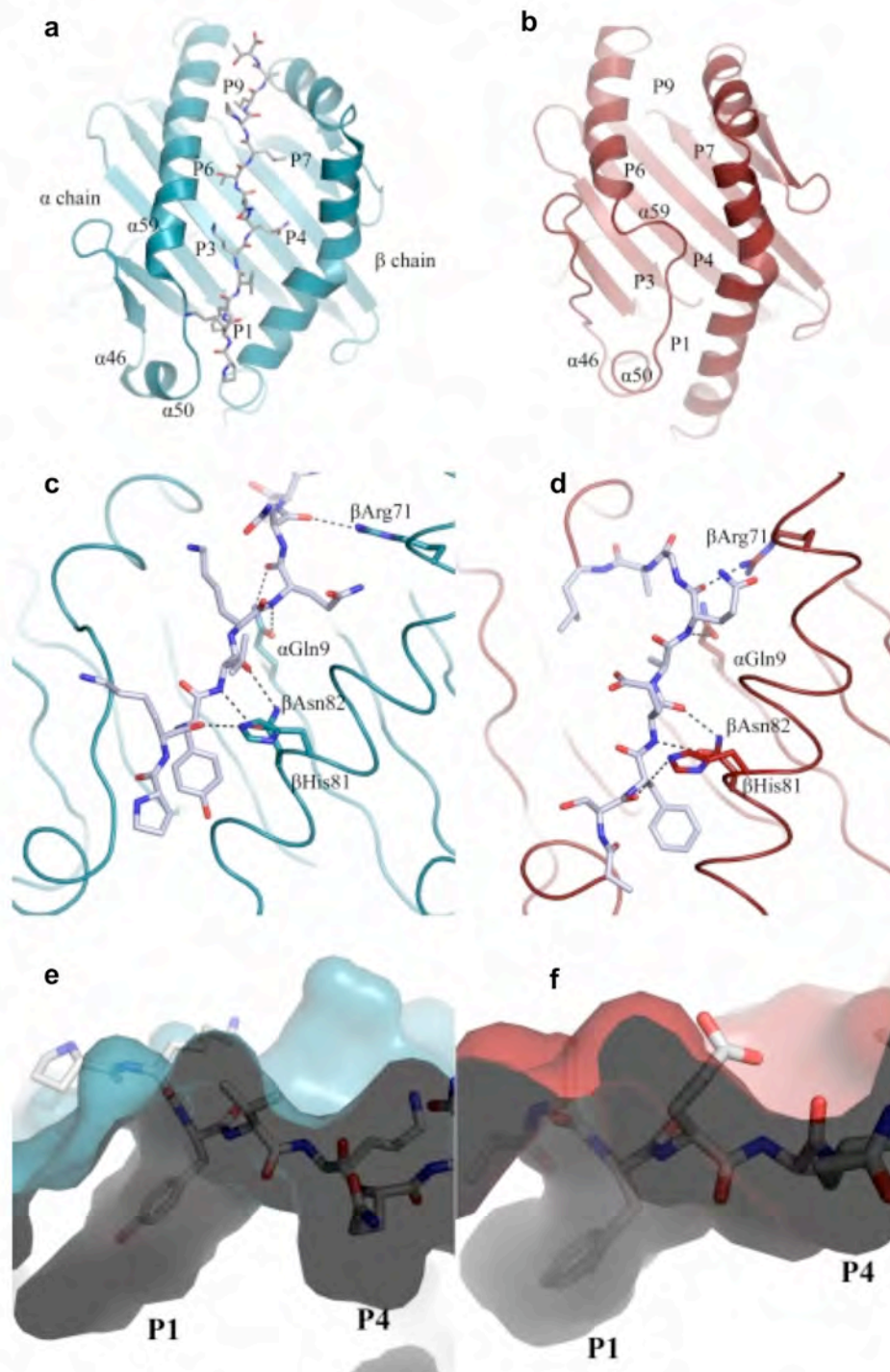
FIGURE 2.5 Molecular dynamics model of peptide free HLA-DR1 (a) Ribbon

diagram of DR1 (blue) bound to the HA-peptide. The peptide is shown as stick

with carbon atoms in white; and nitrogen and oxygen atoms in blue and red,

respectively. Pocket locations within the peptide-binding site are labeled. (b)

Ribbon diagram of the peptide-free HLA-DR1 (red). (c,d), hydrogen-bonding

interactions for the peptide-loaded (c) and peptide-free (d) proteins. (e,f) Surface

side-view of the N-terminal region of the peptide-binding site for the peptide-

loaded (e) and peptide-free (f) proteins. In (d and f), α50-59 of the peptide-free

form is shown in stick representation as for the HA peptide. Figures were

generated using PyMol.

changes are observed in the helical regions that flank α50-59, in the adjacent

α46-49 loop, and in beta subunit helical regions (compare Fig. 2.5 a and b).

After moving into the peptide-binding site, the main chain of the α50-59

region is able to satisfy essentially all of the hydrogen bonds in this region lost

upon removal of the peptide. In the conserved arrangement observed in class II

MHC-peptide crystal structures, the backbone of a bound antigenic peptide forms

six hydrogen bonds with the side chains of non-polymorphic DR1 residues Gln

α9, Arg β71, His β81 and Asn β82 (Fig. 2.5 c). In the molecular dynamics model

of the peptide-free form of DR1, each of these hydrogen-bonding interactions is

observed, by direct hydrogen bonding between the main chain atoms of DR1

α53-57 and side chains of Gln α9, Arg β71, His β81 and Asn β82 (Fig. 2.5 d).

Movement of the α50-59 region into the peptide binding site also results in

occupancy of the P1-P4 side-chain binding pockets. These pockets line the

peptide binding site, and accommodate side chains of the bound peptide. The

P1 pocket of DR1 is the major determinant of peptide binding, and usually

accommodates a large hydrophobic side chain (Sato, Zarutskie et al. 2000). In

the molecular dynamics model of the peptide-free form of DR1, the side chain of

Phe α54 binds into the P1 pocket, in the same orientation as observed for an

aromatic P1 residue from a crystal structure of peptide-loaded DR1 complexes

(Fig. 2.5e and f).   The P4 pocket is shallower than the P1 pocket and open at

the end, and in DR1 exhibits a weaker preference for residues with some

aliphatic character. In the molecular dynamics model of the peptide-free form of

DR1, the side chain of Gln α57 binds into the P4 pocket, essentially identically to Gln at the corresponding position in a bound peptide.

Experimental probes of conformational differences between peptide-free and peptide-loaded HLA-DR1

We attempted to evaluate whether or not the striking alterations predicted by the molecular dynamics simulations corresponded to actual conformational differences between peptide-free and peptide loaded proteins, using conformation-specific superantigen and antibody probes of DR1 structure. Superantigens are soluble bacterial toxins that bind to class II MHC proteins and T cell receptors, causing polyclonal T cell activation independent of peptide antigen (Sundberg, Deng et al. 2007). Superantigen binding sites on the DR alpha subunit have been determined by X-ray crystallography of superantigen-MHC-peptide complexes (Sundberg, Andersen et al. 2003), but superantigen binding to peptide-free DR1 has not been described. Conformation-specific antibody probe of DR1 structure also are available, although the binding sites have been characterized only by domain-swap or mutagenesis experiments. In general, most of these antibodies bind to both peptide-free and peptide-loaded DR1 (Stern and Wiley 1992). MEM-264 and the related MEM-265, MEM-266, and MEM-267 antibodies (Carven, Chitta et al. 2004) are exceptions to this pattern, in they preferentially bind to peptide-free DR1 (Carven, Chitta et al. 2004). Although differential binding to peptide-free and peptide-loaded DR1 has

been described for these antibodies, there has not been a quantitative

comparison. Finally, LB3.1, a commonly used anti-DR antibody, also has been

reported to exhibit differences in reactivity with peptide-free and peptide-loaded

DR1 (Carven, Chitta et al. 2004), although again a quantitative analysis has not

been reported. To evaluate in a quantitative manner the differential binding of

these conformationally-specific superantigen and antibody probes, we used

surface plasmon resonance (SPR) to characterize their binding to peptide-free

and peptide-loaded DR1 prepared by refolding purified DR1 alpha and beta

subunits in the absence or presence of peptide (see Methods). As previously

observed (Zarutskie, Sato et al. 1999), the peptide-free and peptide-loaded

preparations exhibited characteristic differences in hydrodynamic radius and

stability to SDS-induced subunit dissociation (Frayser, Sato et al. 1999) (Fig.

2.6).

Staphylococcal Enterotoxin C3 (SEC3) The interaction of the bacterial

superantigen SEC3, a tight-binding derivative of staphylococcal enterotoxin C3

(SEC3), with peptide loaded DR1 has been characterized previously by X-ray

crystallography and SPR experiments (Anderson and Gorski 2003) Contact

residues between SEC3 and peptide-loaded DR1 have been mapped by

crystallography and by mutagenesis, and include Tyr13, Asp17, Gln18, Met36,

Ala37, Leu60, Ile63, Ala64, and Lys67 on the α chain (Sundberg, Andersen et al.

2003). None of these residues move appreciably during molecular dynamics

simulation of the empty protein. To evaluate this experimentally, peptide-free and

FIGURE 2.6

a
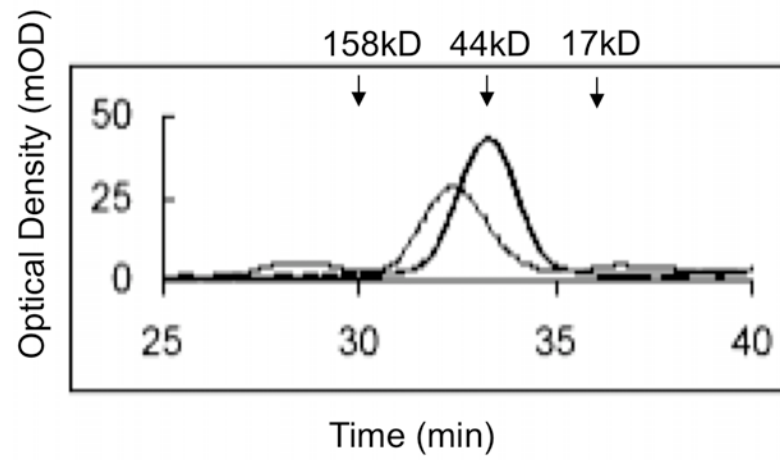
b
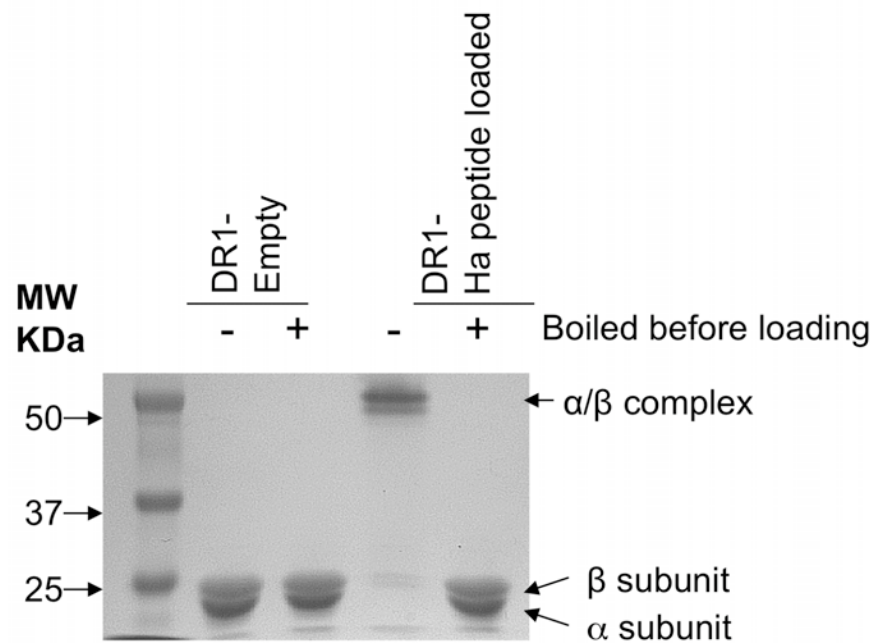
FIGURE 2.6 Characterization of peptide loaded and peptide-free DR1. (a)

analysis of peptide-free DR1 and peptide-loaded DR1 by gel filtration (Superdex

200). Peptide-free DR1 (dotted line) has a larger hydrodynamic radius than the

peptide-loaded DR1(solid line). Arrows indicate position and molecular weight of

standard proteins. X axis represents time in minutes, Y axis represents optical

density (milli Au). (b) 12% SDS-PAGE analysis of peptide-free DR1 and peptide-

loaded DR1. Peptide-free DR1 dissociates into alpha and beta subunits in SDS

whereas peptide-loaded DR1 is resistant to SDS dissociation until boiled.

peptide-loaded DR1 were immobilized to a streptavidin-dextran surface using a C-terminal biotin (Cochran and Stern 2000) and binding to varying concentrations of soluble SEC3 was followed by SPR. Essentially identical SEC3 binding behavior was observed for peptide-free and peptide-loaded DR1 (Figure 2.7 a-c). SPR data were fit to a kinetic model, yielding apparent K_D values for peptide-free and peptide-loaded DR1 of 14 µM and 11 µM, respectively. Equilibrium analysis of these same data yielded apparent K_D values of 6.1 and 8 µM. These values are similar to a previously reported K_D value for peptide-loaded DR1 binding to SEC3, 4.6 µM (Andersen, Lavoie et al. 1999) To confirm these results, we performed this experiment in the opposite orientation, with SEC3 immobilized via standard amine coupling and with peptide-free or peptide-loaded DR1 in the mobile phase. Again, we obtained similar K_D values for peptide loaded and peptide-free DR1 6.0 and 6.1 µM, respectively (Table 2.1). Overall these data demonstrate that SEC3 binding does not distinguish between peptide-loaded and peptide-free DR1. Because this epitope is not predicted to move upon release of peptide, these observations are consistent with the model.

Monoclonal antibody MEM-264 MEM-264 is a monoclonal antibody that previously has been shown to bind specifically to the peptide-free conformation of DR1 (Carven, Chitta et al. 2004).The MEM-264 epitope has been mapped by overlapping peptides and alanine scanning mutagenesis, and corresponds to a discontinuous region on the β subunit helical region including residues 53-67 (Carven, Chitta et al. 2004). In the molecular dynamics model for peptide-free

FIGURE 2.7
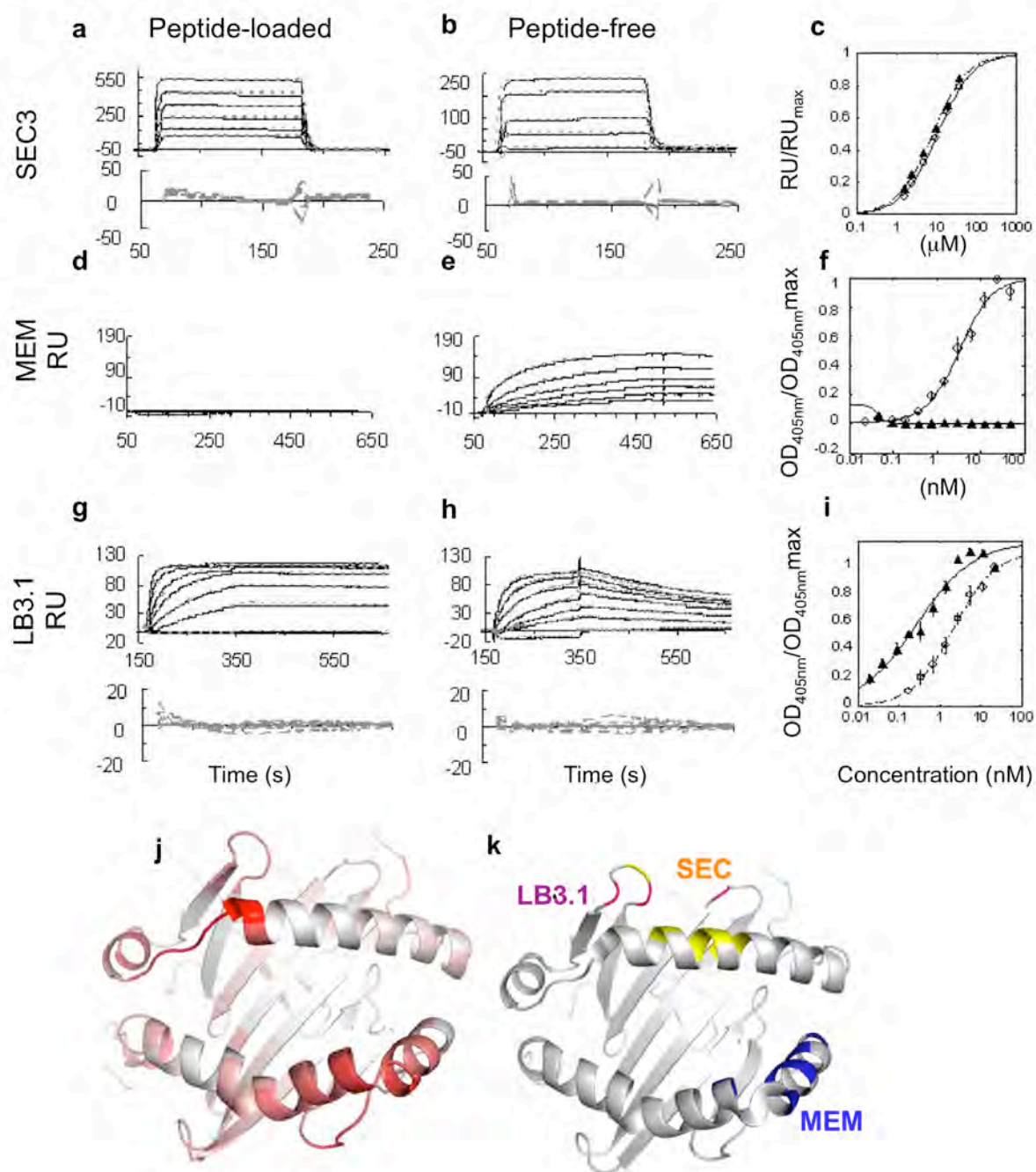
FIGURE 2.7 Binding of peptide-loaded and peptide-free DR1 to conformationally sensitive probes. (a-c) SEC3 binding to immobilized bio_DR. (a) SPR using peptide-loaded DR1. b) SPR using peptide-free DR1. Residuals shown below SPR traces (c) Equilibrium RU values vs. DR concentration, open circles, peptide-free DR1, closed triangles, peptide-loaded DR1. (d-f) DR1 binding to immobilized MEM264. (d) SPR using peptide-loaded DR1. (e) SPR using peptide-free DR1. (f) ELISA of MEM264 binding empty, open circles, and loaded, closed triangles, DR1. (g-i) DR1 binding to immobilized LB3.1. (g) SPR using peptide-loaded DR1. (h) SPR using peptide-free DR1.Residuals shown below. (i) ELISA of immobilized LB3.1 binding to peptide-free (open circles) and peptide-loaded (closed triangles) DR1. (j-k) Comparison of experimental to model data**.** (j) Ribbon diagram of the peptide-binding site of DR1, colored by peptide-free to peptide-loaded $C\alpha$ distances at the end of the dynamics runs. Larger distances shown in darker red. (k) same view but colored to indicate sites of conformational probe interaction: The yellow region represents DR1 residues that interact with the superantigen SEC3, magenta resides that interact with the conformationally sensitive antibody LB3.1, and blue residues in the peptide-free protein that interact with the antibody MEM264 specific for the peptide-free protein.

DR1, this entire region is predicted to move significantly relative to the rest of the β subunit. We performed a SPR binding analysis with immobilized MEM-264 and either peptide-free or loaded DR1 in the mobile phase (Fig. 2.7 d and e). We found robust binding to immobilized MEM-264 for peptide-free DR1, with an apparent K_D of approximately 24 nM. Peptide-loaded DR1 did not bind to MEM-264 at concentrations up to 2µM. In addition, we compared binding of peptide-free and peptide-loaded DR1 using an equilibrium sandwich ELISA assay (Fig. 2.7 e). Half maximal binding of peptide-free DR1 to MEM-264 was observed at 5.3 nM, whereas no binding was observed for peptide-loaded DR1 at concentrations up to 2mM. Overall these data suggest that peptide-loaded DR1 binds to MEM-264 at least 400-fold more weakly than does peptide-free DR1.

<u>Monoclonal antibody LB3.1</u> LB3.1 is a conformationally sensitive monoclonal antibody which has three residues known to be important in the binding interaction, all in the loop region proximal to the α50-59 strand (Fu and Karr 1994). During the simulation, Gln α18 does not move appreciably, Met α36 moves ~5Å but similarly in the peptide-loaded and peptide-free models, and Lys α39 moves and packs differently against the alpha-subunit helix in the peptide-free and peptide-loaded models. Of these, Gln α18 and Met α36 also are in the SEC3 epitope. Differential binding of LB3.1 to peptide-free and peptide-loaded DR1 has been observed previously (Carven, Chitta et al. 2004) but not quantified. We used SPR and ELISA to quantify differences in LB3.1 binding to peptide-free and peptide-loaded DR1. SPR analysis using immobilized LB3.1

and serial dilutions of peptide-loaded and peptide-free DR1 indicated a significant difference in binding kinetics (Fig 2.7 g and h), with tighter binding of the peptide-loaded form. Kinetic analysis revealed apparent K_D values of 76nM for peptide-loaded DR1 and 2.3nM for peptide-free DR1.   We used ELISA to evaluate the binding interaction under equilibrium conditions (Fig. 2.7 i). Once again, tighter binding of LB3.1 to the peptide-loaded form was observed, with half-maximal binding observed at 0.47 nM and 2.1 nM for the peptide-loaded and peptide-free species respectively (Table 2.1). Overall, these experiments confirm that peptide-free and peptide-loaded DR1 have distinct binding affinities for LB3.1.

DISCUSSION

Previous work has shown that peptide-free and peptide-loaded forms of DR1 have different physical characteristics, including hydrodynamic radius, chemical and thermal stability, and far-UV CD and near-UV fluorescence spectra (Zarutskie, Sato et al. 1999). In general, these changes can be induced by binding a wide variety of peptides regardless of length, affinity, or sequence characteristics, provided that the P1 site is occupied (Chou and Sadegh-Nasseri 2000; Sato, Zarutskie et al. 2000).These observations support the notion that there are conformationally distinct forms of the protein based on peptide occupancy (Sadegh-Nasseri, Stern et al. 1994; Boniface, Lyons et al. 1996; Runnels, Moore et al. 1996; Rabinowitz, Vrljic et al. 1998; Natarajan, Assadi et al. 1999; Zarutskie, Sato et al. 1999). Our goal in this work was to gain insight

into structural changes that can occur in the absence of bound peptide. Because conditions for crystallization of peptide-free DR1 have yet to be determined, it is necessary to approach structural questions by alternative methods. Using molecular dynamics in conjunction with experimental data can help to elucidate particular structural events that might otherwise remain obscure.

Two important features of the interaction of peptides with class II MHC proteins have been identified: hydrogen bonds between conserved MHC residues and the peptide main chain amides, and binding of several peptide side chains into pockets in the MHC peptide binding site (McFarland and Beeson 2002). Hydrogen bonding interactions involving the peptide N-terminal region in general appear to be more important than those involving the C-terminal region (McFarland and Beeson 2002), and for DR1 variants the P1 pocket dominates the overall peptide binding behavior (Sato, Zarutskie et al. 2000). In the molecular dynamics model for the peptide-free form of DR1, the key hydrophobic P1 pocket becomes engaged by Phe α54, and the secondary pocket P4 by Gln α57. Conserved MHC hydrogen bonding residues along the peptide binding groove become engaged by the α50-59 loop region. By the end of the simulation, the peptide-free DR1 has satisfied all of the N-terminal binding interactions that were lost by initial removal of the peptide in a manner consistent with the original bonds made by the peptide-DR1 interaction.

We used conformationally-dependent antibody and superantigen probes in order evaluate the concordance of the model with experimental data. Overall,

there is good agreement between the predicted MHC backbone movement and the degree to which the probes are sensitive to the presence or absence of peptide (Fig. 2.7 j and k). The SEC3 epitope is predicted to remain stationary, and our data show no significant differences in binding to peptide-loaded and peptide-free DR1. The MEM264 epitope overlaps with an area in the peptide binding region predicted to undergo a large global movement upon peptide release, and previous results (Carven, Chitta et al. 2004) and those shown here demonstrate a dramatic difference in the reactivity of this antibody for peptide-loaded and peptide-free DR1. The LB3.1 epitope has not been comprehensively mapped, although a few residues within the epitope have been identified using DR-IE (human-mouse) chimeric molecules (Fu and Karr 1994). Residues Gln α18 and Met α36 are also included in the SEC3 epitope, but Lys α39 is unique to the LB3.1 epitope. This residue undergoes a rigid body as well as a side chain reorientation movement in the model. Partial shielding of the residue could account for the observed difference in LB3.1 binding to peptide-free and peptide-loaded DR1, although it is possible that other residues not yet identified contribute to LB3.1 binding. Overall, the observed binding to peptide-free and peptide-loaded DR1 for each of the conformational probes that we tested was consistent with predictions from the molecular dynamics models for the peptide-free protein. While this concordance indicates that molecular dynamics may provide a useful model for the peptide-free conformation, none of the available

conformational probes directly addresses the key prediction of motion of α50-59 into the peptide binding site, which remains to be validated experimentally.

Peptide-free DR1 has been shown to exist in at least two kinetically defined states, peptide receptive and peptide averse (Rabinowitz, Vrljic et al. 1998; Natarajan, Assadi et al. 1999; Joshi, Zarutskie et al. 2000; Sato, Zarutskie et al. 2000). The peptide receptive form is observed immediately after release of a bound peptide, and is characterized by rapid binding of added peptide. In the absence of peptide, the peptide-receptive form converts to the peptide-averse form, with $t_{1/2} \sim$ min (Rabinowitz, Vrljic et al. 1998). The peptide-averse form binds peptide much more slowly, in a process that requires a slow unimolecular conformational change (Joshi, Zarutskie et al. 2000). The predicted conformational change in the peptide-free model could account for the peptide averse form of DR1. It is plausible that upon peptide release, the binding groove is not obstructed and therefore could bind subsequent peptide directly, whereas once the peptide binding groove is engaged by the α50-59 region, the protein would be in the peptide-averse form, and would have to undergo a conformational change in order to allow space for the peptide to enter the binding groove.

In addition to catalyzing peptide binding and release, the peptide exchange factor HLA-DM has also been shown to stabilize the peptide-receptive form of MHC II and to prevent conversion to the inactive form (Pierre, Denzin et al. 1996; Kropshofer, Arndt et al. 1997; Zarutskie, Busch et al. 2001; Grotenbreg,

Nicholson et al. 2007). A key residue in the interaction with DM and DR1 is DR1 Phe α51. When Phe α51 is mutated to Val or Ser the catalytic ability of DM is abolished (Doebele, Busch et al. 2000). Interpreting this result in light of the dynamics model, interaction of DM with this residue could prevent the α50-59 region from engaging the peptide binding groove, inhibiting formation of the averse form. Interestingly, occlusion of the P1 pocket of DR1 by Glyβ86Tyr also has been reported to abolish DM activity (Chou and Sadegh-Nasseri 2000; Narayan, Chou et al. 2007). Such a mutation might prevent α50-59 closing into the peptide binding site, and in fact reduced formation of a peptide-averse state has been reported for this mutant (Chou and Sadegh-Nasseri 2000; Narayan, Chou et al. 2007).

The structures of class I and class II MHC proteins are similar, despite having different domain/subunit organizations and different modes of peptide binding (Brown, Jardetzky et al. 1993). The α50-59 region, proposed herein to occupy the HLA-DR peptide binding site in the absence of peptide, represents a prominent difference between the structures of class I and class II MHC proteins (Brown, Jardetzky et al. 1993). In class I MHC proteins, the α1 helix continues unbroken through this region, extending from residue 56 (equivalent to HLA-DR α52) to residue 86 (equivalent to HLA-DR α78), whereas in class II MHC proteins, this region is an extended strand interrupting flanking helical regions. This structural difference may be related to differences in the conformational changes induced in the absence of peptide, which have been characterized for

both class I (Fahnestock, Tamir et al. 1992; Bouvier and Wiley 1998) and class II MHC proteins (Zarutskie, Sato et al. 1999). A crystal structure of a class I MHC protein with a pentapeptide epitope occupying only the C-terminal end of the binding site (Glithero, Tormo et al. 2006) and molecular dynamics studies of peptide-free class I MHC proteins (Zacharias and Springer 2004; Sieker, Springer et al. 2007) suggest that for class I MHC proteins the N-terminal side of the peptide binding site could be conformationally stable in the absence of peptide, with conformational changes predicted in the C-terminal end (Zacharias and Springer 2004; Sieker, Springer et al. 2007). By contrast, crystal structures of class II MHC-peptide complexes carrying truncated penta-, hexa-, and hepta-peptide analogs occupy the N-terminal side of the peptide binding site, leaving the C-terminal end empty but not conformationally altered (Bolin, Swain et al. 2000). Recently, a study of dipeptide-triggered ligand exchange of DR1 suggested that short peptides can prevent closure of the N-terminal side of the peptide-binding site predicted by molecular dynamics to occur in the absence of peptide (Gupta, Hopner et al. 2008). Finally, normal mode analysis of DR1 and HLA-A2 (Nojima, Takeda-Shitaka et al. 2002; Nojima, Takeda-Shitaka et al. 2003) also highlighted differences between their potential dynamic motions, with the N-terminal side of the binding site predicted to be more flexible for class II MHC proteins and the C-terminal side more flexible for class I MHC protein.

In summary, this work presents a molecular model for the conformational change induced by peptide removal from an MHC II protein. The model was

derived from molecular dynamics calculations and tested using experimental

conformational probes. Development of a model for the peptide-free form of DR1

can help to interpret the conformational changes known to occur within the

protein during peptide binding and release, and can provide insight into possible

mechanisms for DM action.

ACKNOWLEDGEMENTS

METHODS

Generation of DR1:

DR1 was expressed, purified and folded as previously described (Frayser, Sato

et al. 1999). Briefly, the extracellular domains of DR1 subunits were expressed

individually as inclusion bodies in *Escherichia coli*. Subunits were purified by

anion exchange chromatography and then diluted into folding buffer in the

presence or absence of a 5 fold molar excess of the HA peptide

(PKYVKQNTLKLAT). Folded peptide-free or peptide-loaded DR1, was purified

by affinity chromatography on an LB3.1-protein column and by gel-filtration

chromatography to remove any aggregated protein. Pooled fractions were concentrated to 1mg/ml and stored at 4°C. For some SPR studies, DR1 with a cysteine modification at the C-terminus of the alpha subunit was prepared by expression in insect cells as previously described (Cochran and Stern 2000). Briefly, DR1-a$_{cys}$ was expressed in S2 insect cells in serum free medium and purified from culture supernatant by LB3.1 affinity and gel filtration chromatography. This material is substantially free of peptide (Stern and Wiley 1992). To generate loaded complex, purified DR1a$_{cys}$ was incubated with excess peptide in binding buffer (100mM phosphate pH 5.0, 0.02% NaN$_3$, 1 mM EDTA, 50mMNaCl, 0.05% octyl glucoside, 2mM dithriothreitol (DTT), 0.01mg/ml PMSF) for 3 days at 37°C. Peptide-free and peptide-loaded DR1a$_{cys}$ were purified as described above for *E. coli* derived protein.

ELISA:

A sandwich ELISA was used to measure binding of peptide-free or peptide-loaded DR1 to LB3.1 and MEM264 as previously described (Stern and Wiley 1992). Plates were developed with ABTS and read on a Polarstar plate reader (BMG Labtech) at 405 nm absorbance. Half-maximal binding concentrations were obtained from a 4 -parameter binding equation fit to the data.

Biacore:

We used a BIAcore 2000 surface plasmon resonance biosensor for the SEC3 experiments and a Biacore 3000 for all other SPR experiments (Biacore AB, Uppsala, Sweden). Biotinylated DR1 was immobilized using Sensor Chip SA. All other experiments used standard carbodiimide-mediated amine coupling to Sensor Chip CM-5. Data were background-subtracted using an unmodified reference surface. The data were fit to the 1:1 binding with baseline drift model provided by BiaEval software. Fit residuals are shown in Fig. 4, and generally represent <10% of the overall signal. The LB3.1 and MEM264 were regenerated with 20mM NaOH for 1.5 or 1 minutes respectively, followed by a 2 minute stabilization in running buffer. For the other SEC3 and DR1 surfaces, bound protein eluted rapidly and a separate regeneration protocol was not needed.

Molecular Dynamic Simulation:

Each simulated system consisted of one protein molecule in a cubic box with a distance of 3.0 nm from its periodic image, with approximately 30,200 molecules of water. Coordinates for the peptide-bound form of DR1 were downloaded from the Protein Data Bank (PDB code: 1SJE) (Zavala-Ruiz, Strug et al. 2004). The peptide-free form of the DR1 was prepared by removing the sixteen residue peptide from the peptide-binding grove. SEC3 was removed from both structures.

The energy of the system was minimized with the steepest descent algorithm, followed by a 600 ps of positional restraint dynamics to generate the starting point for molecular dynamics. The GROMOS9643a1 force field (Kony, Hunenberger et al. 2007) was used, and all simulations were carried out at constant temperature (298 K) , pressure (1 atm), and number of molecules using a Berendsen weak coupling bath with a coupling constant of 0.1 ps for temperature and 0.5 ps for the pressure (Berendsen 1984). A twin range cut-off of 0.9/1.4 nm for van der Waals interactions was applied, and the particle mesh Ewald algorithm was used for long range electrostatic interactions (Essmann 1995). Neighbor lists were utilized and updated every five steps, and all protein and water bond lengths were constrained using the LINCS and SETTLE algorithm, respectively (Hess 1997).

The length of the simulation was determined by monitoring the convergence of various mechanical properties of the system. The simulation was stopped when the value for the root mean square deviation (RMSD) did not fluctuate more than 3.0 Å from its average value during 2 ns. As described (Villa, Balaeff et al. 2005) if the simulation reached an RMSD that oscillates around a constant value, it can be assumed the system has converged to a stable or a metastable structure. For both systems, the simulations were terminated after 60 ns with a time step of 2 fs. The coordinates were saved every five picoseconds and the analysis was performed using GROMACS v.3.2.1 simulation package

(Berdensen 1995). All molecular graphics images were generated using the

Visual Molecular Dynamics (VMD) software (Humphrey 1996).

CHAPTER III

The class II MHC 3_{10} helix and adjacent extended strand region are key structural determinants that dictate HLA-DM susceptibility and peptide exchange

Corrie A. Painter, Maria P. Negroni, Katherine A. Kellesberger,

Zarixia Zavala-Ruiz, James E. Evans and Lawrence J. Stern

Author Contributions

C.A.P. and L.J.S designed research, C.A.P determined crystal structures and performed most of the functional studies of mutant proteins, M.P.N. and Z.Z.R. produced and/or analyzed mutant proteins, K.A.K and J.E.E. performed and/or analyzed H-D exchange studies; C.A.P. and L.J.S. interpreted results

ABSTRACT

HLA-DM is required for efficient peptide exchange on class II MHC molecules, but its mechanism of action is controversial. A recently proposed mechanism for HLA-DM action posits spontaneous release of peptide from the P1 pocket as a prerequisite for productive HLA-DM interaction. Using a hydrogen-deuterium exchange technique, we show that MHC-peptide hydrogen bonds in the vicinity of the P1 pocket are disproportionally stable, inconsistent with a spontaneous release mechanism. Instead, we observe that interaction with HLA-DM is driven by a conformational change of the fully peptide-bound MHC protein. We trapped an intermediate state of the class II MHC-peptide complex by substitution of αF54, resulting in a protein with increased HLA-DM binding affinity, weakened MHC-peptide hydrogen bonding, and increased susceptibility to DM-mediated peptide exchange. Structural analysis reveals a set of concerted conformational alterations near the putative DM-binding interface that can explain these phenomena.

INTRODUCTION

HLA-DM (DM) facilitates peptide exchange on class II MHC (MHC II) proteins, and is required for efficient peptide loading *in vivo* (Morris, Shaman et al. 1994). MHC II molecules assemble in the endoplasmic reticulum with the class II – associated invariant chain chaperone, which is subsequently cleaved by endosomal proteases leaving a short fragment known as CLIP bound in the MHC peptide binding groove (Machamer and Cresswell 1982; Blum and Cresswell 1988). DM facilitates the exchange of CLIP for peptides generated by endosomal proteolytic digestion of endogenous and exogenous proteins, resulting in a library of peptide antigens bound to MHC II proteins that are transported to the cell surface for inspection by antigen receptors on CD4+ T cells (Denzin and Cresswell 1995; Sloan, Cameron et al. 1995; Kropshofer, Vogt et al. 1996). *In vitro* experiments have corroborated the roles for DM as a peptide exchange factor (Kropshofer, Vogt et al. 1996; Vogt, Kropshofer et al. 1996; Weber, Evavold et al. 1996; Doebele, Busch et al. 2000) as well as a molecular chaperone that prevents peptide free MHC II molecules from becoming inactive and from forming aggregates (Denzin, Hammond et al. 1996; Kropshofer, Arndt et al. 1997).

Despite intensive investigation, details regarding the structural nature of how DM and MHC II interact have not been forthcoming. Although crystal structures have been determined for isolated MHC II proteins as well as for DM, there is scant evidence for the structural mechanism involved in DM facilitated

peptide binding and exchange. Part of the difficulty in developing a complete understanding of the interaction of DM and MHC II may be due to the presence of multiple conformers of DM (Busch, Reich et al. 1998) as well as MHC II (Zarutskie, Sato et al. 1999; Chou and Sadegh-Nasseri 2000; Verreck, Fargeas et al. 2001). At least for MHC II, the conformers believed to be involved in interaction with DM are thought to be kinetically unstable in that they undergo rapid isomerization to an inactive conformation (Zarutskie, Busch et al. 2001) and may not be amenable to structural analysis using conventional high-resolution methods such as x-ray crystallography. Previous work using directed screens (Doebele, Busch et al. 2000; Pashine, Busch et al. 2003), leucine zippered proteins (Busch, Pashine et al. 2002), and tethered peptide approaches (Stratikos, Mosyak et al. 2002) has identified residues on lateral surfaces of both DM and MHC II that are critical for the functional interaction. However, structural characterization of the DM-MHC II complex, dynamic changes that occur as a result of the interaction, and how formation of the complex facilitates peptide exchange have not been described.

Due in part to the paucity of structural information, details regarding the interaction of DM with MHC II have been controversial and several models have been put forward. These models fall into two general mechanistic categories: one that suggests that DM catalyzed peptide release is mediated by disruption of the conserved hydrogen bond network between the peptide and the MHC II (Weber,

Evavold et al. 1996),and another category that suggests that the action of DM is more complex (Busch, Rinderknecht et al. 2005).

Disruption of the MHC-peptide hydrogen bond network was put forth as an attractive target for DM because it allows for a peptide sequence-independent exchange mechanism (Weber, Evavold et al. 1996). Peptides are bound by MHC II molecules in a canonical, extended polyproline-II conformation with conserved hydrogen bonds between the peptide backbone and conserved MHC II main-chain and side-chain atoms (McFarland and Beeson 2002). In total, ~16 hydrogen bonds are formed with the peptide backbone. In this model category, DM-induced disruption of one or more critical hydrogen bonds results in catalyzed peptide exchange (McFarland, Katz et al. 2001; Stratikos, Wiley et al. 2004; Narayan, Chou et al. 2007). However, mutagenesis of the MHC II side chains involved in this interaction has shown for the most part that disruption of individual H-bonds do not diminish DM catalysis. One study proposed that the βH81 H-bond was responsible for the entire mode of DM catalysis (Narayan, Chou et al. 2007), however two other groups have found that this as well as other point mutations do not prevent the effect of DM (Ferrante and Gorski ; Zhou, Callaway et al. 2009). In addition, disruption of this H-bond network by either truncation or methylation of the peptide has revealed that augmentation of DM-mediated peptide catalysis occurs when the N-terminal peptide H-bonds are disrupted (Stratikos, Wiley et al. 2004). These studies show that while disruption of the H-bond network can augment DM-mediated peptide release, the

relationship between the hydrogen bond network and the actual catalytic mechanism of DM remains unknown.

Models that put forth a more complex mechanism for DM catalysis include roles for conformational heterogeneity (Sadegh-Nasseri, Natarajan et al. 2010) (Anders, Call et al. 2011), and the involvement of the peptide side chains in addition to the cooperativity of the H-bond network in regards to DM function (Belmares, Busch et al. 2002). The MHC II P1 side-chain binding pocket, a major determinant for the peptide-MHC interaction(Sato, Zarutskie et al. 2000), has been investigated as a target for DM action. One study suggests that DM recognizes a flexible conformation of MHC II with alterations of the P1 pocket relative to the canonically "rigid" crystal structures to date (Chou and Sadegh-Nasseri 2000), while another recent study has suggested that the occupancy of the P1 pocket may be a critical determinant for DM susceptibility (Anders, Call et al. 2011). In the latter study, spontaneous release of the peptide from the P1 pocket, was put forth as prerequisite to DM interaction. In contrast to a model that focus on interactions in the P1 pocket, a study of many MHC II and peptide variants suggests that interactions along the entire peptide binding groove contribute to the susceptibility of DM (Belmares, Busch et al. 2002). In addition, it has also been suggested that DM functions by reducing the cooperativity of peptide side chain interactions along the length of the peptide, while mediating peptide exchange by way of a "push-off" mechanism (Ferrante, Anderson et al. 2008).

In this work, we describe a structural and dynamic framework for how conformational heterogeneity of MHC II may influence DM susceptibility. We used a novel mass-spectrometry approach to establish the relative strength of the individual hydrogen bonds along the backbone of MHC II- bound peptide. Through targeted mutagenesis of MHC II residues in the vicinity of the peptide N-terminus and P1 pocket, we identified a point substitution that leads to alterations within the hydrogen bonding network, increased susceptibility to DM mediated peptide exchange , and greatly increased DM binding affinity. Structural characterization of the protein revealed an altered MHC II conformation in a molecule contacted at the presumptive DM interaction site, with alterations in the alpha subunit 3_{10} helical region (α45-50) and flanking extended strand region (α51-54). These changes appear to be key structural determinants for DM interaction and peptide exchange.

RESULTS

Measurement of MHC-peptide hydrogen bond strengths using hydrogen-deuterium exchange mass spectrometry

The MHC II-peptide hydrogen bonds are believed to be of fundamental importance to the MHC II-peptide interaction (McFarland, Beeson et al. 1999; McFarland, Katz et al. 2001; Bandyopadhyay, Arneson et al. 2008), but their role in DM-mediated catalysis has been controversial (Belmares, Busch et al. 2002)

(Ferrante and Gorski ; Narayan, Chou et al. 2007; Zhou, Callaway et al. 2009)·(Vogt, Kropshofer et al. 1997), in part because of a lack of methods to examine the strength of these bonds directly. We devised an experimental protocol that uses amide hydrogen-deuterium exchange (H/Dx) and mass spectrometry to examine the strengths of the MHC II-peptide hydrogen bonds in native, unlabeled, soluble MHC II-peptide complexes. Amide hydrogens exchange with solvent on an experimentally useful time scale of milliseconds to hours, with the exchange rate depending on the strength of the amide hydrogen bond (Marcsisin and Engen). Analysis of amide H/D exchange rates by mass spectrometry has been useful in studies of protein folding and structure, but can be limited by the need to fragment large proteins into peptides sufficiently small for high-resolution mass analysis (Tsutsui and Wintrode 2007). Here, we were able to strip the peptide from the MHC II under conditions that minimize further exchange, so that conventional high-resolution LTQ HPLC/MS could be used to evaluate H/Dx in MHC II-peptide amide bonds by direct examination of the released peptide, which retained the pattern of deuterium incorporation obtained as a result of amide protection by MHC II binding.

The experiment is diagrammed in Figure 3.1a. Preformed complexes of HLA-DR1 and influenza-derived HA peptide (MHC II-pep) in aqueous solution were transferred to a D_2O solution, inducing exchange between macromolecular amide hydrogens and solvent deuterons. At various times the reaction was quenched by transfer to ice-cold pH 2.7 buffer, which removes the peptide from

the MHC, while preserving the pattern of amide H/D present in the MHC-peptide complex. Peptide was separated from MHC II by in-line C4 and C18 reverse-phase microcolumns, and peptide mass measured by high-resolution mass

FIGURE 3.1
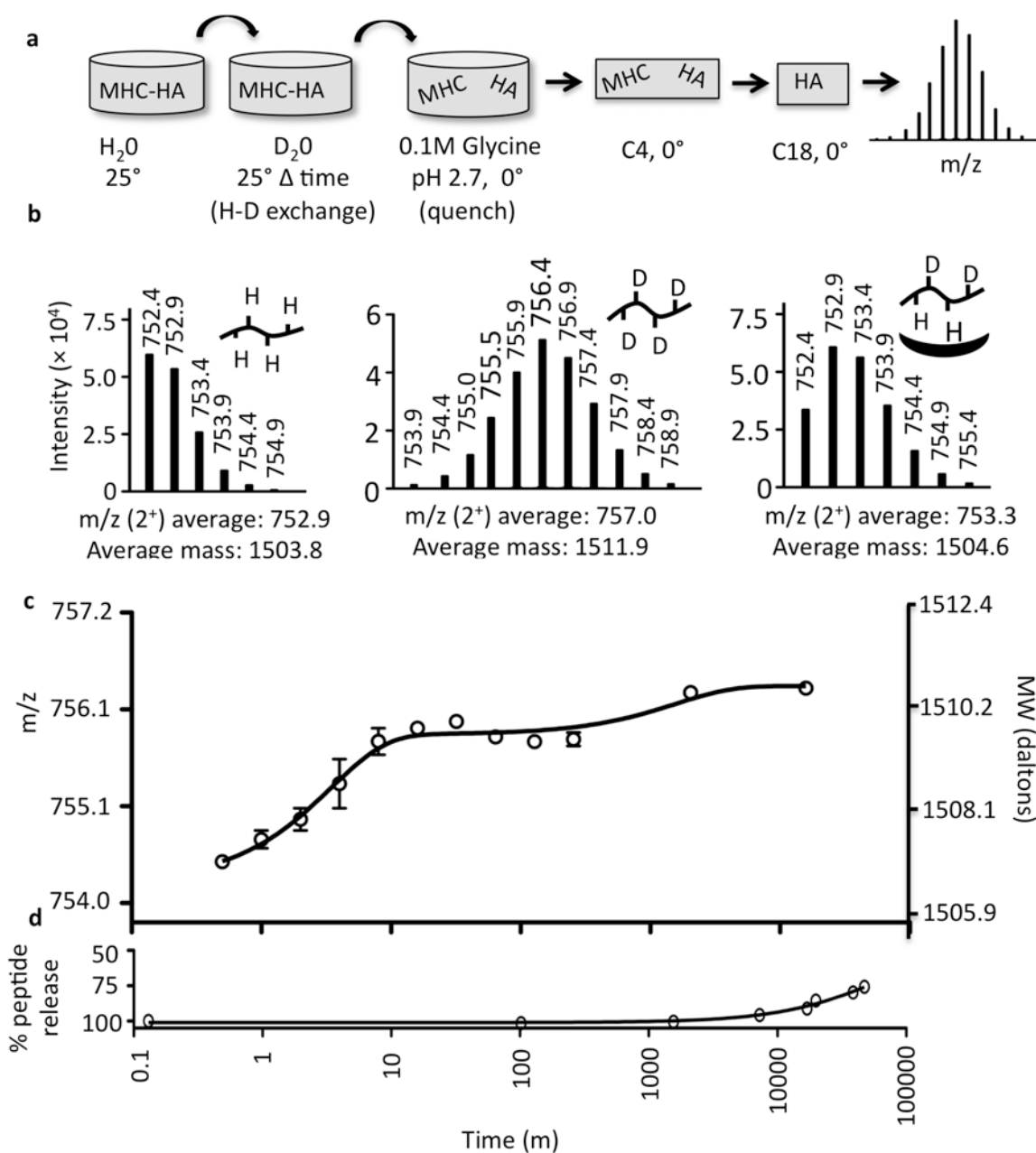
Figure 3.1. Hydrogen-Deuterium exchange mass spectroscopy to evaluate MHC II-peptide hydrogen bonding strengths. (a) Schematic showing experimental design. WT was pre-loaded with HA peptide, then diluted into D_2O for variable lengths of time. The reaction was quenched by dilution into ice cold glycine buffer pH 2.7, which also releases peptide from the MHC II. Sample was then injected onto an on-line series of columns, with the MHC II retained by the C4 column and the HA is retained on and chromatographically eluted from the C18 column into the electrospray ion source of a Thermo LTQ ion trap mass spectrometer for mass analysis. (b) Mass spectra of free and MHCII-bound HA peptide . *Left panel,* mass spectrum of the HA peptide showing the expected isotopic distribution for the $[M+2H]^{2+}$ ion of the unlabeled peptide. The weighted intensities of the ion masses are averaged to obtain the average mass of the peptide. *Center panel*, mass spectrum of the HA peptide after equilibration in D_2O. *Right panel*, mass spectrum of HA peptide eluted from MHC II-complex after 30 second incubation in D_2O, showing MHC-mediated protection from H-D exchange at most of the peptide amide positions. (c) Average mass of the HA peptide eluted from MHC II complex for various times of incubation in D_2O. Data were fit to a two phase exponential association model. (d) Peptide dissociation assays were performed by measuring the decay of polarization for Alexa-488 labeled HA peptide from pre-bound complex.

spectrometry.   The distribution of stable isotopes gives a series of peaks in the MS spectra (Fig. 3.1b). For the free HA peptide in H_2O solution, the average mass (1503.8) and the ion distribution pattern (Fig. 3.1b, left) correspond with that expected for the HA peptide sequence and the known hydrogen, carbon, nitrogen, and oxygen isotope abundances (Fig. 3.2). For the free HA peptide transferred to 90% D_2O solution, the average mass increases to 1511.9, with corresponding changes in the mass spectrum (Fig. 3.1b, center). The average mass change, +8.1 Da, corresponds to addition of 12 D, after accounting for back-exchange during the analysis (Fig. 3.2), and consistent with the twelve amide bonds present in the 13-mer HA peptide. For the MHC II-HA complex immediately after transfer to 90% D_2O, the average mass is 1504.6 (Fig. 3.1b, right). Thus, interaction with the MHC II protein protects ~90% of the peptide amide from exchange.

With increasing time in D_2O, additional H/D exchange is observed, with multiphasic kinetics (Fig. 3.1c). The time dependent H/D exchange kinetic is fit well by a two-phase exponential rise equation that describes an unresolved initial phase ($t_{1/2} < 1$min), a fast phase with half-time of a few minutes, and a much longer slow phase, with a half-time of ~18hr (Table 3.1). The slow phase is still substantially faster than the rate of peptide release (Fig. 3.1d). Overall this analysis reveals that the bound peptide's amide NH bonds exchange at dramatically different rates.

FIGURE 3.2
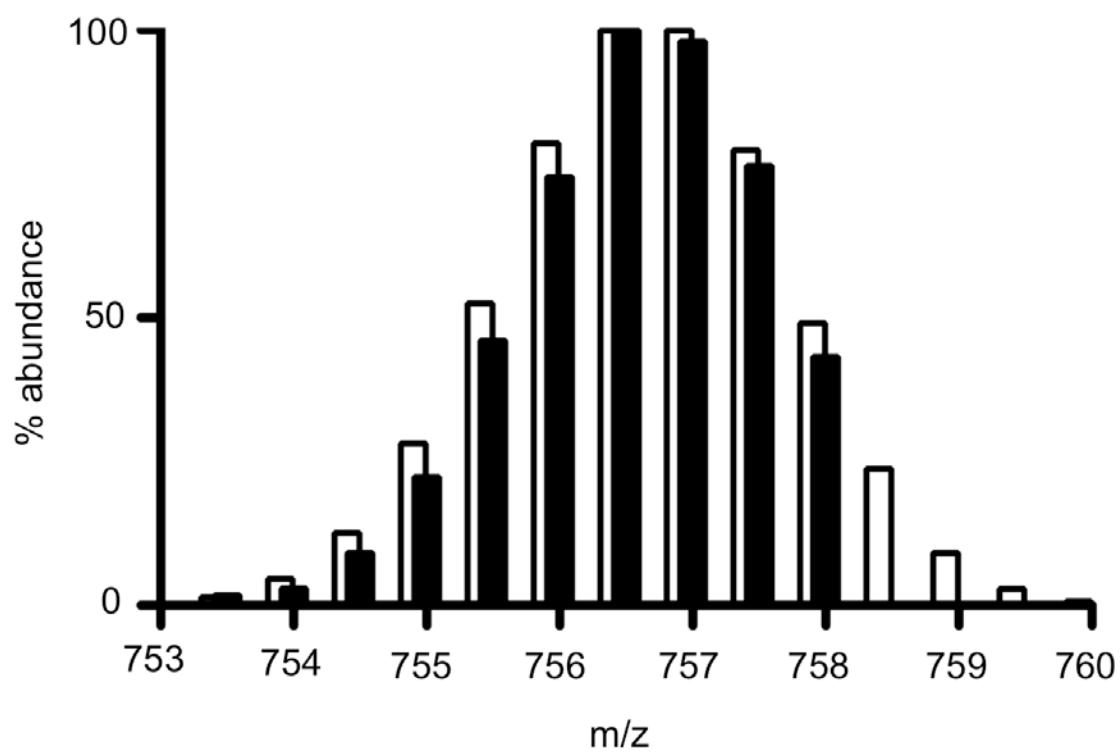
FIGURE 3.2. HDx Back-exchange fitting. Hydrogen-deuterium exchange

isotope distribution pattern in 90% D2O. Closed bars, observed isotope

distribution, open bars, calculated isotope distribution with 28% back exchange

TABLE 3.1 Peptide hydrogen-deuterium exchange parameters

MHC-HA complex	Unresolved[a] initial amplitude[b] fraction (95% CI)	Fast phase amplitude[a] fraction (95% CI)	Fast phase half-life $t_{1/2}$ min (95% CI)	Slow phase amplitude[b] fraction (95% CI)	Slow phase half-life $t_{1/2}$ hr (95% CI)
WT	0.31 (0.24-0.37)	0.38 (0.26-0.50)	2.4 (1.7-4.0)	0.13 (0.06-0.24)	18.1 (7.4-∞)
αF54C	0.36 (0.33-0.39)	0.28 (0.17-0.39)	4.7 (3.1-9.3)	0.24 (0.13-0.35)	1.76 (1.2-3.7)

[a] $t_{1/2} < 1$ min

[b] Amplitudes reported as fraction of total exchange observed for uncomplexed peptide

We were able to assign several individual peptide amides to particular

kinetic phases using multidimensional electron transfer dissocation (ETD) mass

spectrometry. ETD is an ion fragmentation method that can be used inside the

mass spectometer to produce peptide fragments for MS/MS sequence analysis

(Mikesh, Ueberheide et al. 2006). Peptides are fragmented between NH and Cα

atoms (Fig 3.3a) producing sets of c-series and z-series ions (Fig 3.3b),

analogous to the b-series and y-series of conventional collison-induced

dissociation (CID) (Mikesh, Ueberheide et al. 2006). Unlike CID, however, ETD

does not result in H/D scrambling (Zehl, Rand et al. 2008), so that the ion

fragments retain the pattern of deuterium incorporation present in the eluted

peptides. Thus, different peptide fragments exhibit different kinetics of deuterium

incorporation, depending on the protection from D_2O exchange for the particular

amide NH atoms present in that fragment. For example the c3 fragment has very

little deuterium incorporation even at 512 minutes, whereas the c6 fragment is

substantially exchanged by 2 min (Fig 3.3c). We were able to measure

deuterium incorporation rates for 6 c-series ions (c2,c3,c5,c6,c8,c9) and seven z-

series ions (z4,z5,z7,z9,z10.z11,z12), although with weaker signals for the z-

series (complete analysis in Table 3.2). By subtracting the mass differences

(ΔMW) for adjacent c-series (or z-series) ions, the contributions of particular

peptide NH atoms (or pairs of NH atoms) can be obtained. Figure 3.3d shows

such a $\Delta\Delta$MW analysis, with the extracted H/D exchange of each peptide NH

FIGURE 3.3
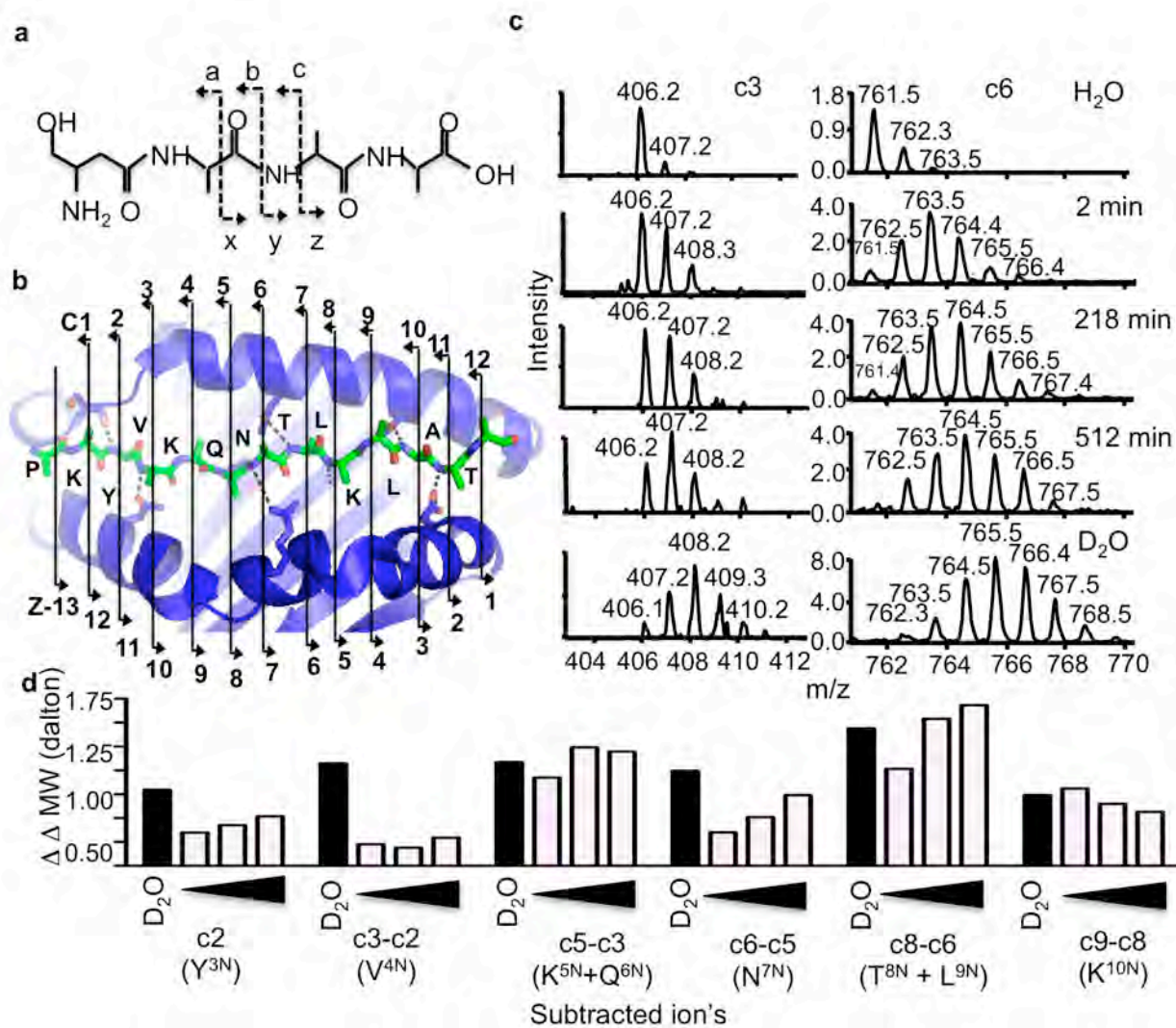
FIGURE 3.3. HDx mapping by ETD of HA peptide.

(a) Schematic representing the N to C-terminus of a peptide backbone. Dashed lines with opposing arrows represent potential ion series that are possible upon backbone cleavage by different methods. Fragmentation by ETD produces c and z ions. (b) Cartoon representation of peptide binding groove with backbone of HA shown in stick. Letters indicate the residue at each position along the backbone. Dashed lines represent amides that are protected by bonding to the MHC II through direct hydrogen bonding or through ordered solvent. Hydrogen bonding partners on the MHC II are indicated in stick. c and z fragmentation pattern is shown by opposing arrows as in (a). (c) Representative data for the HA C3 ion (left) and the C6 ion (right) with no deuterium incorporation (H_2O), with deuterium incorporation at various time points (2, 218 and 512 minutes) while bound to the MHC II, and for the fully unprotected HA (D_2O). (d) Deuterium incorporation for each amine group along the peptide backbone for different times of incubation in D_2O. The Y axis represents the change in molecular weight for the unexchanged ion (ΔMW), which is then subtracted between sequential ion fragments in order to obtain the amount of deuterium incorporation of each amide at that time point ($\Delta\Delta MW$). Black bars represent the fully exchanged ion fragment in D_2O, and the open bars represent an increase in time, with triangles representing 2, 218 and 512minutes. The c-series sequential ions and the corresponding amine group are indicted below

TABLE 3.2 ETD m/z for the c and z ion series

Ion	Ion sequence	HA no H_2O Calc. (m/z)	HA no H_2O (m/z)	HA D_2O (m/z)	WT-HA (D_2O exchange) (m/z) 2min	128min	512min	F54C-HA (D_2O exchange) (m/z) 2min	128min	512min
C1	P (+K_2 NH)	115.1	[a]		[a]	[a]	[a]	[a]	[a]	[a]
C2	PK (+Y_3 NH)	243.2	243.22	244.01	243.56	243.64	243.73	243.61	243.78	243.83
C3	PKY (+V_4 NH)	406.2	406.34	408.21	406.91	406.95	407.15	407.22	407.56	407.47 [b]
C4	PKYV (+K_5 NH)	505.3	505.51							
C5	PKYVK (+Q_6 NH)	633.4	633.75	636.71	635.26	635.61	635.76	635.19	635.99	635.93
C6	PKYVKQ (+N_7 NH)	761.4	761.83	765.78	763.68	764.2	764.58	763.7	764.91	764.81 [b]
C7	PKYVKQN (+T_8 NH)	876.5	875.94							
C8	PKYVKQNT (+L_9 NH)	976.5	977.07	982.46	979.94	980.98	981.5	979.82	981.53	981.78
C9	PKYVKQNTL (+K_{10} NH)	1089.6	1090.20	1096.33	1093.87	1094.76	1095.2	1093.7	1095.51	1095.43
C10	PKYVKQNTLK (+L_{11} NH)	1217.7	1218.37	[c]	[c]	[c]	[c]	[c]	[c]	[c]
C11	PKYVKQNTLKL (+A_{12} NH)	1330.8	[c]	[c]	[c]	[c]	[c]	[c]	[c]	[c]
C12	PKYVKQNTLKLA (+T_{13} NH)	1401.9	[c]	[c]	[c]	[c]	[c]	[c]	[c]	[c]
Z2	(-A_{12} NH) AT	175.1	[a]	[a]	[a]	[a]	[a]	[a]	[a]	[a]
Z3	(-L_{11} NH) LAT	288.2	[a]	[a]	[a]	[a]	[a]	[a]	[a]	[a]
Z4	(-K_{10} NH) KLAT	416.3	416.43	419.21	417.33	418.21	418.39	417.30	418.41	418.46
Z5	(-L_9 NH) LKLAT	529.3	529.70	533.21	531.38	532.19	532.61	531.33	532.46	532.78 [b]
Z6	(-T_8 NH) TLKLAT	630.4	630.92							[b]
Z7	(-N_7 NH) NTLKLAT	744.4	744.90	749.32	746.99	748.76	748.68	747.16	749.10	749.09
Z8	(-Q_6 NH) QNTLKLAT	873.5	872.51							[b]
Z9	(-K_5 NH) KQNTLKLAT	1000.6	1001.05	1007.41	1004.67	1006.07	1006.35	1004.45	1006.51	1006.73
Z10	(-V_4 NH) VKQNTLKLAT	1099.7	1100.30	1106.98	1104.10	1105.97	1106.24	1103.92	1106.44	1106.53
Z11	(-Y_3 NH) YVKQNTLKLAT	1262.7	1263.31	1271.05	1267.19	1268.97	1269.20	1267.38	1269.73	1269.79
Z12	(-K_2 NH) KYVKQNTLKLAT	1390.8	1392.14	1400.76	1396.56	1398.58	1398.70	1396.54	1399.28	1399.79

98

atom (or pairs of NH atoms) at various times shown in open bars and the fully exchanged mass difference shown in black bars. Corresponding z-series data are shown in Fig. 3.4a with an overall summary of both c-series and z-series data in Fig. 3.5. It is readily apparent that the Y3 and V4 positions are the most strongly protected of all the peptide NH, indicating that these participate in the strongest hydrogen bonding interactions with the lowest spontaneous exposure rate. These positions flank the P1 side chain binding pocket. Thus it would be highly unlikely for the P1 side chain to spontaneously escape the P1 pocket, and so we sought other explanations for the key role of this region in DM-mediated peptide exchange catalysis.

Substitution of αF54 dramatically increases susceptibility of MHC II to DM-catalyzed peptide dissociation

To determine the relevance of the region proximal to the P1 pocket for DM catalyzed peptide dissociation, we engineered mutations in the extended strand region of the alpha subunit at residues αF51, αS53, and αF54 (Fig 3.6a, Table 3.3), and at residues surrounding the P1 pocket αL45, αF48, βF89, and βW153 (Fig 3.7, Table 3.3), As a control, we also mutated αQ57, located on the alpha subunit helix one turn beyond the extended strand region. Recombinant proteins carrying the mutations were expressed in *E. coli* and refolded *in vitro* using standard methods (Frayser, Sato et al. 1999). Each of the proteins bound to the

FIGURE 3.4
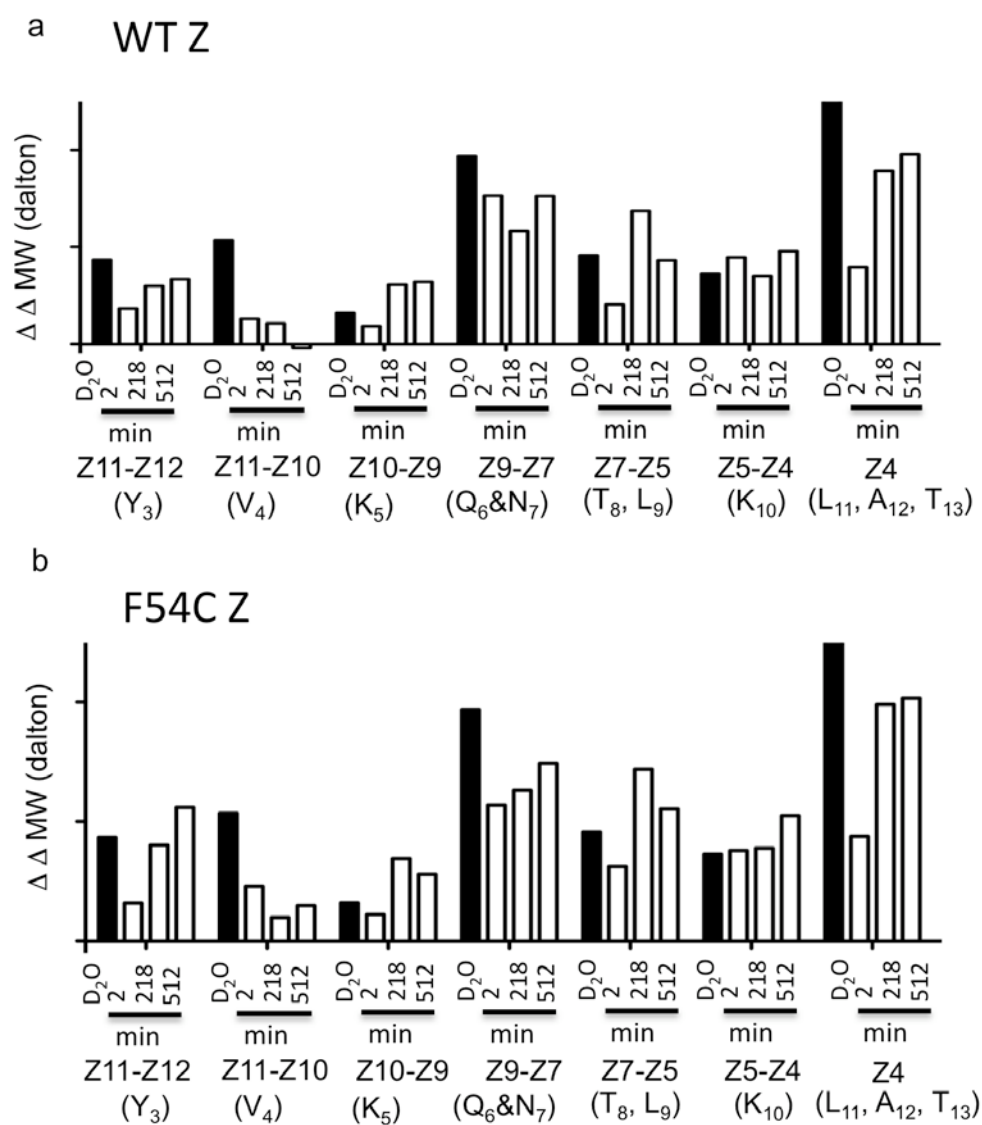
FIGURE 3.4. **ETD ΔΔMW for the z ion series**; Change in molecular weight

plotted for each amine group along the peptide backbone. The y-axis represents

the change in molecular weight of the deuterated ion from the unexchanged ion

which is then subtracted between ion fragments in order to obtain the amount of

deuterium incorporated at each amide. Top panel shows z series calculations for

the HA alone or in complex with WT MHC II, bottom panel shows HA alone or in

complex with F54C MHC II. Black bars represent the fully exchanged ion

fragment in D_2O, and the open bars represent the time course in which the MHC

II HA complex was incubated in deuterium. Determination of the incremental

mass incorporated for each amine was calculated as the ΔΔMW; the deuterium

incorporation for each ion was calculated as the difference in mass between the

deuterated ion and it's corresponding ion in H2O (ΔMW), these differences were

then subtracted for neighboring ions in order to obtain the incremental mass

increases for each amine along the backbone. The subtracted ion species are

indicated and the amine group which corresponds to the fragment is indicated

below in parenthesis.

FIGURE 3.5
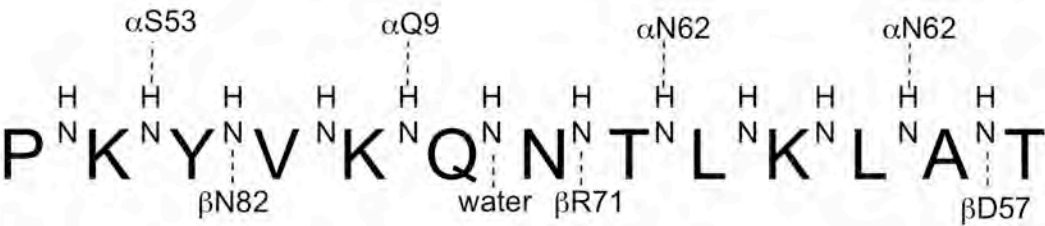
WT c series	n/a	m	s		u		m		f	u	n/a
WT z series	n/a	f	s	f		m		f	u	m
F54 c series	n/a	m	m		f		f		f	u	n/a
F54 z series	n/a	f	m	f		m		f	u	m

FIGURE 3.5. **Summary of HDx data for HA peptide NH bonds in complex with WT and F54C HLA-DR1**.

The HA peptide sequence is shown with amide NH groups involved in hydrogen bonding interactions depicted by dashed lines. Individual NH or groups of NH atoms were characterized as having slow, medium, fast, or unprotected (very fast) HDx based on comparison of ΔΔMW values to corresponding values unbound peptide as follows: slow is <30% exchanged at all time points; medium is < 80% exchanged at 2min and 128 min (usually at all time points); fast is < 80% at 2 min, but > 80% exchanged at later points; unprotected is >80% exchanged at 2 min (and usually at all time points)

FIGURE 3.6
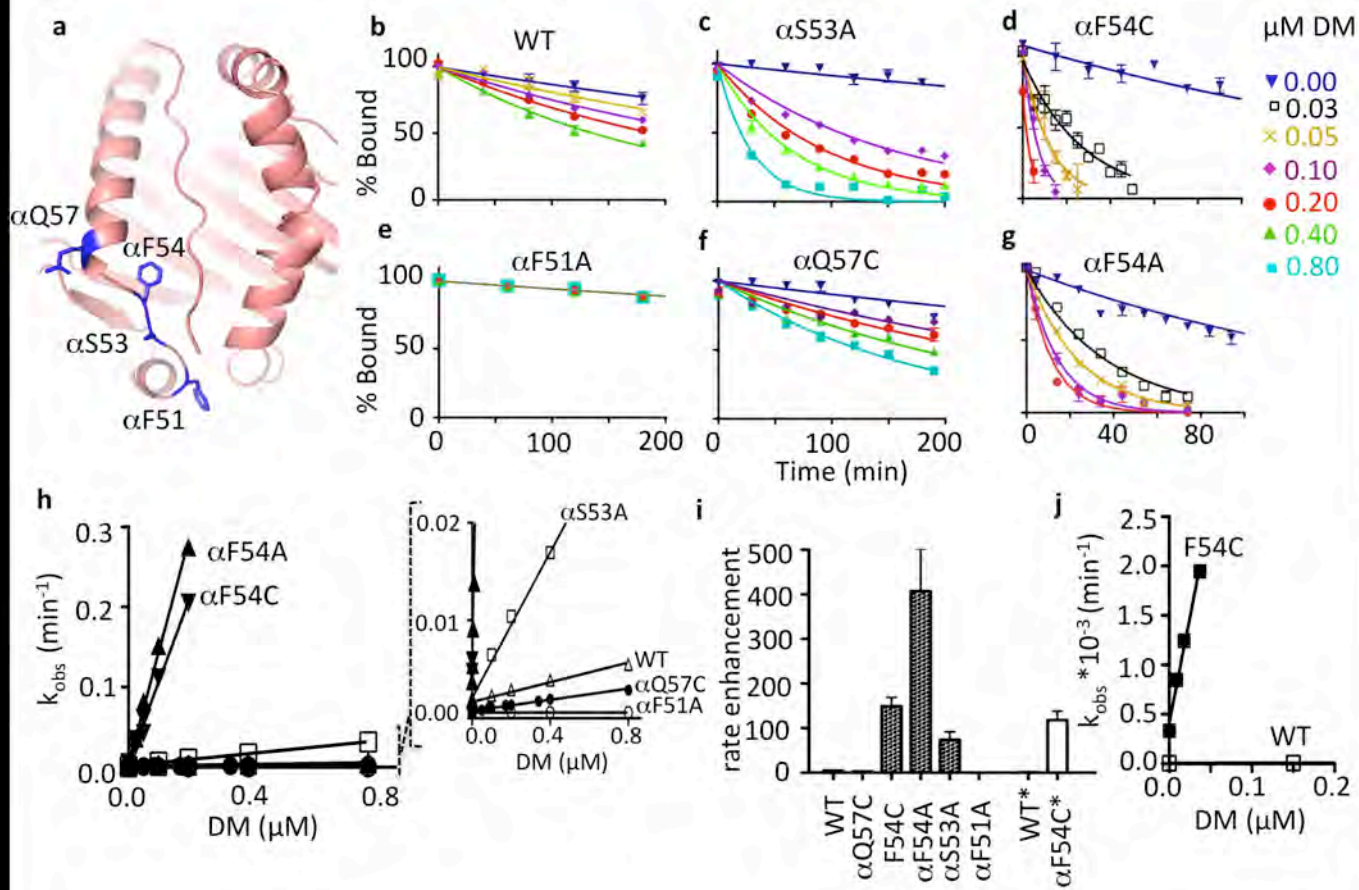
FIGURE 3.6. **Substitution of αF54 results in a dramatic increase in the rate of DM catalyzed peptide exchange.** (a) Schematic representation of the peptide binding groove of MHC II with mutated residues shown in blue. (b-g) Peptide release assays performed by monitoring decay of Alexa 488-CLIP polarization signal in the presence of unlabeled peptide and various concentrations of DM. (h) The k_{obs} values for each exponential decay were plotted against the concentration of DM. Inset with expanded y-axis to show the slopes for WT, αQ57C and αS53A. (i) DM-mediated rate enhancements were calculated for each mutant by dividing the slope of the k_{obs} vs. [DM] plots by the intrinsic dissociation rates. Closed bars, data for MHC II-CLIP. Open bars, data for MHC II-HA. (i) The k_{obs} values for the exponential decay in the HA peptide dissociation assays were plotted against the concentration of DM with complexes labeled on the graph.

FIGURE 3.7
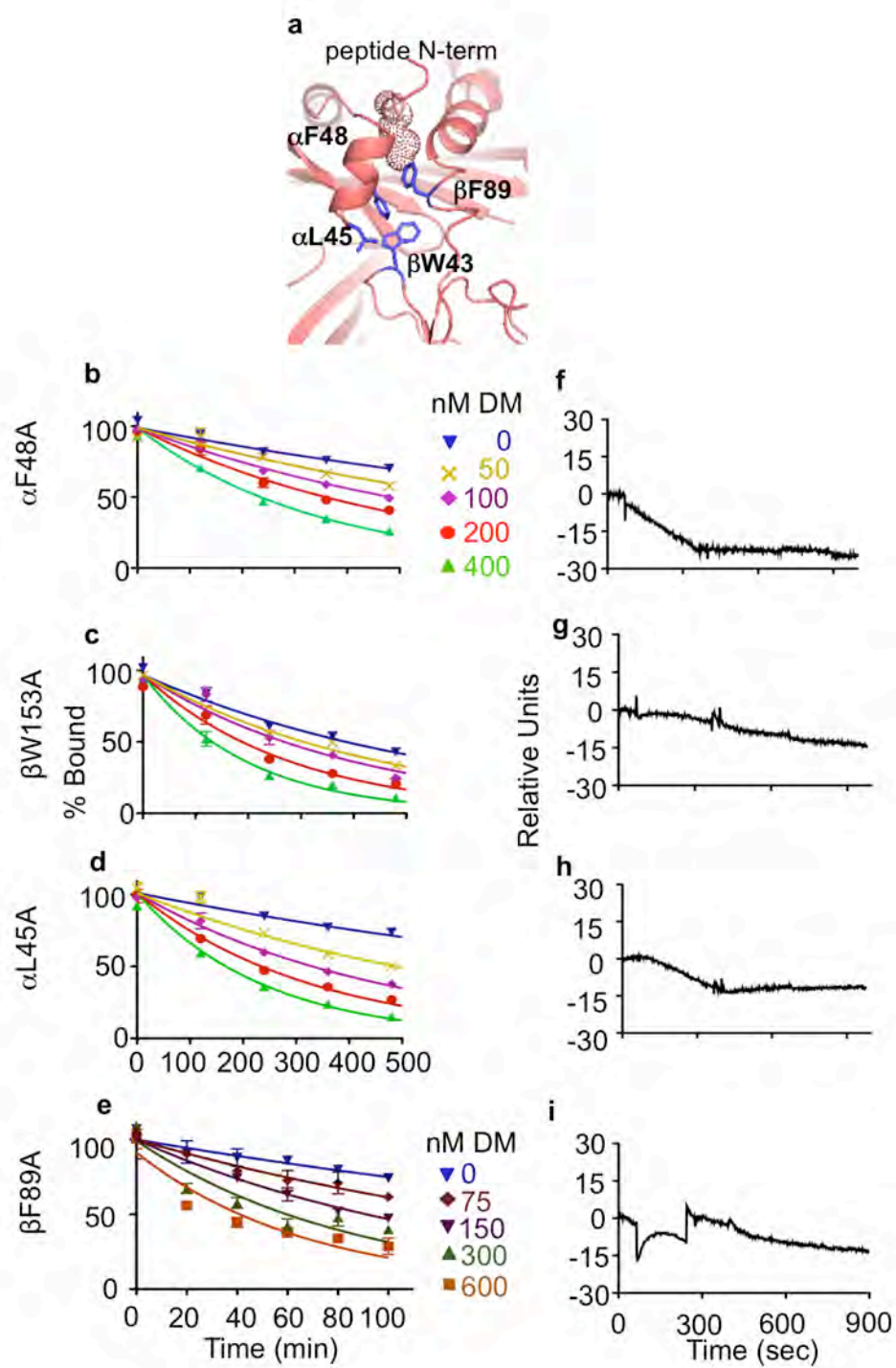
FIGURE 3.7. Mutation of other residues around the P1 pocket does not alter the effect of HLA-DM on peptide release. (a) Cartoon diagram of N-terminal region of the peptide binding groove. Residues mutated to alanines are represented in blue stick. (b-e) Dissociation of Alexa-488 labeled CLIP peptide from αF548A (b), bW153A (c), αL45A(d) and βF89A (e) show similar patterns of release. (f-i) SPR analysis shows that no binding is detected for any of these point mutations when 2.5 µM DM is injected in the mobile phase.

TABLE 3.3 MHC-peptide binding parameters

MHC II	$t_{1/2}$, intrinsic[a] hrs (95% C.I.)	k_{off}, intrinsic[b] $*10^{-3}$ min^{-1} (SD)	k_{off}, intercept[c] $*10^{-3}$ min^{-1}	DM susceptibility[d] $*10^{-3}$ min^{-1} μM^{-1} (SD)	Rate enhancement[e] μM^{-1} (SD)
WT	19.0 (17.1-21.5)	0.6 (0.1)	0.67 (0.04)	2.8 (0.3)	4.6 (1.0)
aQ57C	24.7 (20.5-31.0)	0.5 (0.1)	0.57 (0.01)	1.3 (0.5)	2.8 (1.2)
aF54C	2.0 (1.8-2.2)	5.7 (0.4)	8.6 (4.3)	847 (94)	149 (20)
aF54A	4.5 (4.2-4.8)	2.6 (0.2)	1.7 (2.1)	1057 (226)	407 (95)
aS53A	36.6 (33.9-40.0)	0.31 (0.03)	1.5 (0.7)	22.9 (5.1)	73.9 (17.9)
aF51A	19.8 (17.7-22.4)	0.6 (0.05)	none	none	none
aF48A	10.0 (7.9-13.6)	1.2 (0.2)	0.9 (0.1)	7.3 (0.9)	6.1 (1.3)
aL45A	10.1 (8.8-11.7)	1.1 (0.2)	1.1 (0.1)	10.5 (0.7)	9.5 (1.8)
βF89A	4.0 (2.6-8.1)	2.9 (0.7)	3.0 (4.0)	19.6 (2.9)	6.8 (1.8)
βW153A	6.8 (6.2-7.4)	1.7 (0.2)	1.8 (0.1)	6.0 (1.2)	3.5 (0.8)
WT[f]	1988.0 (1889-2098)	0.0058 (0.0003)	0.0059 (0.0001)	0.006 (0.005)	1.0 (0.1)
aF54C[f]	31.9 (28.8-35.7)	0.362 (0.042)	0.41 (0.07)	42.75 (0.01)	118 (20)

[a] Measured for a MHC II-peptide dissociation reaction performed in the absence of DM. Values in parentheses represent the 95% confidence interval for 3 or more replicates.

[b] Intrinsic dissociation rate, k_{off}. Values in parentheses represent the standard deviation of 3-6 replicates.

[c] Y-intercept extrapolated from linear regression of the k_{off} vs [DM] plot. Values in parentheses represent uncertainty from the linear fit.

could be loaded with peptide using a standard protocol. We monitored the intrinsic rate of peptide dissociation from the mutant proteins using Alexa488-labeled CLIP peptide in a fluorescence polarization assay (Fig 3.6b-g, triangles, Fig 3.7). Dissociation time courses fit well to single exponential decays, with $t_{1/2}$ and k_{off} values shown in Table 3.3. The mutations had varying effects, ranging from a 9.5-fold increase in dissociation rate for αF54C to a 1.9-fold decrease for αS53A.

We tested the susceptibility of the MHC II mutant proteins to DM in a functional assay, where increasing concentrations of DM resulted in an increased rate of peptide dissociation (Fig 3.6b-g). In the range tested, peptide dissociation rate constants increased linearly with increasing DM concentration for each of the mutant proteins (Fig 3.6h, Fig. 3.8), with the slope reflecting the susceptibility of each mutant protein to DM-mediated peptide dissociation. The DM-susceptibility of the control mutant αQ57C (Fig. 3.6f) was similar to WT (Fig 3.6b). Substituting αF51 by alanine resulted in a protein that was resistant to DM (Fig 3.6e). Other mutations at this position in the context of another MHC II previously have been shown to block DM-mediated peptide dissociation (Doebele, Busch et al. 2000). Mutation of residue αS53 to alanine increased the susceptibility to DM, with αS53A approximately seven-fold more sensitive to DM than WT (Fig 3.6c).

FIGURE 3.8

DM (µM)
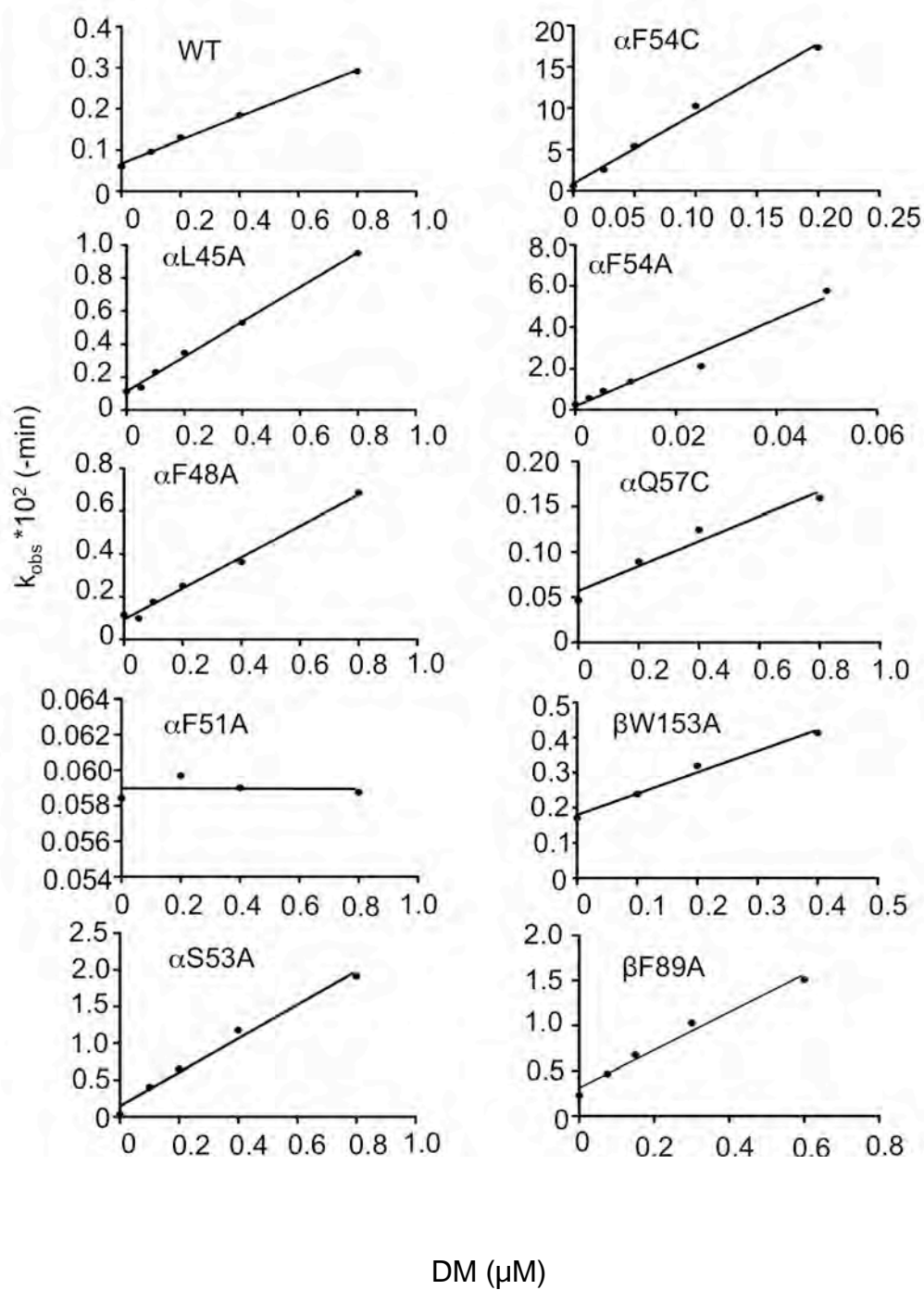
FIGURE 3.8. Effect of DM on peptide dissociation rates for point mutants.

Each plot shows the Linear regression of K_{obs} vs [DM]. The DM enhancement factor was calculated by dividing slope of the linear dependence on DM by the intrinsic peptide dissociation rate for each of the mutants.

In contrast, large effects on susceptibility to DM were observed upon substitution of αF54. Both αF54C and αF54A were exquisitely sensitive to DM, with concentrations as low as 25nM DM inducing large increases in peptide dissociation rates (Fig 3.6d,g). Values for the slopes of the DM-dependent rate profiles, i.e. the DM susceptibility, were 302 and 378 times greater for αF54C and αF54A, respectively, as compared to WT (Fig 3.6h, Table 3.3).

Previous studies have used the slope of the DM susceptibility curve divided by the intrinsic dissociation rate constant, i.e. the fold-enhancement in peptide release per unit of DM or the specific rate enhancement, as a measure of DM's catalytic efficacy towards a particular substrate (Weber, Evavold et al. 1996; Stratikos, Wiley et al. 2004). Even after this normalization, the αF54 mutations still are extreme outliers, with specific rate enhancement over 400 μM^{-1} for αF54A, almost 90-times greater than for WT (Fig 3.6i, Table 3.3). Similar values were obtained regardless of whether intrinsic dissociation rates were determined by experiments performed in the absence of DM or by extrapolation of DM-dependent rate profiles (Table 3.3). The extreme sensitivity of αF54C to DM was not restricted to the CLIP peptide, as it was also observed for the HA peptide (Fig 3.6i, open bars, Fig 3.6j, Fig. 3.9).

These results indicate that substitution of αF54 does not substantially impair MHC II-peptide interactions, but does make the MHC II protein particularly susceptible to DM-mediated peptide release.

FIGURE 3.9
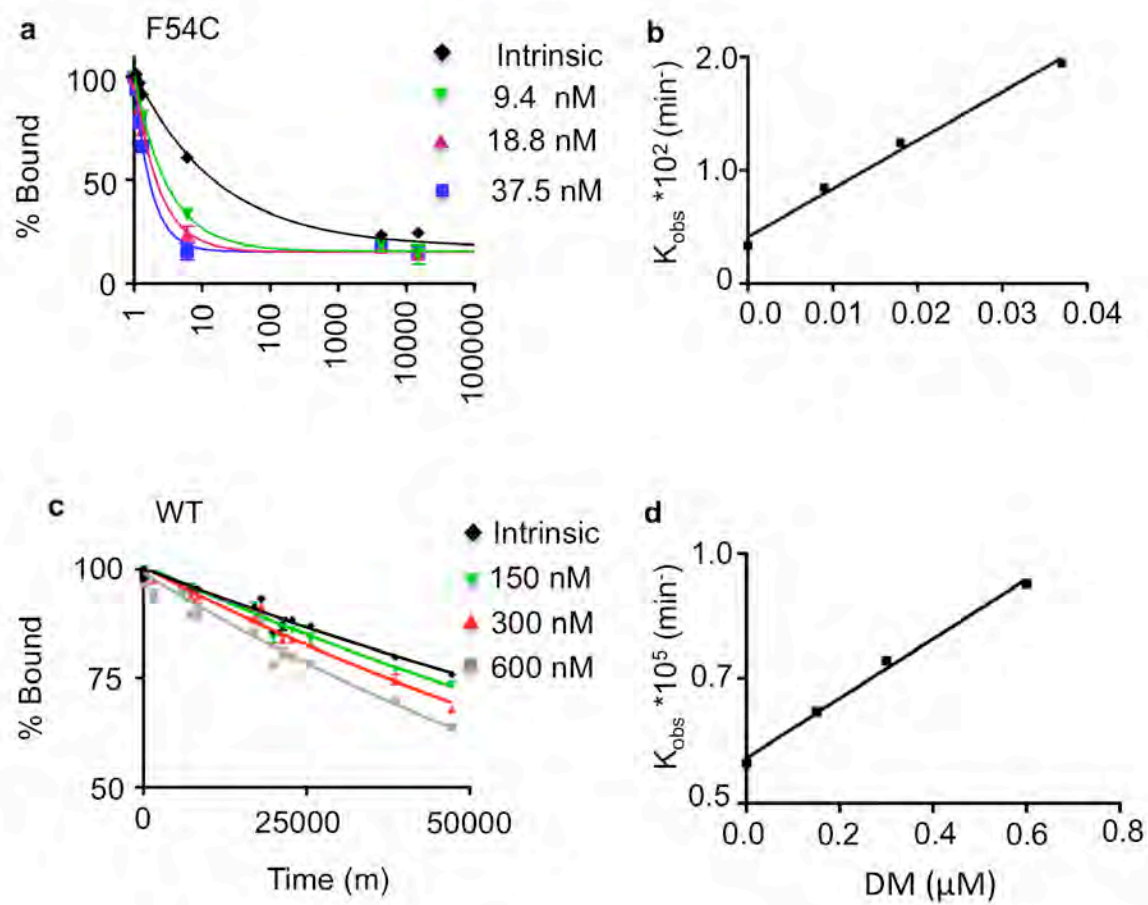
FIGURE 3.9. Kinetics of HA peptide release from WT and αF54C MHC II.

Peptide release assays performed by monitoring decay of polarization signal in the presence of unlabeled peptide with or without a dilution series of DM. Concentrations of DM are color and symbol coded. The linear dependence on DM for peptide release was plotted as K_{obs} against the concentration of DM.

Substitution of αF54 weaken MHC-peptide hydrogen bonding interactions

In previous work, it was shown that disruption of key hydrogen bonds in the vicinity of the P1 pocket by chemical modification led to augmented DM susceptibility (Stratikos, Wiley et al. 2004). Coupled with our observation that the αF54C mutation greatly increased DM susceptibility, we hypothesized that this substitution altered the peptide-MHC II hydrogen bond network. We determined the effect of the αF54C mutation on the overall hydrogen bond network and mapped changes to individual hydrogen bonds using the HDx/MS/MS approach outline above for the WT-HA complex. The amplitudes of the unresolved initial H/D-exchange phases are the same for both WT and αF54C (Fig 3.10 b). The fast phase amplitudes also are similar for WT and αF54C, as are the respective half-lives for this phase (Table 3.1). However, the slow phase of HDx is significantly different for αF54C and WT with half-lives of 1.8 and 18.1 hrs, respectively (Table 3.1). The enhanced rate of hydrogen exchange into the bound peptide for αF54C indicates weakened MHC II-peptide hydrogen bonding and increased structural dynamics leading to increased exposure of several peptide amide NH groups.

In order to resolve the particular amide NH groups involved in each phase, we employed ETD/MS/MS as outlined above for the WT-HA complex. Overall the pattern of deuterium incorporation is similar for αF54C as for the WT-HA complex (Fig. 3.10c), however, the relative strengths of the Y_3 and V_4 hydrogen bonds,

FIGURE 3.10
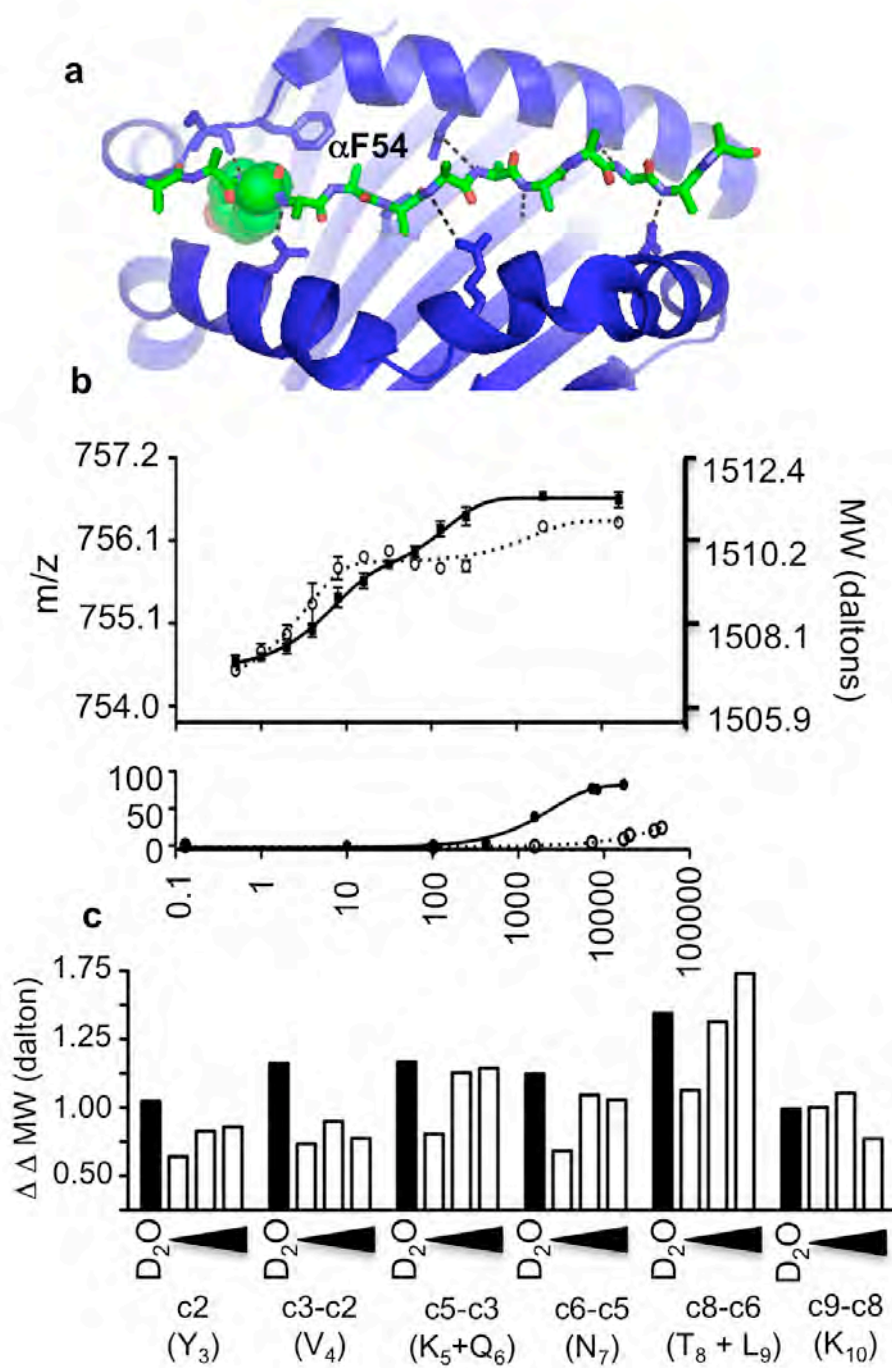
FIGURE 3.10. Mutation of αF54 alters the H-bonding properties between the MHC II and peptide. (a) Cartoon representation of the peptide binding groove with αF54 shown in stick, in addition to other conserved MHC II residues that participate in the H-bond network to the peptide backbone. The P1 tyrosine side chain is shown as spheres. (b) Hydrogen deuterium exchange assay (top) Average mass for HA peptide was determined at various time points as a fraction of total deuterium incorporation for free HA. HA bound to αF54C is shown as a solid line and that bound to WT is dotted. Both sets of data were fit to a two phase exponential association model. (d) Peptide dissociation assays were performed by measuring the decay of polarization fro alexa-488 labeled HA peptide from pre-bound complex. (c) Deuterium incorporation for each amine group along the peptide backbone for different times of incubation in D_2O. The Y axis represents the change in molecular weight for the unexchanged ion (ΔMW), which is then subtracted between sequential ion fragments in order to obtain the amount of deuterium incorporation of each amide at that time point ($\Delta\Delta MW$). Black bars represent the fully exchanged ion fragment in D_2O, and the open bars represent an increase in time, with triangles representing 2, 218 and 512minutes. The c-series sequential ions and the corresponding amine group are indicted below

which are on either side of the alpha 54 position (Fig. 3.10a), exchange faster

than for the WT-HA complex (Fig. 3.10c; Fig 3.11) For the WT-HA complex,

these hydrogen bonds represent the most stable of the interactions, and would

be expected to correspond to those most important in determining the overall

peptide-MHC lifetime. Our results suggest that the αF54C mutation disrupts

these key hydrogen bonds in the N-terminal region of the peptide binding groove.

Substitution of αF54 dramatically increases binding to DM

We hypothesized that the disruption of the hydrogen bond network by the

αF54C substitution and its greater DM susceptibility would be accompanied by

increased MHC II-DM binding affinity. We tested this idea using surface plasmon

resonance. Because the physiological MHC II-DM interaction occurs at low pH in

endosomal / lysosomal compartments, we performed binding experiments at pH

5.6. We immobilized peptide-free WT and each of the mutants, and measured

the binding of various concentrations of DM (Fig. 3.12). Specific, saturable, dose-

dependent binding was detected for both αF54 variants (Fig. 3.12b,c), but not for

WT (Fig. 3.12a) αS53A (Fig. 3.12e), αQ57C (Fig. 3.12d), or αF51A (Fig. 3.12f).

Equilibrium binding analysis revealed $K_{d,app}$ values of 0.5 µM and 0.7 µM for

αF54A and αF54C, respectively (Fig. 3.12g).

We performed several experiments to verify the specificity of the tight

binding observed for αF54A and αF54C to DM. First, we observed substantially

FIGURE 3.11

F54C HA

c3

c6

H₂O

2 min

218 min

512 min

D₂O

Intensity

m/z
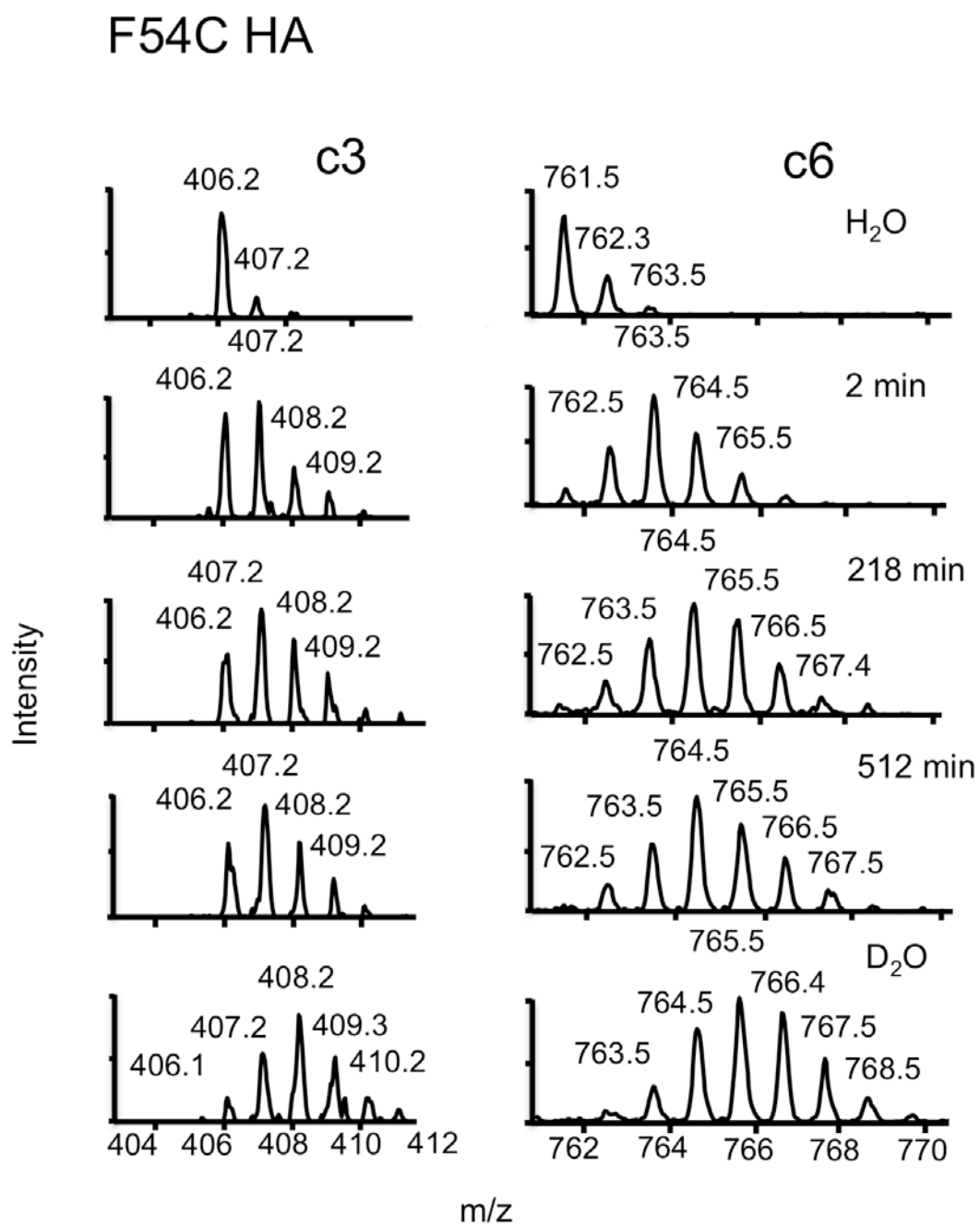
FIGURE 3.11. αF54C ETD representative data. Representative ETD data for HA alone in H2O, D2O or in various states of protection by the αF54C MHC II. The C3 (left) and the C6 (right) ion series are shown.

a WT

RU 30 20 10 0 -10

DM
MHC II

b αF54A

c αF54C

2.5 μM
0.0 μM

d αQ57C

RU 20 10 0 -10

e αS53A

f αF51A

0 250 500 750

g

RU 30 20 10 0

αF54C
αF54A

K_D 0.7 μM
K_D 0.5 μM

b/f

b

0 1 2 3
μM DM

h αF54C

800

400

0

0 400 800
Time (s)

i WT

pH 5.6
pH 7.0

0 400 800
Time (s)

j

RU 300 200 100 0 -100

DM

0 200 400 600

1500 1000 500 0 -500

LB3.1

0 150 300 450
Time (s)

300 200 100 0 -100

DM

0 200 400 600

k αF54C-CLIP

RU 100 75 50 25 0

300 nM
0.0 nM

0 500 1000
Time (s)

l WT-CLIP

100 75 50 25 0

300 nM

0 500 1000
Time (s)

m αF54C-CLIP

100 80 60 40 20 0

K_D 0.13 uM

b/f

b

0 0.1 0.2 0.3 0.4
DM (μM)

FIGURE 3.12. SPR analysis of αF54C/αF54A binding to DM. (a-f) Various

concentrations of DM were flowed over immobilized WT and mutant MHC II. Only

the 2.5 μM DM concentration is shown for αQ57C, αS53A, and αF51A. At the

concentrations tested, binding was observed only for αF54C and αF54A. (g)

Equilibrium analysis of values obtained from DM binding to immobilized αF54C,

circles, and αF54A, triangles, with Scatchard plot shown as inset. .(h,i) 10uM DM

was injected over immobilized αF54C (h) or WT (i) at pH 7.0, solid line, or at pH

5.6, dotted line. Binding for αF54C was greatly reduced at higher pH and no

binding was detected for WT at either pH tested. (j) Blocking experiment showing

DM (5 μM) binding to immobilized αF54C-CLIP (left panel), followed by anti-MHC

antibody LB3.1 (center) and subsequent diminishment of DM (5 μM) binding. (k,l)

Equilibrium analysis of αF54C-CLIP (k) or WT-CLIP(l) binding to immobilized

DM. (m) Equilibrium analysis of values obtained from αF54C binding to

immobilized DM, with Scatchard plot shown as inset.

reduced binding of DM to immobilized αF54C at pH 7.0 relative to pH 5.6 (Fig. 3.12h), consistent with known pH dependence of the interaction (Ullrich, Doring et al. 1997). We did not observe binding of DM to WT at either pH (Fig 3.12i) Second, binding was abrogated by preincubation with a monoclonal antibody (LB3.1) specific for a conformational epitope on MHC II (Fu and Karr 1994) near the presumptive DM binding interface (Doebele, Busch et al. 2000) (Fig 3.12j). Finally, DM binding was observed also for CLIP peptide complexes of αF54C but not WT (Fig. 3.12k,l,m).

These results indicate that αF54 substitutions, which increase sensitivity to DM-mediated peptide release, also increase the binding affinity for DM.

The crystal structure of αF54C-CLIP shows a conformational change in the vicinity of a critical DM contact residue.

To investigate the structural basis for the altered hydrogen bond strengths, the increased DM susceptibility and the increased DM binding activity of αF54C in, we determined its 2.3 Å crystal structure in complex with the CLIP peptide (Table 3.4). For comparison, we also determined the 2.7 Å crystal structure of WT bound to CLIP, using crystals that were obtained from streak seeding with αF54C crystals. In this way, we were able to obtain a nearly isomorphous data set for WT-CLIP in the same unit cell as αF54C-CLIP. Previously determined crystal structures for WT-CLIP differed in unit cell and crystal packing

123

TABLE 3.4. Data collection and refinement statistics (molecular replacement)

	F54C_CLIP	WT_CLIP
Data collection		
Space group	$P2_12_12_1$	$P2_12_12_1$
Cell dimensions, a, b, c	65.001, 94.870, 154.090	65.290, 95.840, 151.629
Resolution (Å)	50.0 – 2.3 (2.38-2.30)*	50 – 2.7 (2.75-2.70) *
R_{merge}	6.9 (41.0)	12.5 (40.2)
I / sI	31.6 (4.8)	19.8 (4.1)
Completeness (%)	100 (100)	99.9 (99.5)
Redundancy	7.4 (7.5)	7.0 (6.8)
Refinement		
Resolution (Å)	44.0 – 2.3 (2.38-2.30)	38.6 – 2.7 (2.75-2.70)
No. unique reflections	43,063	26,411
R_{work} / R_{free}	18.9/22.1	19.3/23.5
No. atoms	6751	6419
Protein	6374	6253
Water	487	166
Main Chain B-factors		
ab (mol1)	16	28
peptide (mol1)	16	33
ab (mol2)	22	27
peptide (mol2)	32	34
Waters	20	23
R.M.S.D.		
Bond lengths (Å)	0.004	0.002
Bond angles (°)	0.82	0.63
R.M.S.D. NCS		
a1b1 pep domain	0.62	0.46
a2 domain	0.56	0.32
b2 domain	0.31	0.21

(Gunther, Schlundt et al.). For the structures reported here, both WT and αF54C crystal structures have 2 molecules in the asymmetric unit. For the WT-CLIP structure, both molecules (blue and green in Fig. 3.13a-e) overlay with no major deviations in RMSD except for an exposed loop near βP108 that shows large RMSD deviations between most MHC II structures solved to date. Overall the structure of αF54C (purple and red in Fig. 3.13a-e) was very similar to WT, except for a region proximal to the αF54C mutation (indicated by carets in Fig. 3.13b,f), for which large differences were observed specifically in one of the two molecules in the asymmetric unit (Fig. 3.13f-i). Residues in an altered conformation include the region around αM36, in the loop between two strands of the beta sheet platform that forms the floor of the peptide binding site, the short 3_{10} helix encompassing residues αL45 to αF50 at the edge of the binding site, and the extended stand region, αF51-αF54C.

The conformational changes involving the αL45 to αF51 region of molecule 2 of αF54C can be seen in the ribbon diagrams shown in Figure 3.14a-c. The conformational change results in a ~20° reorientation of the short 3_{10} helix, together with a partial unwinding towards a more canonical alpha-helical pitch (compare Fig. 3.14b,c). These changes are accompanied by a concerted set of rotamer changes in residues that surround the P1 pocket. In addition to a reorientation of the αF51 residue, a large change is observed for αF48, which

FIGURE 3.13

126
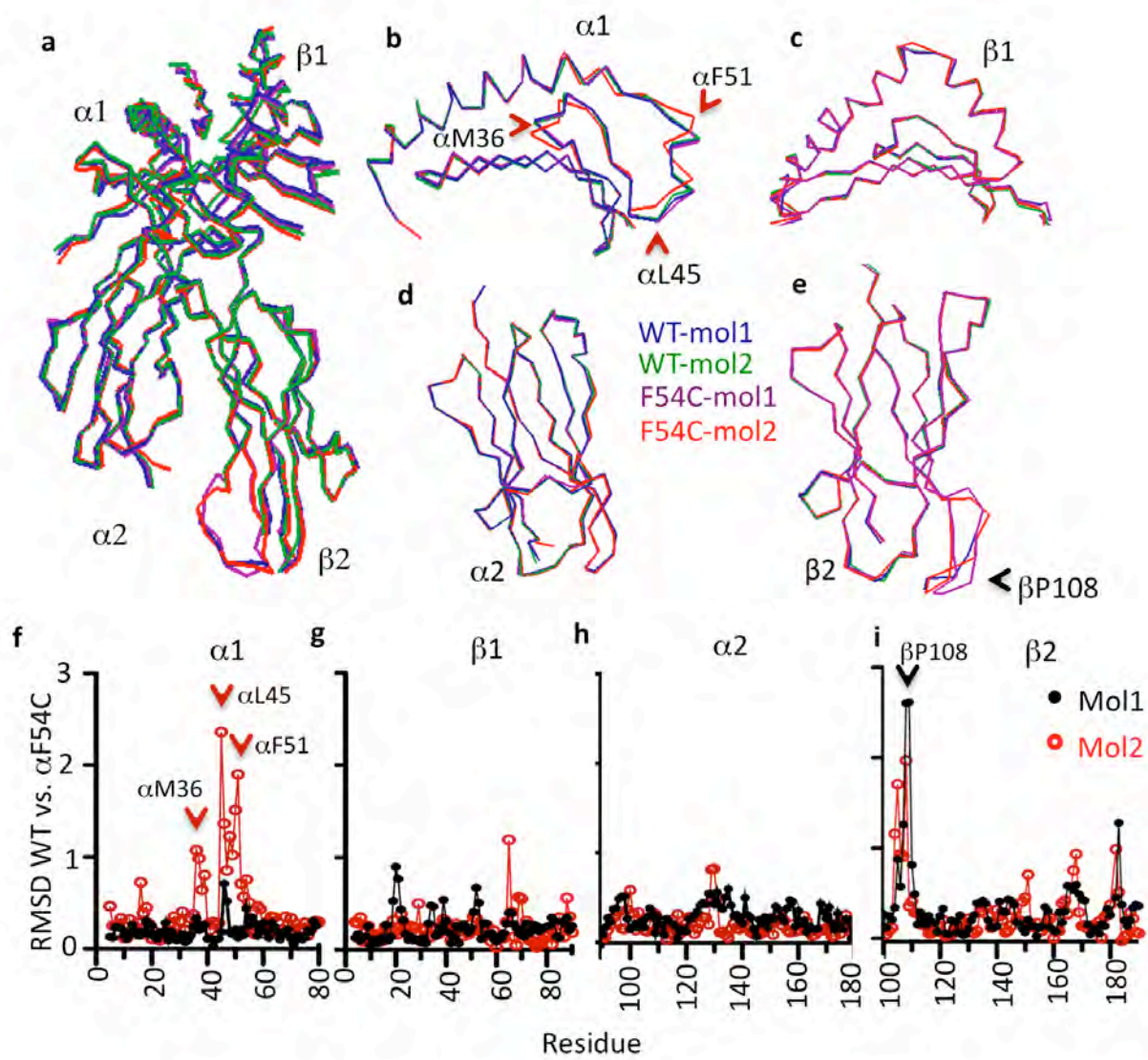
FIGURE 3.13. An altered conformation of the 3$_{10}$ helix and adjacent strand region for one molecule in the asymmetric unit of the αF54C structure. (a-e) Structure alignment of C-alpha traces of WT and αF54C, with molecules 1 and 2 of WT in blue and green, and molecules 1 and 2 of αF54C in purple and red. (a) Alignment of entire protein for all of the molecules. (b-e) Individual domain alignments for all of the molecules, (b) The α36-α54 region of αF54C shows a deviation from the other molecules when the alpha 1 domains are aligned. (c-e) The β1 and α2 domains do not show any significant deviations between WT and αF54C, although the β2 shows deviations around the βP108 position. Carets indicate residues that undergo significant deviations. (f-i) Main chain RMSD values after alignment of the individual domains comparing the WT to the αF54C; black, Mol1 of WT is aligned with Mol 1 of the αF54C, red, Mol2 of the WT structure is aligned with Mol2 of the αF54C structure. Carets indicate residues with the largest RSMD between WT and αF54C. The βP108 region is a partially disordered loop and shows deviations in both WT and αF54C.
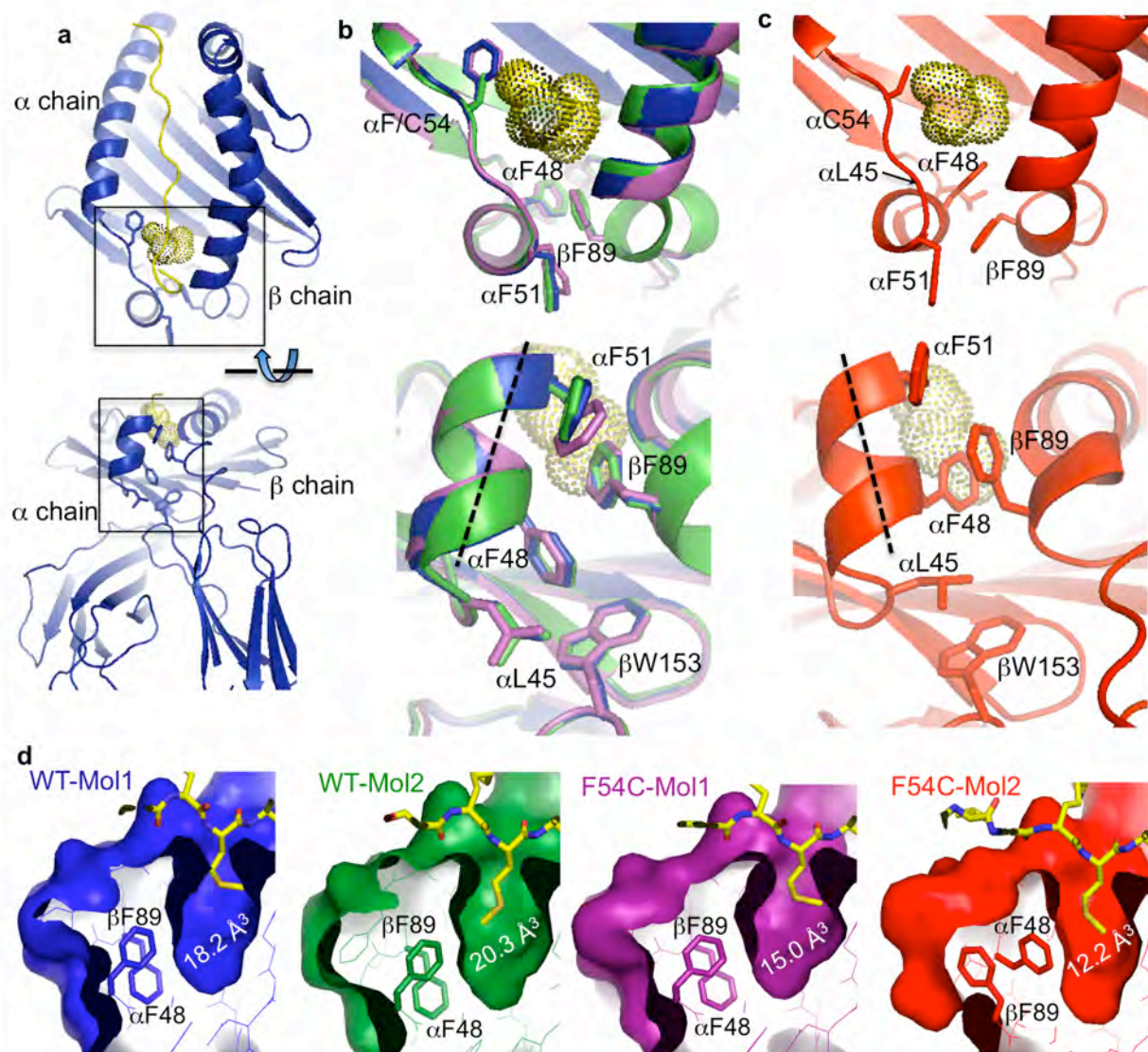
FIGURE 3.14

FIGURE 3.14. X-ray crystal structures of WT and αF54C bound to the CLIP peptide. (a) *Top panel*, ribbon diagram of WT peptide binding groove with CLIP peptide shown in yellow. The peptide M91 side chain which occupies the P1 pocket is shown in dots, top view. *Bottom panel*, 90° rotation showing the end-on view of the WT structure. Boxes indicate regions expanded in (b-c). (b) *Top panel*, overlay of WT mol1 (blue), WT mol2 (purple) and αF54C mol1 (green) with M91 side chain shown in dots, residues αF48, αF51 and β89 shown in sticks. *Bottom panel,* 90° rotation showing this region with the additional residues αL45 and βW153. Dotted line represents helical axis. (c) αF54C mol2 (red) shown with the same alignment as molecules in panel (b). (d) Surface representation of the P1 pockets for (a) WT mol1 (blue) WT mol2 (green) αF54C mol1 (purple) αF54C mol2 (red) with calculated surface area shown below the methionine residue engaged in the P1 pocket. Changes in the P1 pocket are mediated primarily by the rearrangement of residues αF48 and βF89, which are shown in sticks.

positions its side chain on the side of the P1 pocket, displacing βF89 which also

undergoes a rotamer change placing it more distal from the P1 pocket. The

largest change is seen at αL45, which moves to contact with the βW153,

replacing the contact normally made by the αF48 side chain. The

rearrangements of αL45, αF48, and βF89 resulted in changes in the shape and

volume of the P1 pocket (Figure 3.14d).

The conformational changes in the 3_{10} helix and adjacent strand region

appear to be due to a crystal contact at the αF51 position in molecule 2 of the

asymmetric unit (Fig. 3.15). The contact is observed for both WT (Fig. 3.15a) and

αF54C (Fig. 3.15b), but only in the mutant is the conformational change induced.

These changes result in lowered B-factors for the 3_{10} helix and adjacent strand

region relative to the remainder of the $\alpha1\beta1$ peptide-binding domain (Fig. 3.16).

However, B-factors for the bound peptide increase as a result of the

conformational change (Fig 3.16). The αF51 position is known to be critical

determinant for DM binding and activity (Doebele, Busch et al. 2000), and

contact with another molecule at the αF51 position may simulate the effect of a

contact at this position with DM, thus providing a model where changes resulting

in weaker MHC-peptide interactions may lead to peptide release.

FIGURE 3.15
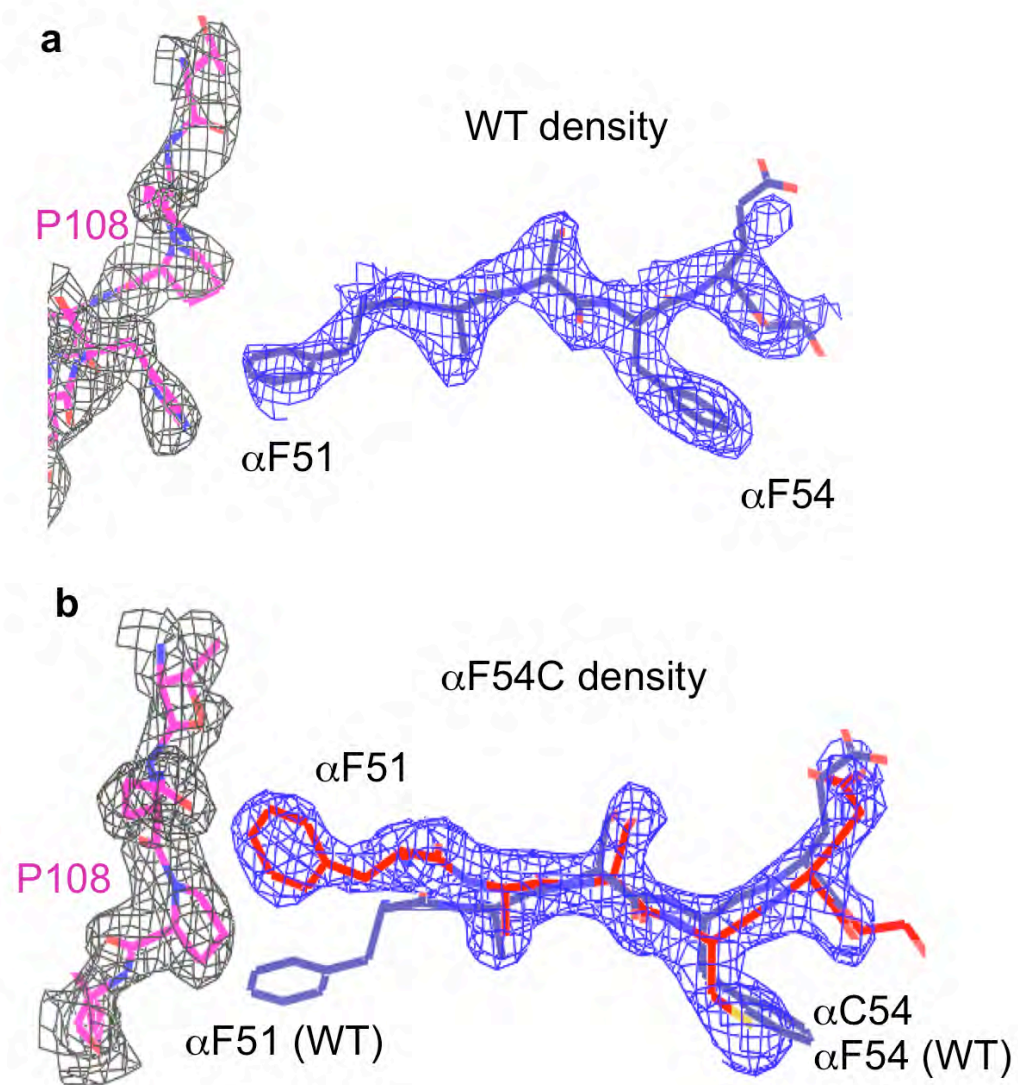
FIGURE 3.15. Conformational change in αF54C Mol2 is induced by a crystal contact at αF51, whereas a similar contact in WT has no effect. (a) 2|Fo-Fc| omit electron density (blue) contoured at 1σ and stick representation model (blue) for WT mol2. A crystal contact at the αF51 residue is made by a residue (P108) from the β2 domain of another molecule in the crystal, shown with grey density and pink model in stick representation. The αF54 position is noted. (b) Density (blue) and model (red) for the F54C mol2, contoured as in panel (a). The αC54 position is noted. The blue model for WT is shown aligned to the αF54C mol2 structure.

FIGURE 3.16

WT Mol 1

αF54

B-factor
Range (Å²)
α45-56 (33)
α1β1   (28)
Peptide (32)

F54C Mol 1

αC54

B-factor
Range (Å²)
α45-56 (29)
α1β1   (16)
Peptide (16)

WT Mol 2

αF54

B-factor
Range (Å²)
α45-56 (33)
α1β1   (27)
Peptide (34)

F54C Mol 2

αC54

B-factor
Range (Å²)
α45-56 (23)
α1β1   (22)
Peptide (32)
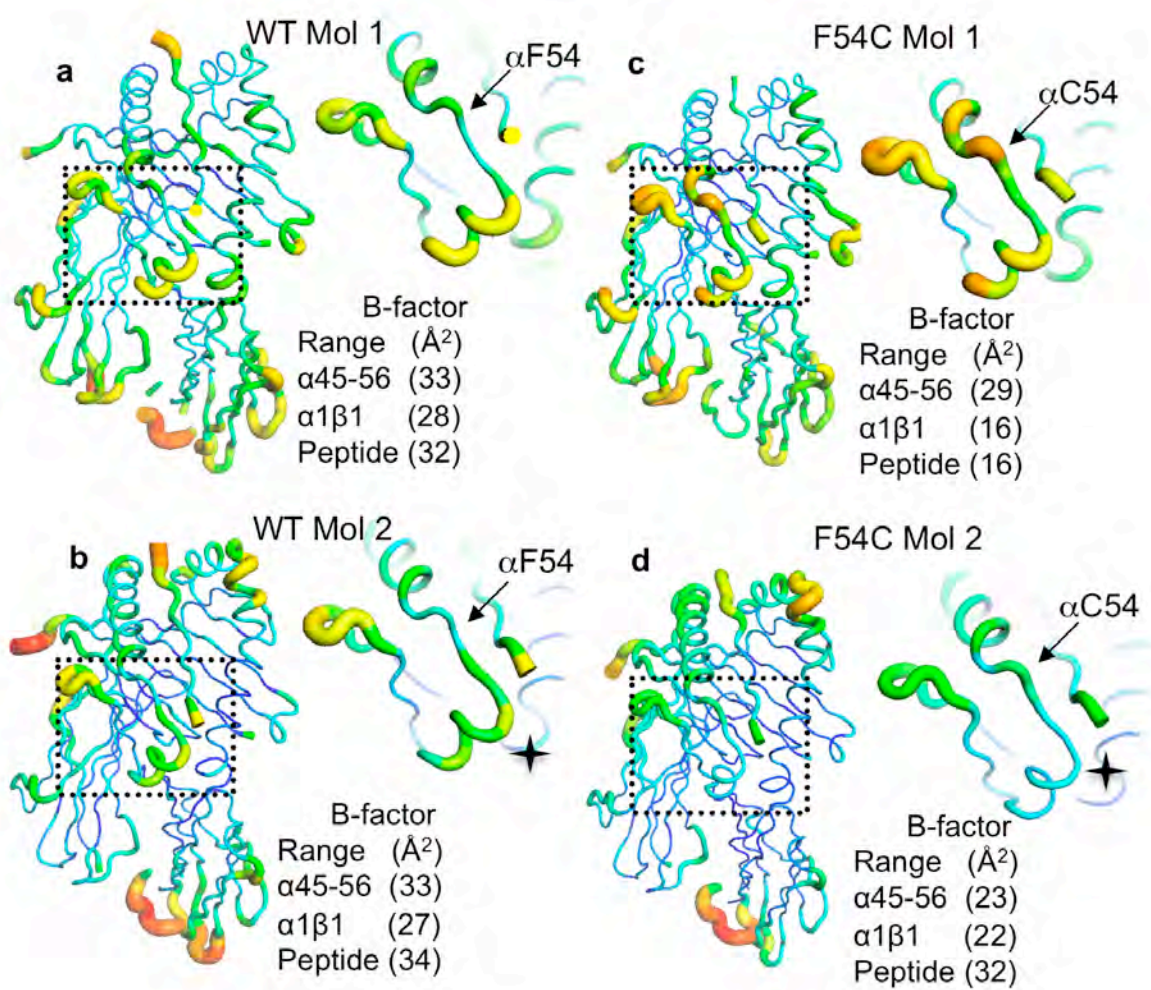
FIGURE 3.16   Crystal contact induced stabilization of αF54C Mol2 but not

WT Mol2 (a-d) B-factor putty representation, with red representing regions with

highest B-factors and blue showing regions with lowest B-factors, shown for both

molecules in the αF54C structure (a-b) and the WT structure (c-d), boxed region

is shown enlarged. The average main chain B-factors for residues α45-56, the

α1β1 domain and the peptide are shown for each molecule. The crystal contact

at αF51 is depicted by a black star for αF54C mol2 (b) and WT Mol2 (d).

DISCUSSION

Substitution of αF54 in the MHC II extended strand region of the peptide binding site results in a protein with greatly increased susceptibility to DM-mediated peptide release, increased DM-binding affinity, and increased MHC-peptide dynamics. The crystal structure of the αF54C mutant is very similar to that of the WT protein, with the exception of a set of conformational alterations near the N-terminus of the bound peptide involving the reorientation of the (α45-50) 3_{10} helical region, the (α41-54) adjacent extended strand as well as changes in the (α39-44) region; adoption of the altered conformation is dependent on contact of αF51, a known DM-MHC II contact site (Doebele, Busch et al. 2000). The increased DM binding and susceptibility to DM-mediated peptide release observed for the αF54C/αF54A mutations are likely to be due to conformational alterations induced proximally as a result of loosening the interaction between the extended strand and the rest of the MHC-peptide complex, as opposed to direct interaction with the α54 residue, which is buried in both conformations and also in the wild-type protein. These observations suggest that this mutation allows the MHC II to adopt a DM-receptive conformation.

Several factors indicate that the conformation observed in the αF54C mutant can be adopted by WT and is relevant to DM-mediated peptide exchange. Modeling studies of MHC II suggest that the N-terminal side of the peptide binding site undergoes conformational alteration concurrent with peptide

135

release (Nojima, Takeda-Shitaka et al. 2003; Gupta, Hopner et al. 2008; Painter, Cruz et al. 2008) (Yaneva, Springer et al. 2009). In a molecular dynamics simulation of peptide-free MHC II (Painter, Cruz et al. 2008), we observed changes strikingly similar to those observed in the αF54C structure determined here, in particular, a change in pitch and partial unwinding of the 3_{10} helix and concerted rotamer changes of αF51,αF45, αF48 and βF89 (Fig. 2.5, 3.17). The P1 pocket, a locus of conformational change in molecule 2 of the αF54C crystal structure, is known as a key determinant of MHC II-peptide interaction (Stern, Brown et al. 1994; Zarutskie, Sato et al. 1999; Tobita, Oda et al. 2003) and has long been proposed by numerous groups to be involved in DM catalyzed peptide exchange(Anders, Call et al. ; McFarland, Beeson et al. 1999; Chou and Sadegh-Nasseri 2000; Stratikos, Mosyak et al. 2002; Pashine, Busch et al. 2003; Nicholson, Moradi et al. 2006; Narayan, Chou et al. 2007; Davies, Lamikanra et al. 2008) (Mosyak, Zaller et al. 1998). Finally, the α39-44 strand, which also rearranges in molecule 2 of the αF54C structure, carries two other residues in addition to αF51 implicated in DM-MHC II contact, αE39, which was identified in a random screen as a residue important in mediating DM's functional effect (Doebele, Busch et al. 2000), and αW43, which was identified by mutagenesis as important in DM-DR binding (Anders, Call et al.). Thus, the altered conformation observed in the crystal structure of molecule 2 of αF54C provides a structural explanation for the involvement of the regions previously implicated in DM-mediated catalysis.

FIGURE 3.17

Stable MHC-peptide complex

Peptide-free MHC conformation

DM

DM receptive conformation
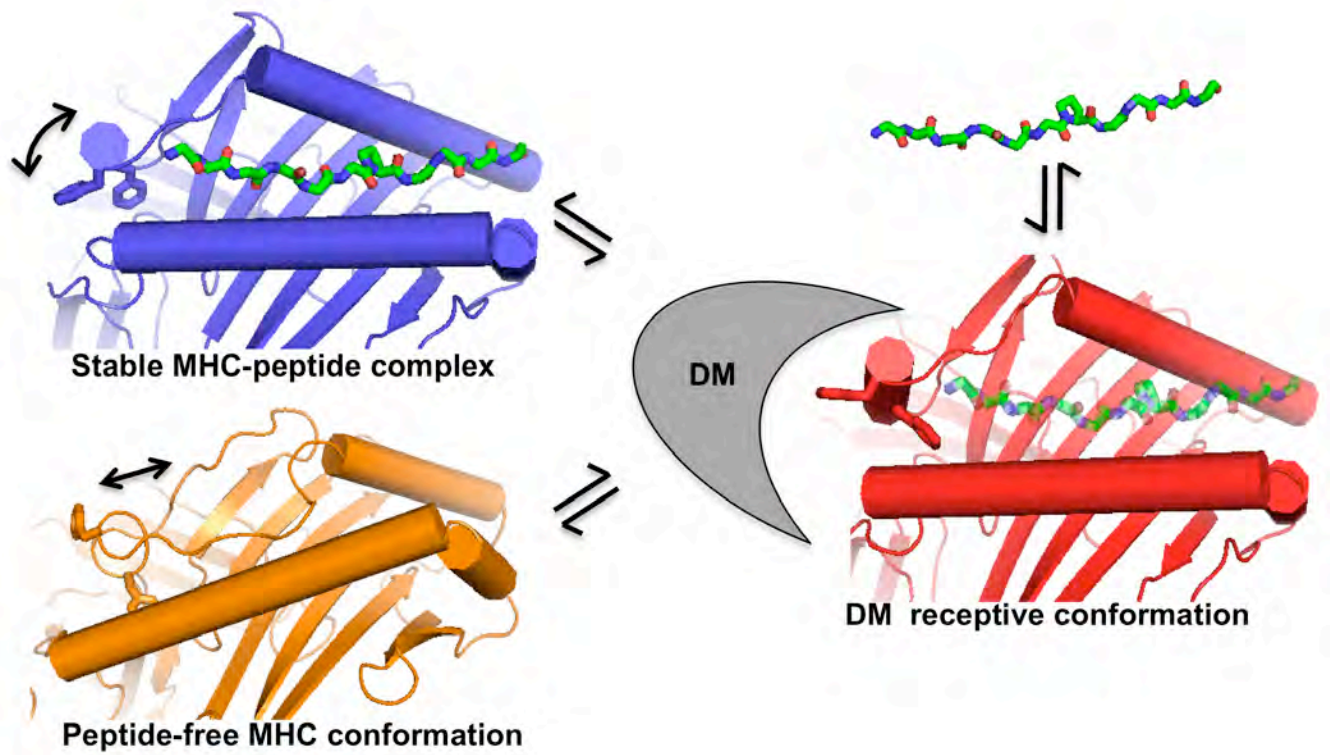
FIGURE 3.17. Model of peptide free WT molecular dynamics simulation shows similar motion in key residues involved with α**F54C-CLIP conformational change.** Top left shows N-terminal region of the simulation starting model with residues αF48, αF51 and β89 shown in sticks. Bottom left; 90° rotation showing the orthogonal view of this region with the additional residue αL45. Right panels show the same view but after a 20ns molecular dynamics simulation. The dotted lines represent the trajectory of the 3_{10} helical region before (left) and after (right) the simulation

How does substitution of αF54 lead to changes in the 3_{10} helix and flanking strands? The principal contact between the extended strand region α51-54 and the remainder of MHC II is with the αF54 side chain, which lodges in a small hydrophobic cluster with αW43 and other aromatic side chains forming the side of P1 pocket. The side chain of residue αF54 appears to act as an anchor for the extended strand region. Except for main-chain hydrogen bonds formed with the peptide, the extended strand does not otherwise interact with the rest of MHC II, and so replacement of the phenylalanine side chain with alanine or cysteine would facilitate motion of that region. The nature of the structural changes in the entire α39-54 region, and the reduced B-factors for this region in the altered conformation, suggest that it represents a stable alternative conformation. In support of the hypothesis, MHC II proteins that contain glycines at the alpha 52 and 53 positions (G/G) can adopt stable alternate conformations in the 3_{10} helix and adjacent strand region. HLA-DQ alleles are the only such MHC II proteins to contain the G/G motif and therefore may represent a subset of MHC II proteins that have increased lability within the 3_{10} helix and extended strand region. Interestingly, the HLA-DQ2 allele has a deletion at the Serine 53 position is resistant to DM mediated peptide exchange, suggesting that alterations within the extended strand region can influence DM susceptibility (Fallang, Roh et al. 2008).

Notably, the H/D exchange experiments show that several hydrogen bonds are weakened by the αF54C mutation, indicating a global destabilization

of peptide-MHC II interaction. This result is consistent with the crystal structure, for which increased B-factors were observed all along the length of the peptide for molecule 2 of αF54C. Thus, the functional effect of the mutation extends beyond the region immediately adjacent to the αF54 mutation. Cooperative changes along the length of the peptide previously have been associated with DM function (Ferrante and Gorski).

A model for how this conformation might function as an intermediate state in the DM-mediated peptide release pathway is shown in Figure 3.18. In this model, interaction of DM with the MHC II-peptide complex stabilizes a conformation with decreased MHC-peptide hydrogen bonding and rearrangements in the crucial P1 pocket (Fig. 3.18 red). These structural alterations lead to reduced MHC II-peptide binding affinity and facilitated peptide release. DM interaction with this intermediate form persists until binding by a peptide with sufficiently high affinity is able to shift the equilibrium back towards the original MHC II-peptide conformation with release of DM (Fig. 3.18 blue). If an exchange peptide were not available, DM dissociation would lead to formation of the peptide-refractive empty conformation (Fig. 3.18 orange). Thus the mechanism provides a potential role for a "push-off" peptide, recently suggested to be required for DM function (Ferrante, Anderson et al. 2008) Computational studies suggest that the conformation of the peptide-free protein has additional alterations at the N-terminal end of the binding site (Nojima, Takeda-Shitaka et al. 2003; Gupta, Hopner et al. 2008; Yaneva, Springer et al. 2009), with the

Peptide-free start model

Peptide-free 20ns model

FIGURE 3.18. Model for the DM receptive conformation as an intermediate between the stable MHC II-peptide complex and the peptide-free MHC II protein. Top view of the peptide binding groove, with helices shown as cylinders, and peptide main chain and αF51 and αF48 side chains shown in stick. Stable MHC II-peptide complex (blue), from crystal structures MHC II-peptide complexes, with arrow denoting motion of the αF51 and 3_{10} helical region. DM receptive conformation (red), from Mol2 of the αF54C structure. DM is shown as a cartoon surrounding the putative MHC II binding region at the N-terminal side of the binding site. Peptide exchange is facilitated in this form. Peptide-free conformation, from molecular dynamics simulation model of the peptide-free MHC protein (Painter, Cruz et al. 2008). Arrow indicates movement of the entire αF51 to αG57 strand region postulated to be involved in the conversion to the peptide-refractive MHC II conformation (Painter, Cruz et al. 2008).

extended stand region occupying part of the canonical peptide binding site (Painter, Cruz et al. 2008), creating a peptide refractive state. In the model shown in Figure 3.18, association with DM would reverse these interactions, providing a structural explanation for DM's chaperone function (Kropshofer, Arndt et al. 1997; vogt, Moldenhauer et al. 1997) . Whether or not peptide is released, partially bound, or fully bound in the DM-associated intermediate complex is not yet clear. Recently, a model has been put forward for the DM –mediated peptide release mechanism based on DM binding of HLA-DR2 variants, in which spontaneous release of peptide from the P1 pocket facilitates DM interaction (Anders, Call et al.). In contrast, in the αF54C-CLIP complex reported here, the P1 pocket is fully occupied, and there are other structural changes including the 3_{10} helix and adjacent strand regions that appear to facilitate DM interaction. Numerous studies (Natarajan, Stern et al. 1999; Sato, Zarutskie et al. 2000; Tobita, Oda et al. 2003) suggest the P1 anchoring residue, for the alleles used therein, disproportionately stabilize the peptide within the groove. It is plausible that covalently bound MHC II-peptide complexes used within that study induced conformational changes within the MHC II that were not explored through the binding assays employed to develop the spontaneous release model Nonetheless, additional studies will be required to fully elucidate the peptide occupancy of the DM-MHC II complex.

A detailed molecular understanding of the DM mediated peptide exchange mechanism has been elusive due to the lack of a structural model that

encompasses the dynamic interactions between DM and MHC II. The structures reported here describe the first characterization of conformational changes involved in peptide exchange by DM, and provides a struct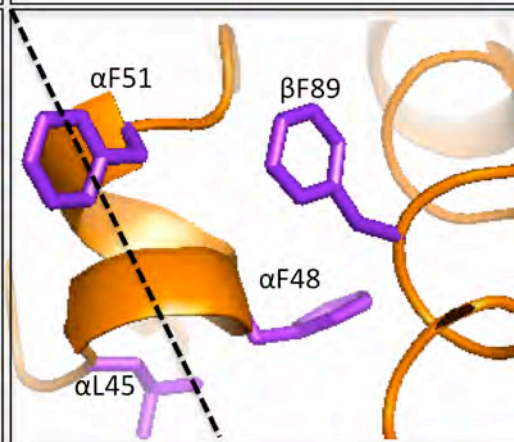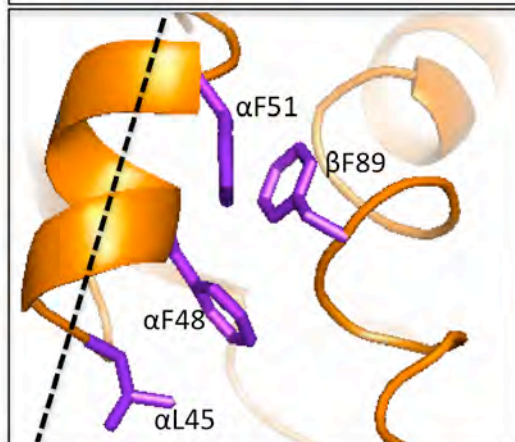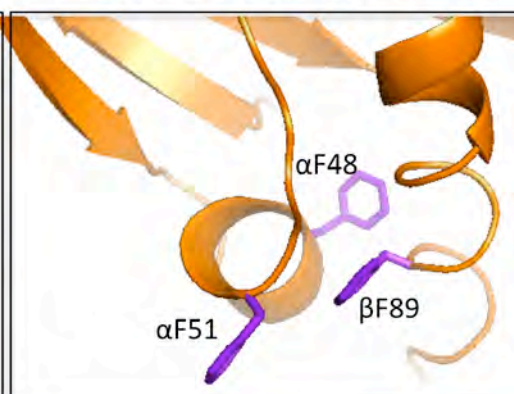ural model for the DM-receptive conformation of MHC II intermediate between a stable MHC II-peptide complex and the peptide-free conformation.

Acknowledgments

Author Affiliations

Department of Pathology, University of Massachusetts Medical School, Worcester, Massachusetts

Maria P. Negroni, Lawrence J. Stern

Department of Biochemistry and Molecular Pharmacology, University of Massachusetts Medical School, Worcester, Massachusetts

Corrie A. Painter, James E. Evans, Lawrence J. Stern

Department of Chemistry, University of Puerto Rico, Rio Piedras, San Juan, Puerto Rico

Zarixia Zavala-Ruiz

Bruker Daltonics, Billerica, MA

Katherine A. Kellersberger

Accession Codes

RCSB064219; RCSB064222

METHODS

Mutagenesis of plasmid DR1

Point mutations were introduced into the alpha and beta chains of the MHC II allele, HLA-DR1 (DRA*0101, DRB1*0101) using the QuickChange site-directed mutagenesis system (Stratagene). For each engineered mutation, a pML1 plasmid vector (Frayser, Sato et al. 1999) containing either the alpha or beta chain of HLA-DR1, was used as a template, and primers designed to introduce the desired mutation were annealed and subsequently extended by temperature cycling using PfuUltra DNA polymerase. The parent DNA template was digested using Dpn1 endonuclease, and the engineered plasmids were then transformed into XL1-Blue competent cells. The sequence of the entire mutant gene was confirmed before plasmids were transfected into *E. coli* BL21(DE3) pLysS cells for expression. Primers were designed using the web based program PrimerX (www.bioinformatics.org/primerx/index.htm).

Protein production

The extracellular domains of the recombinant HLA-DR1 alpha and beta chains were individually expressed in *Escherichia coli* inclusion bodies, isolated by denaturing ion exchange chromatography, and refolded i*n vitro* as previously described (Frayser, Sato et al. 1999). Refolded HLA-DR1 was purified by immunoaffinity chromatography using protein-A coupled conformation-specific anti-HLA-DR1 antibody LB3.1. Eluted protein was further purified by gel filtration (Superdex 200). The protein concentration was measured by UV absorbance at 280 nm using an extinction coefficient of 54,375 M^{-1} cm^{-1} for HLA-DR1.

HLA-DM expression and purification

The soluble DM molecules with FLAG tag (Busch, Pashine et al. 2002) were produced by and secreted from stably transfected *Drosophila* S2 cells and isolated by immunoaffinity chromatography from conditioned medium. Eluted DM complexes were further purified by size exclusion chromatography (Superdex S200).

Peptide labeling/purification

N-terminally acetylated HA peptide (Ac-PKFVRQNTLRLAT-OH) and CLIP peptide (Ac-VSKMRMATPLLMQ-OH) (21st century Biochemicals) were labeled with Alexa-488 tetrafluorophenyl ester (Molecular Probes) through primary

amines at position K2 for HA and K3 for CLIP. Labeled peptides were purified

from unreacted reagents and side products by reverse phase chromatography

(Vydak C18), and subjected to MALDI to confirm the correct molecular weight.

Polarization assays

Peptide complexes were prepared by incubation of WT or mutant MHC II (150

nM) with 25 nM Alexa-488 labeled CLIP for 3 days at 37°C in aluminum covered

96-well non-binding surface, black polystyrene assay plates (Corning) in 200 µl

binding buffer (100 mM Na citrate, 50 mM NaCl, 0.1% octyl glucoside, 5 mM

EDTA and 1 mM PMSF. Intrinsic dissociation reactions were initiated of bound

peptide was monitored after addition of 100-fold excess unlabeled HA peptide in

50 µl binding buffer and were followed using by fluorescence polarization at 488

nm excitation and 520 nm emission, using a BMG Polarstar plate reader. DM-

mediated peptide release was monitored using the same conditions with the

addition of a variable concentration of DM added to the incubation mixture. All

experiments were run in triplicate. Free Alexa-peptide, and unlabelled competitor

controls were included in each experiment; typical values were 30 mP and 300

mP respectively. Dissociation rate constants were determined by fitting data to a

single phase exponential decay model using Graphpad Prism. The rate

enhancement for peptide dissociation by DM was calculated as the slope of the

linear rate vs. DM concentration plot, and the DM-enhancement factor calculated

as this slope divided by the intrinsic (i.e. no DM) rate constant (Weber, Evavold

et al. 1996). Intrinsic rates estimated as the y-intercept of the rate vs. DM concentration plot were similar to the no DM values.

Surface plasmon resonance

All SPR experiments were carried out on a Biacore 3000 instrument using CM5 chips. Running buffer was 10mM sodium citrate pH 5.5, 150mM NaCl, 3mM EDTA and 0.05% (v/v) surfactant P20   Protein was immobilized by standard amine coupling using EDC and NHS to activate the carboxyl groups on the CM5 surface. In the standard ligand coupling procedure, excess activated dextran carboxylate groups are capped with ethanolamine. For surfaces capped this way we observed significant non-specific binding of DM at pH 5.5, presumably because of interactions with non-ionized carboxylic acids from the carboxydextran matrix (pKa ~5). Instead we capped with a different reagent, 2-amino-ethyl-sulfate, which maintains a negative charge at low pH, and observed low non-specific binding at pH 5.5.   Binding experiments were carried out using 2-fold dilutions of peptide-free WT or F54C flowed over immobilized HLA-DM at 30 ul/min. We used a 3 minute binding phase with kinetic injection parameters and followed by dissociation of complex in running buffer for 10 minutes. Regeneration of the DM coupled surface was carried out by flowing 50 mM CAPS pH 11.5 for 30 s until a stable baseline was reached. Binding interactions were fit to a heterologous binding model using BIAeval software.

Protein crystallography

 Crystals of αF54C CLIP complexes were grown at 4°C by hanging drop vapor

diffusion over 12% polyethylene glycol 4000, 100 mM sodium acetate (pH 5.6),

100 mM ethylene glycol, 5 mM DTT with drops containing 1 µl of well buffer with

1 µl of 8.5 mg/ml protein. WT crystals were obtained under the same conditions

by streak seeding crushed F54C CLIP crystals. For x-ray diffraction

experiments, we soaked crystal in a cryoprotectant (well buffer with 25%

ethylene glycol) for 30 seconds prior to flash freezing in liquid nitrogen.

Diffraction data for both the WT-CLIP and the F54C-CLIP, collected under cryo

conditions at the National Synchrotron Light Source (NSLS) on the x29 beamline

(λ=1.1 Å) from single crystals (WT: 0.1 x 0.05 x 0.05, F54C : 0.6 x 0.07 x

0.07mm) using a ADSC Q315 detector, were processed with HKL2000 (McCoy,

Grosse-Kunstleve et al. 2007). Initial phasing was obtained by molecular

replacement using Phaser (McCoy, Grosse-Kunstleve et al. 2007) with

coordinates from another HLA-DR1 structure (PDB code: 1PWY) as a search

model. Multiple rounds of refinement and building were carried out using Phenix

(Adams, Afonine et al.) and COOT (Emsley and Cowtan 2004).

Hydrogen /deuterium exchange

WT and αF54C were pre-loaded with HA peptide, buffer-exchanged into PBS pH

7.2 and concentrated to a final protein concentration of 55 µM. The exchange

assays were performed by diluting the MHC II-peptide complexes, or HA peptide alone, 1:10 into PBS in D_2O, followed by incubation at 25°C over the time course indicated in figure 6. At each time interval we quenched the reaction by diluting the exchange mixture 1:10 into 1M glycine pH 2.7 at 4°C. These conditions minimize the exchange of amide H/D. Samples were then flash frozen on dry ice and stored at -40° until we measured the deuterium incorporation of the peptide backbone amide nitrogens of the HA peptide by LCMS. All components of the LCMS in contact with the sample were chilled to 4° prior to data collection. Samples were thawed on ice and 5 ul was added to 5 ul ice cold buffer A (0.1% TFA in 2% ACN) and immediately injected by syringe into the on-line chromatography system. Chromatography was carried out using 2 Acclaim PepMap μ-precolumns (Dionex) in series. The first was a 1X15mm, C4 PepMap300 column connected in series to the second, a 1X15 mm C18 PepMap100 column. Mobile phase A, 0.1% TFA in 2% ACN, was flowing at 50 μl/min at the time of injection to capture the MHC-pep complex on the C4 column. The MHC-pep complex quickly dissociates in this solution, and the released peptide remain bound to the C4 column. The peptide is then rapidly eluted from the C4 column and partially retained on the C18 column by switching the mobile phase to 25% ACN (50 μl/min). The peptide is then eluted into the LTQ mass spectrometer for analysis. The LTQ was tuned in the +ESI enhanced mode with resolution on the HA peptide +2 ion by teeing 2 ul/ml HA into the flow stream. We scanned from m/z 450-1600 using capillary temperature 275.00 C°

and source voltage 4.5 kV. Spectra were acquired from m/z 450 to 1600 with a cycle time of ~1 sec corresponding to 10 summed microscans with the maximum ion time set at 200 ms. At each time point an average m/z value was calculated by summing each peak in the isotope distribution weighted by its relative abundance. Average mass values were converted to fractional HD exchange by reference to the average mass observed for unexchanged free peptide in the same experiment. Fractional HD exchange versus time curves were fit to a two-phase exponential rise equation using GraphPad Prism.

The expected isotope distribution for HA peptide was calculated from the atomic formula ($C_{69}H_{119}N_{18}O_{19}$) using Protein Prospector (http://prospector.ucsf.edu/prospector/mshome.htm). For calculation of the expected mass distribution under various conditions, the probability of H-D exchange at each of the 12 peptide main chain amide hydrogens was estimated using a binomial equation, which assumes equal probability of exchange at each position.

$$P(k)= n! / (k!*(n-k)!) * p^k * (1-p)^{(n-k)}$$

where $P(k)$ is the overall probability of finding k events in a total of n tries when each individual event has a probability of p. Here n=12 for the twelve amide positions, p=0.9 for exchange into 90% D_2O, and k is number of hydrogens exchanged.

Electron-transfer induced dissociation mass spectrometry

HA peptide from WT and F54C MHC II complexes, as well as free HA were subjected to hydrogen deuterium exchange and chromatography as outlined in the HDx methods section. For the ETD experiments, we chose 2, 218 and 512 minute time points for deuterium incubation of complexed peptide. Peptide was eluted off the on-line chromatography system and injected into an amaZon quadroploe ion trap intstrument. The ion trap was set to operate in positive ion mode. ETD data analysis: ETD spectra were processed using Bruker Daltonics software. The average mass of each of the ions was determined by calculating the intensity weighted average of the isotope envelope corresponding to each calculated ion species for the c and z generated fragments (protein prospector).

Chapter IV

Conclusions and future directions

The studies in this thesis were designed to address outstanding questions in the field of MHC II peptide presentation. Understanding the conformational variability inherent in MHC II proteins at various stages of the peptide loading process is critical to understanding the basic principles involved with peptide binding as well as for developing a model that can explain the catalytic action of HLA-DM. Utilizing computational, biochemical and structural studies, models of both the peptide free conformation of HLA-DR1 as well as a trapped intermediate in DM mediated peptide catalysis were generated.

Model for the peptide free MHC II

Chapter II of this thesis described a model for the peptide free conformation of the MHC II HLA-DR1. Using molecular dynamics simulation as well as experimental probes sensitive to the peptide occupancy of HLA-DR1, the peptide-free state of the molecule was investigated. The model developed from the simulation revealed novel conformational changes concentrated near the region surrounding the P1 pocket. Strikingly, these alterations in structure maintained the general shape and electrostatic environment of the entire peptide binding groove, and in particular, the P1 pocket. This structural "maintenance" was due to an unraveling of the alpha 50-59 region and subsequent movement into the peptide binding groove with the alpha F54 engaging the P1 pocket in a

similar manner as the original valine side chain of the peptide bound structure. In addition, the canonical hydrogen bonding network was recapitulated between the conserved residues of the beta chain with the unfolded alpha 50-59 region of the alpha chain that moved into the binding groove. Support for this model was generated using monoclonal antibodies as well as other MHC II binding proteins with epitopes on HLA-DR1 that were predicted to have altered accessibility due to the conformational changes induced upon peptide removal. There was good agreement with the binding of these probes to regions of HLA-DR1 that were predicted to undergo no change, moderate, or large changes based on the simulation model.

Previous work has shown that there is more then one conformation of peptide-free MHC II proteins. Kinetic studies have determined that there are peptide averse as well as peptide receptive conformations, with the peptide receptive form generated immediately upon peptide release slowly and reversibly converting to a peptide-averse state over a few minutes (Rabinowitz, Vrljic et al. 1998). However, detailed structural models of these states have not been defined. The model put forth in chapter II of this thesis presents a peptide free conformation, however whether this conformation reflects a peptide binding averse or receptive conformation is unknown. It is conceivable that this model represents an averse form and that the engagement of the P1 pocket by the αF54 as well as the "maintained" hydrogen bonded N-terminal peptide binding region occlude the groove from potential peptide binding events. It could also be

155

that this model represents the kinetically unstable peptide receptive conformation and that engagement of the hydrophic P1 pocket allows the structure to not collapse or be altered so that productive binding could occur in the presence of peptide.

Future studies designed to address the conformational differences between the peptide averse and receptive states, and whether the model put forth from the molecular dynamics simulation of the empty MHC II represents either of these kinetically described species are needed. One possibility would be to test the hypothesis that engagement of the alpha F54 into the P1 pocket blocks peptide binding, and therefore creates a peptide averse conformation. Mutation of the phenylalanine to an alanine would eliminate the anchor effect of the bulky hydrophobic side chain into the P1 pocket. Previous studies have developed methods for the assaying the fraction of peptide receptive and averse (Rabinowitz, Vrljic et al. 1998; Grotenbreg, Nicholson et al. 2007). Using peptide binding assays, the rate of peptide association could be measured both for freshly generated peptide free MHC II protein as well as for peptide free MHC II that was in an equilibrium state between averse and receptive. This would allow a comparison to be made between WT MHC II, theoretically able to form the F54 engaged averse conformation with a F54A mutant, which would be unable to form the same "stable" averse conformation. If the model represented a peptide averse conformation mediated by F54 engagement, we would expect to see a larger percent of the peptide receptive conformation in a F54A mutant.

In addition to addressing this hypothesis, further information regarding the nature of the conformational state of the peptide free MHC II could be ascertained by developing a panel of monoclonal antibodies directed against the alpha chain of HLA-DR1. In a similar manner to work that has been done on the beta chain, monoclonal antibodies raised against the denatured alpha subunit could be screened for differential reactivity for peptide loaded and peptide free HLA-DR1 (Carven, Chitta et al. 2004). One confounding issue with this method is that the alpha chains for MHC II HLA-DR alleles are very similar in humans and mice, therefore, development of hybridomas specific for human HLA-DR-alpha would need to be carried out in an MHC II knockout strain in order to maximize the amount of epitopes generated.

MHC II conformation dictates HLA-DM susceptibility and peptide catalysis

Chapter III of this thesis described a model for an MHC II conformational intermediate in the DM catalyzed peptide exchange reaction. Using a novel hydrogen deuterium exchange mass spectrometry approach to mapping MHC-peptide interaction, the relative strengths of the individual hydrogen bonds along the backbone of the peptide were measured while the peptide was bound to MHC II. The hydrogen bonds flanking both sides of the P1 pocket were shown to be the strongest of those along the peptide backbone. A point mutant at the alpha 54 position of HLA-DR1 was generated and shown to have weakened hydrogen bonds flanking the P1 pocket relative to WT MHC II-peptide. This

mutation resulted in an MHC II with exquisite susceptibility to DM mediated peptide release as well as an increase in affinity for DM relative to wild type MHC II. Crystallization studies of the F54C and WT CLIP bound complexes revealed an intact hydrogen bond network, therefore the differences observed in the strengths of the hydrogen bonds between the F54C and WT peptide complexes must be due to a dynamic process.

These structural studies revealed that the F54C complex showed a conformational change in one molecule of the asymmetric unit, which was induced by a crystal contact at the alpha F51, an important DM contact residue. The F54C and WT structures were nearly isomorphic with similar crystal contacts, however, no such change was induced in the WT structure.

The alpha F54 lodges into a hydrophic cluster that anchors the P1 proximal strand region to the rest of the MHC II. It was postulated that removal of the bulky hydrophobic phenylalanine side chain by the F54C mutation, resulted in an MHC II that could adopt alternate conformations. The fact that the alpha F51, which is not directly adjacent to the mutated F54 residue, participated in a crystal contact resulting in the entire 3_{10} helix and adjacent strand region adopting an altered conformation suggests that this region would undergo a concerted change if DM contacted the same residue.

Interestingly, the model that was generated from the molecular dynamics simulation described in chapter II of this thesis, revealed a similar set of concerted changes involving the alpha 3_{10} helix and adjacent strand region. Due

to the striking similarities, it is reasonable to think that the model for the peptide free MHC II and the crystal structure of the contacted F54C converge on a conformation accessible to the WT MHC II. The conformational changes present in both models may represent a kinetically unstable form of the protein such as those that have been described for the peptide receptive and/or the DM susceptible conformation of MHC II.

Because of the increased affinity of the F54C MHC II for DM, it may be possible to generate a co-crystal of the MHC II-DM complex. A possible reason for the lack of a complexed crystal structure thus far, may be a result of the weak affinity of the soluble ectodomains of WT MHC II and DM. In addition, crystallization attempts may be stymied because the interaction may only proceed through an unstable intermediate that would not be amenable to crystallization. The F54C mutant may overcome these barriers and allow for a stable MHC II-DM complex.

There is considerable debate in the field regarding the conformation of MHC II that DM recognizes. A recent model suggests that DM only recognizes an MHC II that is partially empty with no occupancy of the P1 pocket (anders 2011). Other models however, suggest that DM recognizes alternate conformations of the MHC II itself, with a particular emphasis on the structure, rather then the occupancy, of the P1 pocket (Sadegh-Nasseri, Natarajan et al.). The data presented in Chapter III of this thesis would support the latter model suggesting that structural rearrangements of the N-terminal peptide binding domain

determine susceptibility to DM, regardless of peptide occupancy. A definitive crystal structure of the co-MHC II-DM and/or ternary MHC II-pep-DM complex could help resolve these outstanding questions regarding the mechanism of DM mediated peptide catalysis. However, direct structural analysis would still leave questions related to the dynamic nature of this interaction unanswered, therefore other biochemical approaches could be employed to help elucidate the nature of the peptide MHC II interaction and how DM functions to alter these interactions. One such approach that would be particularly useful for defining the role of the canonical hydrogen bond network in terms of peptide affinity for MHC II, would be to expand on the hydrogen deuterium exchange / electron transfer dissociation mass spectrometry (HDx/ETD) work presented in chapter III of this thesis.

Using this approach, a number of different questions related to the peptide MHC II interaction could be addressed. First, what is the relationship between MHC II pocket engagement of the peptide side with the hydrogen bond network. Numerous studies have tried to address this issue by manipulating at least one component of the MHC II-peptide interaction, and or by comparing alleles and extrapolating information based on intrinsic differences between the various complexes (Ferrante and Gorski ; Weber, Evavold et al. 1996; Busch, Rinderknecht et al. 2005; Narayan, Chou et al. 2007; Zhou, Callaway et al. 2009) Applying HDx/ETD systematically to different MHC II-peptide complexes may broaden our understanding of how the two types of interactions that bind peptide

within the MHC II binding groove are related. One could use a panel of peptides that engage the pockets of the MHC II differently, and directly measure the effects along the hydrogen bonding network. Applying this methodology to different MHC II proteins may uncover inherent differences between how the allotypes bind peptides.

We have not applied the HDx/ETD method to determining the effect of DM on the MHC II-peptide complex, although this method could generate compelling information regarding the mechanism of DM induced peptide exchange. The rate of HDx is dependant on pH, and is quenched at pH 2.6. DM mediates peptide exchange in acidic compartments and has been shown to be inactive at neutral pH, therefore the ideal pH to perform the assay would need to be empirically determined. A balance would have to be found for a pH that was low enough to enabled DM to function, while at the same time, high enough such that the rate of hydrogen deuterium exchange was still on a useful time scale.

Another approach that could be employed to get a greater understanding of the dynamic nature of the peptide-MHC II interaction would be to use NMR. If the individual chains of the 50kD complex could be labeled and their respective peaks could be assigned, then the dynamic nature of the H-bond network extending from the MHC II to the peptide could be studied. In addition, the stability of the MHC II protein could be measured as a function of peptide affinity, of P1 occupancy and of peptide sequence.

In appendix I of this thesis, structural alterations in HLA-DQ alleles were examined. This analysis revealed that HLA-DQ alleles which contained a G/G motif at the alpha 52 and 53 positions were able to adopt alternate conformations in the alpha 3-10 helix and extended strand region. These motions are similar to what we see in the F54C structure, which is exquisitely susceptible to DM. It seems plausible that there is a connection between the lability we observed in the F54C protein and the changes observed around the alpha strand G/G region of the DQ alleles. One hypothesis that can be derived from these similarities is that the G/G/ motif in the HLA-DQ alleles creates a more DM susceptible MHC II. This hypothesis could be directly addressed by many of the methods described in Chapter III of this thesis. In particular, peptide release assays with titrations of DM as well as SPR binding experiments would be particularly useful in determining whether these alleles were more susceptible then MHC II proteins without the alpha G/G motif to DM mediated peptide release.

The work presented in this thesis addresses MHC II conformational variability. By developing models for both the peptide free form of HLA-DR1 as well as a DM susceptible form of HLA-DR1, this work has expanded our understanding of the conformational heterogeneity of MHC II at various stages of the peptide loading process. The future studies proposed within this chapter would be valuable in broadening our overall understanding of the dynamic nature of proteins involved in antigen presentation.

APPENDICES

A.1 Structural alterations in the alpha 3-10 helix for HLA-DQA1*01 alleles

A.2 Expression of HLA-DR1 in *E. Coli* (Fermentation)

A.3 Inclusion body prep for HLA-DR1 subunits

A.4 Making Urea Solutions

A.5 Urea HQ Inclusion body Purification for HLA-DR1

A.6 Refolding HLA-DR1

A.7 Folded HLA-DR1 ELISA

A.8 Preparation of Antibody Protein A Immunoaffinity Column

A.9 Immunoaffinity purification of HLA-DR1

A.10 Loading HLA-DR1 with peptide

A.11 LCMS/HDx for MHC II bound or free peptide

A.12 Peptide sequences

A.13 HLA-DR1 protein sequence

A.14 HLA-DR1 alpha gene sequence

A.15 HLA-DR1 beta gene sequence

A.16 Primers used to generate point mutants in HLA-DR1

A.17 Using Fluorescence Polarization to measure KD_{app} and Peptide off rates

A.1. Structural alterations in the alpha 3-10 helix for HLA-DQA1*01 alleles.

There are many outstanding questions regarding DM catalyzed peptide exchange. In particular, structural changes in both DM and MHC II have been recognized as playing a role in the interaction of these molecules, although details have not been well defined (Sadegh-Nasseri, Natarajan et al. ; Ullrich, Doring et al. 1997; Chou and Sadegh-Nasseri 2000; Zarutskie, Busch et al. 2001; Rotzschke, Lau et al. 2002; Belmares, Busch et al. 2003; Narayan, Chou et al. 2007). Therefore we have analyzed existing MHC II structures in order to gain insight into regions of structural variability that have been identified as being important regions for the DM-MHC II interaction (Doebele, Busch et al. 2000; Pashine, Busch et al. 2003). Work presented in this thesis has identified the alpha 3_{10} helix and adjacent strand region proximal to the P1 pocket as regions that undergo conformational changes at various stages of the peptide loading process. In addition, the work presented here suggests that lability within the alpha strand region of HLA-DR1 is a key determinant in DM mediated peptide catalysis.

Our mutagenesis work has shown that when HLA-DR1 alpha F54 is mutated to an alanine or cysteine, the protein becomes exquisitely susceptible to DM, has altered peptide binding dynamics, and an increased propensity to adopt an alternate conformation. Examination of the structures for all MHC II peptide complexes to date has revealed that, with the exception of the region

around the prominent kink in the beta subunit alpha helix encompassing residues 57-70, the architecture of the peptide binding domain is maintained, and that side chain polymorphisms give rise to alterations in pocket structure. However, the HLA-DQ alleles have structural variations in the alpha 3_{10} helical region, which correspond to the same regions that show alterations in both our empty dynamics simulation as well as our F54C structure. The HLA-DQ alleles have been associated with disease, yet surprisingly little has been done towards understanding the structural differences that are apparent for this subset of MHC II proteins. Upon alignment of different MHC II proteins, the HLA-DQ structures were clear outliers and showed deviations from the other MHC II structures in the same regions that we described in our empty simulation model and our αF54C structure (Fig 1.5, 1.7); the latter of which we believe to have important implications for the dynamic nature of DM catalyzed peptide exchange.

Intriguingly, each of the HLA-DQ alleles aligned show alterations in 3_{10} helical and adjacent strand region (Fig. 1.5, 1.7). The HLA-DQ0602 structure (1UVQ; A1*0102/B1*0602) and the HLA-DQ1 (3PL6; A1*0102/B1*0502) have the same alpha chain, yet differ in the conformation of the alpha 3_{10} helix. An LSQ alignment was performed in order to gauge the magnitude of the alterations between the two HLA-DQ alleles when compared to each other and to HLA-DR1 (Fig 1.7). This analysis revealed that the alpha 1 domains for the DQ alleles differed in main chain RMSD by less then 0.7 angstrom along the

entire domain, except for the 3_{10} region from alpha 43 to alpha 55, where the average RMSD between the DQ alleles when compared to each other as well as to HLA-DR1, was around 2.0 angstroms (Fig A.1). Because the 1UVQ and 3PL6 structures have the same alpha chains, we sought to determine whether there were features inherent to the peptide or the beta chain that could cause these disparate conformations in the alpha chain.

The concerted conformational changes in the alpha 3_{10} helical region can be summarized as follows: In the 1UVQ HLA-DQ structure, the hypocretin peptide contains a proline at the P2 position. The crystal structure of the complex shows that the peptide maintains the canonical type II polyproline twist conformation up until the P2 proline, which is next to the beta His 81 of HLA-DQ (Fig A.1.1). The P2 proline could prevent the beta His 81 from adopting its normal rotamer (as seen in all other MHC II structures that have a His at this position) due to steric hindrance. A theoretical alteration of the beta His 81, placing it in its canonical rotamer shows that this change would create a 0.45 angstrom clash with the proline at the P2 position (using coot for the modification and assessing by molprobability in phenix). This could be why there is an alternate rotamer seen in the 1UVQ structure that prevents the beta His 81 from forming a hydrogen bond with the main chain of the peptide. In addition, the beta Asn 82 OD1 cannot form a hydrogen bond to the P2 proline (Fig. A.1.1). Both the beta His 81 and Asn 82 hydrogen bonds have been

FIGURE A.1.1
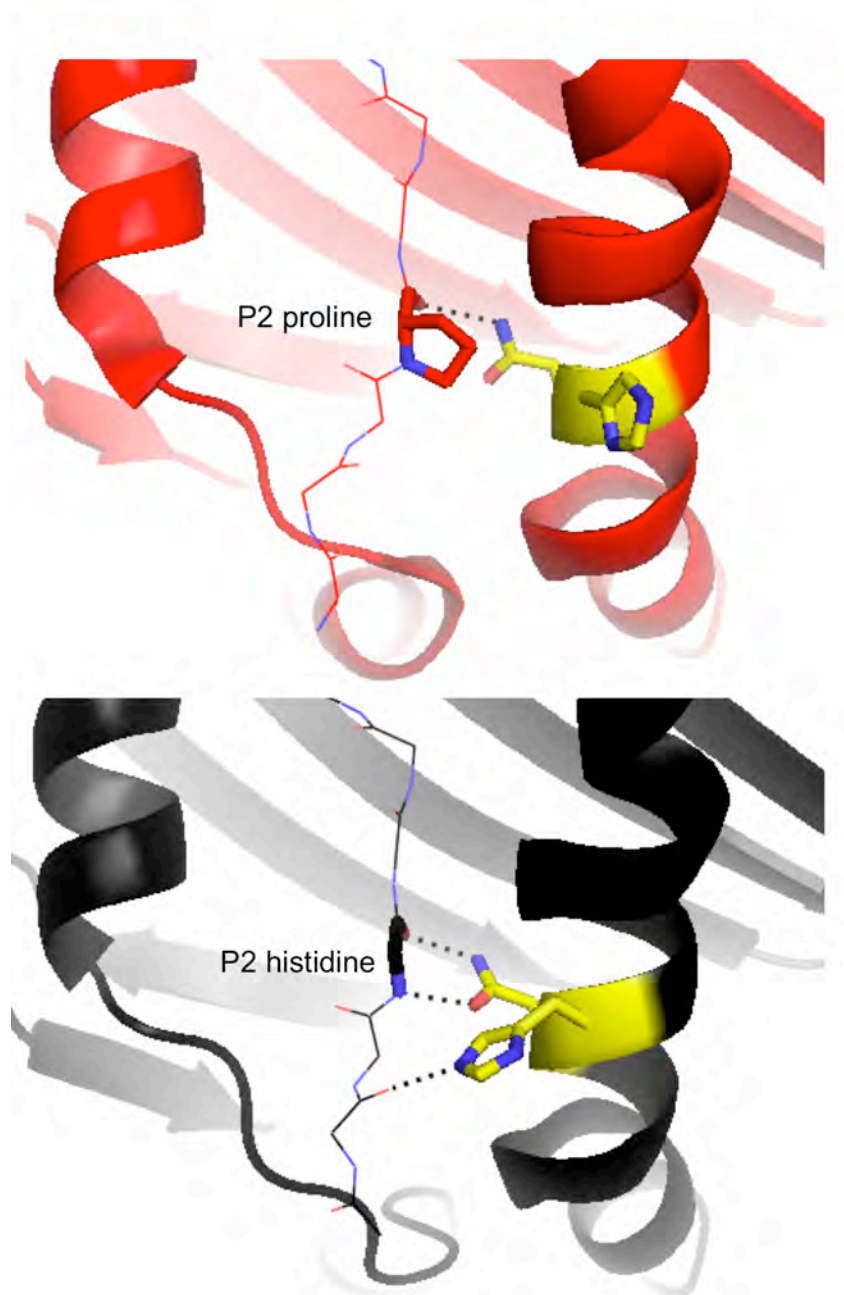
FIGURE A1.1 Proline at the P2 position in the HLA-DQ bound peptide breaks key N-terminal hydrogen bonds. (top) Broken hydrogen bonds due to a proline at the P2 position in 1UVQ . Cartoon diagram of N-terminal region of the peptide binding domain with the peptide backbone shown as lines, with the proline at the P2 position shown in stick. Beta ASN 82 and H81 are shown in yellow. Dashed line indicates the hydrogen bond between the ASN 82 and the carbonyl of the proline. (bottom) Intact N-terminal hydrogen bonds in the 3PL6 structure. The main chain of the P2 histidine is shown in stick and dashed lines indicate hydrogen bonds between both functional groups of beta ASN 82. The beta H81 adopts the canonical rotamer and forms a hydrogen bond with the backbone of the peptide

implicated as key energetic factors in the peptide-MCH II interaction, and when mutated, have been shown to cause nearly spontaneous release of peptide from HLA-DR alleles (Narayan, Chou et al. 2007; Bandyopadhyay, Arneson et al. 2008; Zhou, Callaway et al. 2009). Therefore, the HLA-DQ proteins may have different requirements for the energetic contributions of hydrogen bonds with the beta 81 and 82 residues. Yet another effect of the P2 proline in the 1UVQ structure is that the psi angle of the proline causes the peptide to kink toward the DQ alpha chain (the delta psi between the 1UVQ and the 3PL6 peptides show a 347 degree deviation at the i+1 position).

The HLA-DQA1*01 alleles are unique in that there are glycines at the alpha 52 and 53 positions (G/G), different HLA-DQ alpha chains, and all other MHC II proteins do not contain this motif as assessed by sequence alignment in the IMGT/HLA database. For all MHC II structures to date, the alpha 53 position is the only residue that forms hydrogen bonds with the peptide backbone. In the 1UVQ structure, these hydrogen bonds are maintained, likely because the G/G sequence allows some level of flexibility in this region and can therefore accommodate the kink in the peptide through an alteration in their phi psi angles. Fig A.1.2. shows delta phi psi plots comparing the 1UVQ with the 3PL6 (which have the identical alpha chain, and therefore the same G/G motif) as well as with 1DLH (HLA-DR1), which has an Ala 52 and Ser 53 in place of the G/G. The phi for the alpha Gly 52 and the psi for the alpha Gly 53 show major deviations when the 1UVQ is compared to 3PL6 as well as the 1DLH,

FIGURE A.1.2

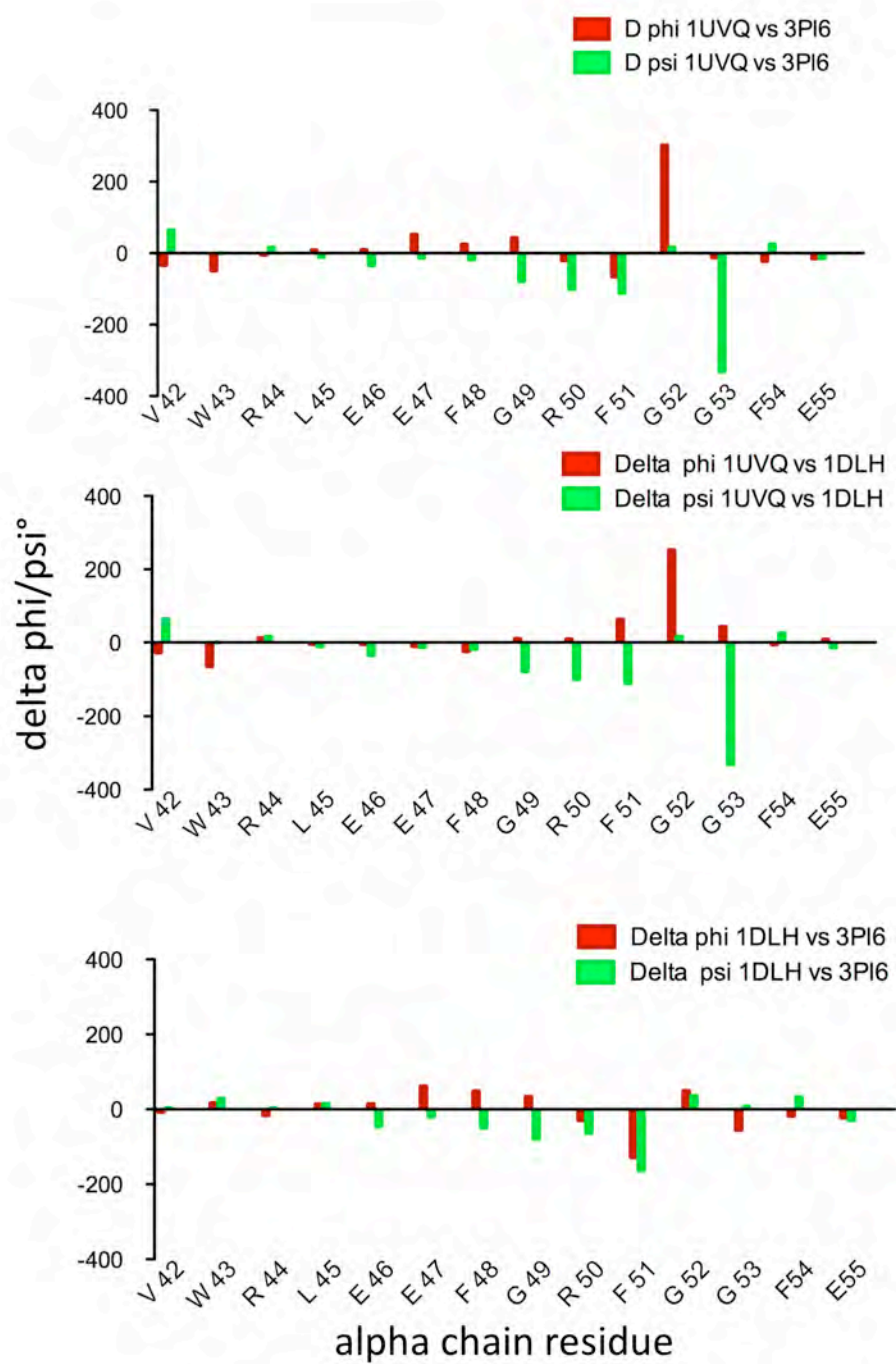**FIGURE A.1.2. The Gly/Gly motif in the extended strand region for some HLA-DQ alleles allows alternate conformations of the alpha 3$_{10}$ helix**. Delta phi psi plots comparing the 1UVQ with the 3PL6 (top), 1UVQ vs 1DLH (HLA-DR1) (middle) and 1DLH vs 3PL6 (bottom), phi values are represented in red and phi are in green. Residues are shown on the x-axis and delta phi/phi are shown on the y-axis

however, there is a relatively small difference for the alpha 52 and 53 positions when the 3PL6 and the 1DLH structures were compared. When phi psi angles for all of the residues that comprise the alpha 3_{10} helix were compared, the only major deviation was at the G/G region, implicating these residues as contributing to the conformational change that propagated along the entire alpha 3_{10} helical region (Fig. 1.7). These analyses suggest that the G/G motif is able to accommodate both canonical and altered conformations.

It is reasonable to think from this analysis that the structure of the peptide is influencing the conformation of the alpha 3_{10} helical region and that a proline in the P2 position is the key structural factor promoting a distortion of the G/G motif in the 1UVQ alpha chain which then propagates to the alpha W43. Interestingly, the W43 in the 1UVQ structure is in a pointed away from the base of the peptide binding groove (Fig. A.1.3). The 1UVQ structure is unique in that this is the only solved MHC II peptide structure to show the alpha W43 in this rotamer. The conformational change in the 3_{10} alpha helix positions the carbonyl from the Gly 52 such that it would clash with the W43 if the W43 maintained it's canonical rotamer, which is normally tucked into a hydrophobic cluster that forms a side of the P1 pocket. Interestingly, the alpha W43 has been implicated in the DM-DR interaction, when mutated, the interaction is abrogated (Anders, Call et al.).

Another HLA-DQ allele, (HLA-DQA1*0501/B1*0201; IS9V) also has structural changes in the regions described above. Interestingly, there is a

FIGURE A.1.3
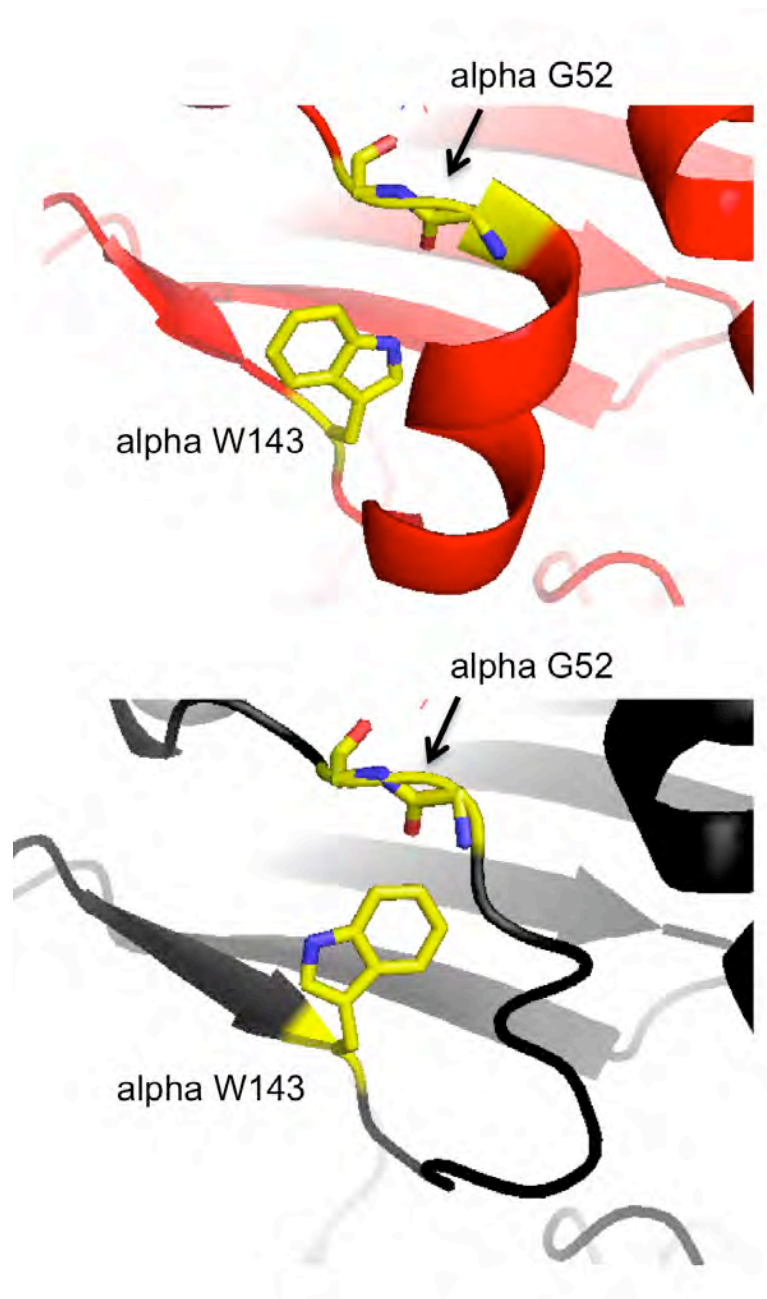
FIGURE A.1.3. Alpha W143 can adopt different rotamers in HLA-DQ alleles that contain the alpha strand Gly/Gly motif. (top) The alpha W143 is pointed away from the peptide binding groove. (bottom) The 3PL6 structure showing the W143 in the canonical rotamer. The alpha Gly 52 is indicated for both structures, note the position of the carbonyl from the Gly 52 would create a steric hindrance on the W43 if the W43 were in it's canonical rotamer (as seen in the bottom panel).

deletion of the alpha Ala 52, which causes the alpha Phe 51 to be tucked into the N-terminal side of the peptide binding groove, which theoretically could inhibit the interaction with DM, since this has been shown to be a critical DM interaction residue (Doebele, Busch et al. 2000). Indeed, this particular HLA-DQ allele has been shown to be resistant to the effects of DM catalyzed peptide exchange(Fallang, Roh et al. 2008). However, based on the analysis for the HLA-DQ alleles that contain the G/G, it can not be ruled out that the Ala 52 deletion influences the lability within the stand region proximal to the P1 pocket and in that way creates a DM resistant phenotype.

Using the SYFPEITHI database, we performed a search for peptides associated with MHC II alleles and found that proline is predicted in the i+1 for peptides known to bind HLA-DQA1*01 alleles, but not for the majority of MHC II alleles (data not shown). A thorough structural analysis of different MHC II alleles complexed with peptides that have a proline at the P2 position may help identify whether the peptide itself can contribute to alterations in the N-terminal peptide binding region. In addition, studies of DM susceptibility for MHC II peptide complexes that have the Gly52 Gly53 motif may also indicate whether flexibility in this region is important for the mechanism of DM mediated peptide release.

A.2 Expression of HLA-DR1 in *E. Coli* (Fermentation)
Protocol from Mia Rushe

***Procedure*:**

Day 1:
1. Streak an LB-amp (or kan if kanamycin resistant strain, chlor also if cells are pLys^s) plate in the evening with BL21 cells of interest from frozen stocks. Incubate at 37˚C overnight.

Day 2:
1. Put streaked plate at 4˚C in morning, sealed with parafilm.
2. Autoclave assembled fermentor filled with 10 L of 1 x LB broth, 1 L of distilled H_2O, 1 L of 1 x LB broth, at least 150 mL 20 % glucose, and 3-125 mL Erlenmeyer flasks.
3. In the early evening, add 83 mL sterilized LB broth to one of the sterile flasks. Add 83 mL Ampicillin (50 mg/mL) and 1.2 mL 20 % glucose. **IF the cells are kanamycin resistant, substitute 83 mL of a 50 mg/mL stock of kanamycin sulfate for ampicillin. If cells are pLys^s, add 83 mL chloramphenicol (35 mg/mL).**
4. Mix well and take a 1 mL blank sample for OD_{600} measurements. You may want to add 1 mL 20 % NaN_3 to prevent growth in the blank sample. Keep this blank in a plastic cuvette.
5. The remaining LB solution will be split into different containers. Pipet 2 mL into a sterile 15 mL conical tube, 20 mL into a 50 mL conical tube, and 20 mL into each of the remaining sterile Erlenmeyer flasks. Label the flasks 1, 2 and 3.
6. Pick one colony from your plate. Add it to your 15 mL tube and vortex vigorously. Take 200 mL of that tube and add it to the 50 mL conical tube and vortex vigorously. Take 200 mL of that tube and add it to Erlenmeyer flask #1 and swirl a lot. Take 200 mL from that flask and add it to Erlenmeyer flask #2 and swirl a lot. Take 200 mL of that flask and add it to Erlenmeyer flask #3.
7. Grow the 3 Erlenmeyer flasks on a shaker table at 37˚C overnight.

1 colony

200 μL   200 μL   200 μL   200 μL

Flask #1   Flask #2   Flask #3

500
colonies/L

5
colonies/L

0.05
colonies/L

0.0005
colonies/L

0.000005
colonies/L
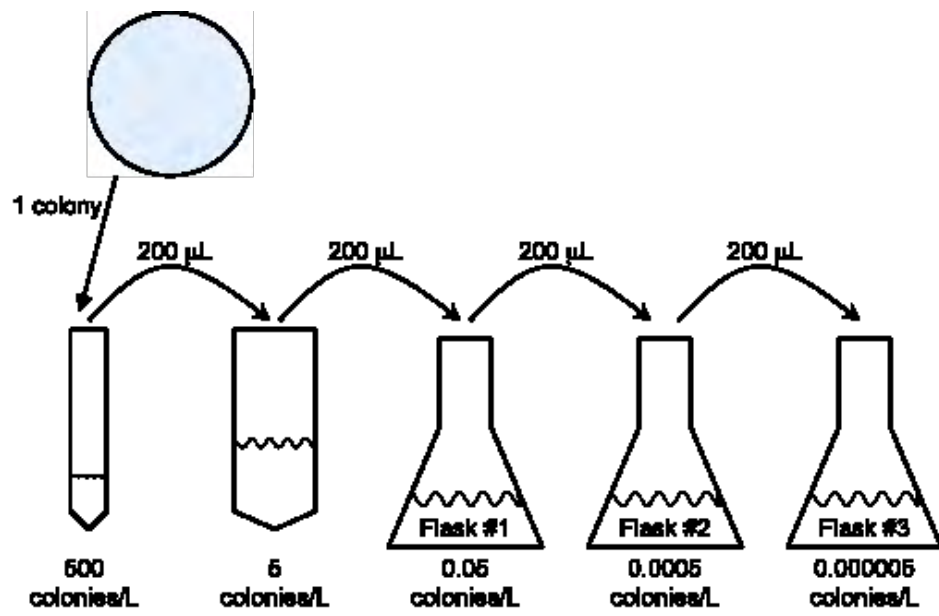
Day 3:
1. Measure the absorbance at 600nm of each flask compared to the blank you saved. Pick the one that is less than 1.0 OD_{600}, but still has measurable growth in it. (0.7 is about ideal.)
2. Set up the fermentor: Add 10 mL of Ampicillin, 50 mg/mL, 100 mL 20 % glucose (sterile), and 200 mL antifoam A. **IF the cells are kanamycin resistant, substitute 10 mL of a 50 mg/mL stock of kanamycin sulfate for ampicillin. If the cells are pLys^s, also add 10 mL 35 mg/mL chloramphenicol.** Mix well. Remove 1 mL as a blank and store in a plastic cuvette, possibly with 1 mL 20 % NaN_3.
3. Run the mixer on the fermentor at ~700 rpm, and run the air at 15 psi and 5 LPM. Watch for excessive foaming and add antifoam if it is necessary. **If you have never set the fermentor up before, ask for help!!
4. Seed the fermentor with 10 mL of the overnight flask you selected.
5. Take samples and check the OD_{600} every hour until you get close to 1.0, and then check more frequently. Do not overgrow!
6. When the OD_{600} reaches 1.0, take a 1 mL sample "not induced." Spin down and re-suspend in 1x urea-SDS loading buffer. Freeze at –20°C.
7. Add IPTG to 0.75 mM final concentration. I use 10 mL of 0.75M IPTG stock (1000 x). Allow to grow for 2-5 hours with IPTG. (Longer for class I MHC subunits)
8. Take a 1 mL sample "induced." Spin down and re-suspend in 1x urea-SDS loading buffer. Freeze at –20 °C until you are ready to check the "not induced" and "induced" samples on a gel by SDS-PAGE.
9. Spin down all the cells at 8000 x g and discard the supernatant. For inclusion bodies, you may freeze the pellet at –20°C, or proceed with the inclusion body prep through the DNAse step and freeze at –20°C.

BL21 MEDIA RECIPES
Protocol from Lauren Angelo

Modified LB Broth	2x YT + Salts	Terrific
10 g/L tryptone	16 g/L tryptone	12 g/L tryptone
5 g/L yeast extract	10 g/L yeast extract	25 g/L yeast extract
0.4-1% glucose	0.4-1% glucose	0.4-1% glucose
5 g/L NaCl	100 mL/L 10x Salts*	100 mL/L
10x Salts*		
5 g/L K_2HPO_4		
10 mM $MgSO_4$		
1 mL/L Trace Elements		

*10x Salts
23.1 g/L KH_2PO_4
125.4 g/L K_2HPO_4
filter-sterilize—do not autoclave. Add to media after other ingredients have been autoclaved

A.3 Inclusion body prep for HLA-DR1 subunits
Protocol from Mia Rushe

Procedure (for pellet from 10 L culture):

1. Spin down cells at 5000 x g—collect supernatant into a container, sterilize with 1% Wescodyne for 10-20 minutes, and then dump down the sink.
2. With a rubber spatula, re-suspend fresh bacteria into a single plastic container with ~200 mL Sucrose Solution.
3. Chop the solution briefly in a homogenizer or polytron. **Do not sonicate!
4. If cells are not pLys^s, add 1 mg dry lysozyme per mL suspension (0.2 g) and stir for 10 minutes. If cells are pLys^s, just stir for 10 minutes.
5. While stirring, add 500 mL Deoxycholate-Triton Solution. Solution will become very viscous due to cell lysis and DNA release.
6. Add 1 mL of 4 M MgCl$_2$ Solution to make 5 mM final concentration.
7. Add 2 mL DNAse Solution. Stir until the solution is the viscosity of water.
8. Freeze overnight at –20˚C, or until ready to complete the prep.
9. Thaw solution in warm water bath.
10. Stir an additional 10 minutes after thawing to allow the DNAse to work again.
11. Spin down in 2 centrifuge bottles at 8000 x g for 20 minutes. Discard supernatant.
12. Re-suspend pellets in 300 mL or more each Triton Solution. Chop briefly, keeping the pellets on ice as much as possible. Spin down at 8000 x g for 20 minutes and discard supernatant.
13. Repeat step 12 three or more times.
14. Re-suspend pellets into 300 mL or more each Tris Solution. Chop briefly, keeping the pellets on ice as much as possible. Spin down at 8000 x g for 20 minutes and discard supernatant.
15. Repeat step 14 two or more times.
16. Re-suspend/dissolve the pellets and chop in ~ 200 mL Urea Solution.
17. Spin down at 20˚C, 15,000 x g for 30 minutes. Filter through a 0.2 mm filter.
18. Freeze at –70˚C until ready to purify by Urea HQ.

INCLUSION BODY PREPARATION FOR HLA-DR1 SUBUNITS
Protocol from Mia Rushe

Solutions (**Note: Do not add DTT until just before use!):

Sucrose Solution
  50 mM Tris, pH 8.0
  25 % sucrose
  1 mM EDTA
  0.1 % NaN$_3$
  10 mM DTT

Deoxycholate-Triton Solution
  1 % Deoxycholic Acid
  1 % Triton X-100
  20 mM Tris, pH 7.5
  100 mM NaCl
  0.1 % NaN$_3$
  10 mM DTT

Triton Solution
  0.5 % Triton X-100
  50 mM Tris, pH 8.0
  100 mM NaCl
  1 mM EDTA
  0.1% NaN3
  1 mM DTT

Tris Solution
  50 mM Tris, pH 8.0
  1 mM EDTA
  0.1% NaN3
  1 mM DTT

Urea Solution
  8 M Urea
  20 mM Tris, pH 8.0
  0.5 mM EDTA
  10 mM DTT

DNAse Solution (**make 50 mL total, not 1L**)
  75 mM NaCl
  50 % glycerol
  2 mg/mL DNAse
  (Sigma D-5025 or DN25)

A.4 Making Urea Solutions
Protocol from Mia Rushe

***Procedure*:**

1. Add concentrated buffer stock solution, any additives (such as EDTA or NaCl), and dry urea (FW = 60.06). Add ddH$_2$O to an appropriate volume to make 8 M Urea.
2. Stir slowly—you can warm in a bucket of water, but do not warm too quickly or too much.
3. After urea is dissolved, add Sigma mixed bed resin TMD-8, ½ teaspoon at a time until the beads stop turning yellow in the solution (i.e. there are a lot of blue beads).
4. Stir slowly another 10 minutes, and then let the beads settle.
5. Filter using a 0.2 mm membrane.
6. Store at –20˚C if you are not going to use immediately.

A.5 Urea HQ Inclusion body Purification for HLA-DR1
Protocol from Mia Rushe

Column: HiTrap Q XL column, GE Healthcare

Buffers: **Solution A**: 8 M urea, 20 mM tris, 1 mM DTT added just before use
　　　Solution B: 8 M urea, 20 mM tris, 1 M NaCl, 1 mM DTT added just
before use
　　　　　For purifying A1S, both solutions should be pH 8.0
　　　　　For purifying B1S, both solutions should be pH 9.0

Procedure:
1. Make approximately 3 L **solution A** and 1 L **solution B**, using the protocol for *Making Urea Solutions*. Use the appropriate pH for the inclusion body you will be purifying. If not using immediately, store at -20°C. Do not add the DTT until just before use.
2. Thaw urea-solubilized inclusion bodies. For B1S, adjust the pH to 9.0 using NaOH. (pH should be 8.0 in frozen inclusion bodies)
3. Equilibrate the HQ column in 1-5 column volumes **solution A**.
4. Flow the inclusion body solution over the column. If it is very concentrated, it may bind better if it is diluted 1:2 in **solution A**. **NOTE: Save flow-through of the column, as the protein is very concentrated and may saturate the column.**
5. Run a gradient of 0-30% **solution B** (1-300 mM NaCl) over 6 column volumes. Collect fractions.
6. Analyze fractions from all major peaks by SDS-PAGE. **NOTE: If the protein peak of interest looks different when run on reducing vs. non-reducing SDS-PAGE, add more DTT to the final inclusion body pool to completely reduce the protein.**
7. Pool peak fractions and measure the concentration of protein using absorbance at 280 nm against a blank of **solution A**. **NOTE: For A1S: 1.3 OD_{280} = 1 mg/mL.   For B1S: 1.7 OD_{280} = 1 mg/mL.**
8. For B1S, adjust the pH back to 8.0. Add EDTA to a final concentration of 5 mM (10 µL 0.5M EDTA stock / mL inclusion body solution).
9. Store in convenient aliquots at -80°C.

　　NOTES: A new HQ column has a protein binding capacity of about 5-10 mg / mL resin. The capcity becomes significantly lower over time with this procedure, possibly in part due to EDTA. Regeneration does not seem to be particularly helpful. Thus, when loading protein, do it slowly and monitor the absorbance of the flow-through to determine when the protein is no longer binding to the resin. The chromatograms will be very messy and inconsistent, but the refolding yield for inclusion bodies purified in this manner is much better.

A.6 Refolding HLA-DR1
Protocol from Mia Rushe

Procedure:

7. Chill Refolding Mix without glutathione to 4°C. Refolding should be done in a container close to the size of the volume of liquid to reduce exposure to air. De-gas solution by sparging with argon for about 20 minutes.
8. Add glutathione (oxidized and reduced) and stir until just dissolved.
9. Stir as rapidly as possible
10. Add peptide—about 5-fold molar excess in a 1x refolding is good, so you should end up with a final peptide concentration of 0.4 mM. You can use the same concentration peptide for a 2x re-folding. **Note: If you want to re-fold empty DR1, simply omit the peptide.
11. Slowly (dropwise) add HQ-purified inclusion bodies in urea. Add 2 (1 x) or 4 (2x) mg of each inclusion body (alpha and beta) per liter of Refolding Mix.
12. After everything is well mixed, cover tightly and store at 4°C for at least 36 hours.

Refolding Mix:
20 mM Tris, pH 8.5
0.5 mM EDTA
25 % glycerol
2 mM glutathione, reduced   ** Add just before use!
0.2 mM glutathione, oxidized   ** Add just before use!

Example 2 x re-folding, 4 L total volume:
80   mL of 1 M Tris, pH 8.5
4   mL of 0.5 M EDTA
1000 g glycerol
2.45 g glutathione, reduced
0.488 g glutathione, oxidized
16   mg DRA1S inclusion bodies (8 mL of 2 mg/mL stock, Urea HQ pure)
16   mg DRB1S inclusion bodies (16 mL of 1 mg/mL stock, Urea HQ pure)
1.6   mmoles Ha peptide (800 mL of 2 mM Ha peptide stock)

A.7 Folded HLA-DR1 ELISA
Protocol from Mia Rushe

***Procedure*:**

1. Coat Immulon IV plate (from Dynex) with 100 µL per well α-DR monoclonal antibody LB3.1 or L243, diluted 1:1000 in plain PBS. Stock is 1.8 mg/mL in PBS, 0.02% NaN$_3$. Incubate plate on nutator for 2 hours at 37°C or overnight at 4°C.
2. Wash each well 3 times with PBST Solution.
3. Block the plate by filling each well to the top with Block Solution. Incubate at least one hour on nutator at 37°C. The plate can be stored at this point if the Block Solution is replaced by Dilution Solution. Store plates at 4°C, covered in packing tape and surrounded by plastic wrap.
4. Remove Block Solution or Dilution Solution in stored plates. Add 50 µL fresh Dilution Solution to each well.
5. Make up standards of folded DR1 in dilution solution. Make high concentration of 2 ng/µL as the high concentration, and dilute 1:2 down to 0.002 ng/µL. Add 50 µL of standard per well, giving 100-0.1 ng/well—make sure to do duplicate measurements of the standards. Also, include a blank measurement.
6. Add samples and diluted samples into wells. A good way to test most refolding mixes is to add 50 µL, 5 µL, and 2.5 µL of sample to give the dilutions, making up the difference to 50 µL with dilution solution (0 µL, 45 µL, and 47.5 µL).
7. Incubate plate on nutator for 1 hour at 37°C, 2 hours at room temperature, or overnight at 4°C.
8. Carefully wash each plate 3 times with PBST, avoiding spillover from neighboring wells.
9. Add 100 µL/well of rabbit CHAMP polyclonal α-DR1 antibody diluted 1:25,000 (or 1:500 of a 1:50 stock solution) in Dilution Solution. Incubate plate on nutator for 1 hour at 37°C, 2 hours at room temperature, or overnight at 4°C.
10. Wash wells 3 times with PBST. ** Follow Alternate Procedure after this point for Europium Staining (following page)
11. Add 100 µL goat α-rabbit IgG peroxidase (HRP) conjugate (from Roche) diluted 1:4000 in dilution solution. No azide should be present at this step, as it inhibits the enzyme. Incubate on nutator 0.5-2 hours at room temperature or 37°C. **Background increases if this step is allowed to sit overnight at 4°C.
12. Wash wells 3 times with PBST.
13. Add 200 µL ABTS Solution to each well.
14. Read absorbance in ELISA plate reader at 405 nm.

15. To stop plate from developing, add 50 µL Stopping Solution to each well.
16. Try several absorbance readings to catch the solutions at the most informative stage of developing—before saturation.
17. Use a 4-parameter curve fit to the standards to determine the MHC class II concentration of the samples.

A.8 Preparation of Antibody Protein A Immunoaffinity Column
Developed by Mia Rishe

Materials:
200 mM Borate: 1.24g /100 mL, titrate to pH 9.0 with NaOH
200 mM Ethanolamine: 1.2mL/100 mL, titrate to pH 8.0
Antibody solution, enough to have 10 mg/5mL matrix
Protein A-coupled matrix; I prefer IPA-400 Fast-Flow.
PBS + 0.02% NaN_3
Dimethylpimelimidate (20 mM final, (MW=259), 5.18 mg/mL)
   *Advice:* Use a fresh bottle (e.g. unopened) every time

Procedure:

1) Mix Antibody and ProteinA matrix in PBS, preferably with as small a volume as possible (ideally ~15 mL if using 5 mL matrix; can be scaled up accordingly). This can be done in a polypropylene centrifuge tube, or directly in the gravity column body (just make sure the ends are sealed) Rotate at room temperature 1 hour or longer. Remove 15 mL of suspension into tube labeled "TOTAL".

2) Spin 2000 rpm 5 min, remove and save supernatant and pellet. Or, if using the column, let the solution drain out. Remove 15 mL of supe into tube labeled "NON-BOUND".

3) Resuspend pellet in 50 mL borate solution, spin/drain, remove supernatant.

4) Resuspend pellet in 15 mL fresh borate solution. Remove 10 mL into tube labeled "BOUND". Add 20 mM final dimethylpimelimidate as solid (77.7 mg for 15 mL) and dissolve. Rotate 30 minutes at room temperature (going longer will over-couple the matrix)

5) Spin/drain to remove supe and check that the pH of the supe is > 8.0.

6) Resuspend pellet in 50 mL ethanolamine, rotate 30 minutes room temperature or longer, spin/drain off supe.

7) Wash pellet with 50 mL ethanolamine, then 50 mL borate, then 50 mL PBS

8) Resuspend pellet in 15 mL PBS. Remove 15 mL of suspension into tube labeled "NON-COUPLED". Store matrix at 4°C in PBS + NaN_3.

Analysis:

Add 10 mL 2x Laemlli buffer to each fraction, boil, and spin in microfuge. Run 10% SDS-PAGE of MW markers, 1 mg mouse IgG, and 10 mL of each fraction taken. Gel should show heavy and light chains in TOTAL and BOUND, and nothing in NON-BOUND and NON-COUPLED. If there is more protein in NON-BOUND than BOUND, try a different binding buffer (PBS works fine for LB3.1/L243). If there is any protein in NON-COUPLED, cycle the matrix through all binding and elution conditions that will be used in the affinity purification procedure, and next time use fresh pimelimidate!

Sample of analysis gel:
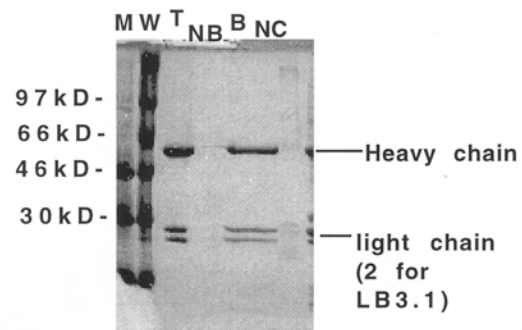
A.9 Immunoaffinity purification of HLA-DR1
Protocol from Mia Rushe

1. Concentrate folding mix and switch buffers into 1x PBS, pH ~7. Make sure there is no glutathione, as that will ruin the antibody column! If the DR1 is from an insect cell prep instead of an E.coli refolding, make sure the supernatant has been filtered through a 0.2 mM filter.
2. Flow the protein solution over a Protein A sepharose pre-column and then the LB3.1 or L243 column by gravity. Be sure to use a safety loop so that the columns don't dry out. Save the flow-through to check on a gel.
3. Wash with at least 10 column volumes of cold PBS
4. Elute using high pH for DR1. Use ~5 column volumes of 50 mM CAPS, pH 11.5 and collect 1 mL fractions into tubes with 300 mL of 300 mM NaPi, pH 6.0 to neutralize them. Make a blank fraction for zeroing the UV-VIS. (**Note: low pH may be used to elute, using 5 column volumes 50 mM glycine, pH 2.6, and collecting 1 mL fractions into tubes containing 300 mL of 300 mM Tris, pH 8.0 in them. This will give a lower yield for DR1, but may be better for other alleles.)
5. Clean the column with pH swings:
    a. 3 column volumes 50 mM glycine, pH 2.6
    b. 3 column volumes 50 mM CAPS, pH 11.5
    c. 3 column volumes 50 mM glycine, pH 2.6
6. Wash the column with at least 10 column volumes of PBSZ—until the pH is neutral.
7. Check the Abs_{280} of the fractions and pool the protein-containing fractions. You may add azide to 0.02%, add peptide if the complex is empty and you wish to load a particular peptide, or dialyze/concentrate into 20 mM tris, pH 8.0 if you wish to further purify by ion exchange.

A.10 Loading HLA-DR1 with peptide
Protocol from Zarixia Zavala-Ruiz

Procedure:

1. Obtain the empty MHC at a concentration of ~ 1 mg/mL, about 20 mM, in a suitable buffer such as PBS pH 7.0 with 0.02% sodium azide and 5 mM EDTA as protease inhibition.
2. Add the peptide of choice to a final concentration of at least 100 mM, or 5-fold molar excess.
3. Incubate the mixture at 37°C for 3 days.
4. Purify the peptide-loaded complex by gel filtration. **Make sure to save a sample of the unloaded complex to test by SDS-PAGE and analytical gel filtration. Peptide loading will shift the MHC complex to a later time on a gel filtration column, and it will often cause SDS stability in a gel, as opposed to the empty MHC, which will break down into subunits.

A.11 LCMS/HDx for MHC II bound or free peptide

Preparation of sample for LCMS/HDx

1. Dry 1 ml of PBS and reconstitute with 1ml of D_2O-H_2O)

2. Add 10 µl of 1 M Gly-HCl (pH 2.7) to 0.6 ml tubes and put on ice

Samples (start timing when mixed w D_2O, incubate at room temp):
   1. 2.6 µl DR1-HA (from Corrie) + 23.4 µl D_2O-PBS
   2. 5 µl HA (from Corrie) + 45 µl D_2O-PBS
   3. 12 µl F54C-HA + 108 µl D_2O-PBS

Take 1, 5 and 5 µl aliquots of samples 1 – 3 respectively at specified time points, mix with 10 µl of 1 M Gly-HCl (pH 2.7) in normal water at 0° and immediately freeze at -80°.

Take 1, 5 and 5 µl aliquots of samples 1 – 3 respectively at specified time points, mix with 10 µl of 1 M Gly-HCl (pH 2.7) in normal water at 0° and immediately freeze at -80°.

LCMS:

   Columns: 1X15 mm C4 (300A) connected to a 1X15 mm C18 (Pepmap). Both columns and injector kept in ice bath.

   Mobile phases: A=0.1% TFA in 2% ACN. B=0.1% ACN in 25% ACN. Flow 50 µl/min. Adjust %B to give ~5 min HA retention time (~18%).

   LCQ: Tune +ESI enhanced resolution on HA +2 ion by teeing 2 µl/min 1 mg/ml HA into flow stream. Scan from m/z 450 – 1600 using the following values.

   Capillary Temp (C): 275.00
   Sheath Gas Flow (): 15.00
   Aux Gas Flow ():   20.00
   Sweep Gas Flow (): 2.00
   Source Voltage (kV):   4.50
   Full Micro Scans: 10
   Full Max Ion Time (ms):   200.00

Sample handling:

Remove one time point from -80°, quickly thaw in hand, draw 5 µl into cooled 10 µl syringe and inject ASAP. After peaks have eluted, inject next time point by same procedure

A.12 Peptide Sequences

HA:
Ac-PKFVRQNTLRLAT-OH

Clip:
Ac-VSKMRMATPLLMQ-OH

A.13 HLA-DR1 Protein Construct

Chain A:
IKEEHVIIQAEFYLNPDQSGEFMFDFDGDEIFHVDMAKKETVWRLEEFGRFAS
FEAQGALANIAVDKANLEIMTKRSNYTPITNVPPEVTVLTNSPVELREPNVLICFI
DKFTPPVVNVTWLRNGKPVTTGVSETVFLPREDHLFRKFHYLPFLPSTEDVYD
CRVEHWGLDE
PLLKHWEFDA

Chain B:
GDTRPRFLWQLKFECHFFNGTERVRLLERCIYNQEESVRFDSDVGEYRAVTEL
GRPDAEYWNSQKDLLEQRRAAVDTYCRHNYGVGESFTVQRRVEPKVTVYPSK
TQPLQHHNLLVCSVSGFYPGSIEVRWFRNGQEEKAGVVSTGLIQNGDWTFQTL
VMLETVPRSGEVYTCQVEHPSVTS
PLTVEWRA

A.14 HLA-DR1 alpha gene sequence

Gene Construct	HLA-DR1 AS (α chain, short) and AL (α chain, long)
Plasmid	Full length in pHN1 (T7 promoter) called pDRA10 Short version in pLM1 (T7 promoter) Amp resistance gene for plasmid production in *E. coli*
Made by	Mia Rushe in Larry Stern's lab
Sites used for cloning	EcoRI and HindIII
Insert size	~580bp AS, ~600bp AL
For production in	*E. coli* BL21 Induce with IPTG
Gene Sequence	gaattcaggaggaatttaaaatgATCAAAGAAGAACATGTGATCATCCAGGCCGAGTT CTATCTGAATCCTGACCAATCAGGCGAGTTTATGTTTGACTTTGATGGTGAT GAGATTTTCCATGTGGATATGGCAAAGAAGGAGACGGTCTGGCGGCTTGAA GAATTTGGACGATTTGCCAGCTTTGAGGCTCAAGGTGCATTGGCCAACATA GCTGTGGACAAAGCCAACTTGGAAATCATGACAAAGCGCTCCAACTATACT CCGATCACCAATGTACCTCCAGAGGTAACTGTGCTCACGAACAGCCCTGTG GAACTGAGAGAGCCCAACGTCCTCATCTGTTTCATCGACAAGTTCACCCCA CCAGTGGTCAATGTCACGTGGCTTCGAAATGGAAAACCTGTCACCACAGGA GTGTCAGAGACAGTCTTCCTGCCCAGGGAAGACCACCTTTTCCGCAAGTTC CACTATCTCCCCTTCCTGCCCTCAACTGAGGACGTTTACGACTGCAGGGTG GAGCACTGGGGCTTGGATGAG *short:* CCTCTTCTCAAGCACTGGGAGTTTGATGCTtaaaagctt *long:* CCTCTTCTCAAGCACTGGGAGTTTGATGCTCCAAGCCCTCTCCCAGAGACT ACAGAGAAC taaaagctt
Protein Sequence	*iqeefk*MIKEEHVIIQAEFYLNPDQSGEFMFDFDGDEIFHVDMAKKETVWRLEEFG RFAS FEAQGALANIAVDKANLEIMTKRSNYTPITNVPPEVTVLTNSPVELREPNVLICFI DKFT PPVVNVTWLRNGKPVTTGVSETVFLPREDHLFRKFHYLPFLPSTEDVYDCRVE HWGLDE *short:* PLLKHWEFDAEND *long:* PLLKHWEFDAPSPLPETTENEND
Protein MW	AS: 21,264; AL: 22,330 Da
Protein pI	AS: 4.75; AL: 4.67
Protein extinction coefficient	28,000 at 280nm (unfolded)

A.15 HLA-DR1 beta gene sequence

Gene Construct	HLA-DR1 B1S (β chain, short) and B1L (β chain, long)
Plasmid	Full length in pHN1 (T7 promoter) called pDRB10 Short version in pLM1 (T7 promoter) Amp resistance gene for plasmid production in *E. coli*
Made by	Mia Rushe in Larry Stern's Lab
Sites used for cloning	EcoRI and HindIII
Insert size	~600bp B1S, ~620bp B1L
For production in	*E. coli* BL21 Induce with IPTG
Gene Sequence	xgaattcaggaggaatttaaaatgGGGGACACCCGACCACGTTTCTTGTGGCAGCTT AAG TTTGAATGTCATTTCTTCAATGGGACGGAGCGGGTGCGGTTGCTGGAAAG ATGCATCTATAACCAAGAGGAGTCCGTGCGCTTCGACAGCGACGTGGGG GAGTACCGGGCGGTGACGGAGCTGGGGCGGCCTGATGCCGAGTACTGG AACAGCCAGAAGGACCTCCTGGAGCAGAGGCGGGCCGCGGTGGACACCT ACTGCAGACACAACTACGGGGTTGGTGAGAGCTTCACAGTGCAGCGGCG AGTTGAGCCTAAGGTGACTGTGTATCCTTCAAAGACCCAGCCCCTGCAGC ACCACAACCTCCTGGTCTGCTCTGTGAGTGGTTTCTATCCAGGCAGCATT GAAGTCAGGTGGTTCCGGAACGGCCAGGAAGAGAAGGCTGGGGTGGTGT CCACAGGCCTGATCCAGAATGGAGATTGGACCTTCCAGACCCTGGTGATG CTGGAAACAGTTCCTCGGAGTGGAGAGGTTTACACC *short:* TGCCAAGTGGAGCACCCAAGTGTGACGAGCCCTCTCACAGTGGAATGGA GAGCAtaaaagctt *long:* TGCCAAGTGGAGCACCCAAGTGTGACGAGCCCTCTCACAGTGGAATGGA GAGCACGGTCT GAATCTGCACAGAGCAAGtaaaagctt
Protein Sequence	*iqeefk*MGDTRPRFLWQLKFECHFFNGTERVRLLERCIYNQEESVRFDSDVGEY RAVTELGRPDAEYWNSQKDLLEQRRAAVDTYCRHNYGVGESFTVQRRVEPK VTVYPSKTQPLQHHNLLVCSVSGFYPGSIEVRWFRNGQEEKAGVVSTGLIQN GDWTFQTLVMLETVPRSGEVYTCQVEHPSVTS *short:* PLTVEWRAEND *long:* PLTVEWRARSESAQSKEND
Protein MW	B1S: 22,185; B1L: 23,059 Da
Protein pI	B1S: 5.98; B1L: 6.23
Protein extinction coefficient	38,930 at 280nm (unfolded)

A.16. Primers used to generate point mutants in HLA-DR1

L45A Forward: GACGGTCTGGCGGGCTGAAGAATTTGGAC
Reverse: GTCCAAATTCTTCAGCCCGCCAGACCGTC

F48A Forward: GGCGGCTTGAAGAAGCTGGACGATTTGCC
Reverse: GGCAAATCGTCCAGCTTCTTCAAGCCGCC

F51A Forward: GAAGAATTTGGACGAGCTGCCAGCTTTGAGG
Reverse: CCTCAAAGCTGGCAGCTCGTCCAAATTCTTC

S53A Forward: GAATTTGGACGATTTGCCGCCTTTGAGGCTCAAGGTG
Reverse: CACCTTGAGCCTCAAAGGCGGCAAATCGTCCAAATTC

F54A Forward: GACGATTTGCCAGCGCTGAGGCTCAAGGTG
Reverse: CACCTTGAGCCTCAGCGCTGGCAAATCGTC

Beta W153A: CCAGAATGGAGATGCGACCTTCCAGACCC
Reverse: GGGTCTGGAAGGTCGCATCTCCATTCTGG

Beta F89A: CTACGGGGTTGGTGAGAGCGCAACA
Reverse: CAACTCGCCGCTGCACTGTTGCGCTC

A.17 Using Fluorescence Polarization to measure KD$_{app}$ and Peptide off rates

Determination of KD$_{app}$

Reagents:
 5X binding buffer (bb)
      -500mM NaCitrate pH 5.0
      -250mM NaCl
      -0.5% Octylglucaside
      -25mM EDTA
      -0.2% Azide
      -note: add 5mM DTT and protease inhibitors to1X just prior to use.
Black low binding polystyrene 96 well plate
12 channel pipette from Mauricio
Alexa-488 labeled peptide
Purified empty DR

Set up:
1. Add 100ul 1x bb to wells a-f 2-12
2. Add 200ul 250nM DR1 (in 1xbb) to wells a-f 1
3. Serially dilute by taking 100ul from a-f 1 and mixing it with next set of wells. Continue to wells a-f 11, but leave a-f 12 with no DR1
4. Add 100ul 1x bb to wells a-f 12 (note: polarization values are not reliable if you don't have at least 200ul volume)
5. Add peptide (HA-FRR alexa 488)to all wells (I added 50ul/well of 250nM peptide for a final concentration of 25nM/well)
6. Seal plate and incubate in the dark at 37⁰ for 3 days.
7. Read by polarization (set gain equal to peptide only well)
8. Fit to the following equation modified from the "Saturation binding with ligand depletion" under the advanced radioligand binding file in GraphPad Prism
Kd=KdnM
b=Kd + X + Bmax
c=-1*X +Bmax
Y=(-b+sqrt(b*b-4*a*c))/(2*a)

Effect of DM on peptide dissociation:

Set up:
1. Add 100ul 1x bb to wells a-f 2-12
2. Add 200ul 600nM DM (in 1xbb) to wells a-f 1
3. Serially dilute by taking 100ul from a-f 1 and mixing it with next set of wells. Continue to wells a-f 10, but leave a-f 11 and 12 with no DM
4. Add 100ul of 200nM DR1 to all wells except a-f 12, to those wells, add 100ul 1x bb
5. Add peptide (HA-FRR alexa 488) to all wells (I added 50ul/well of 250nM peptide for a final concentration of 25nM/well)
6. Seal plate and incubate in the dark at 37⁰ for 3 days.
7. Read plate for time 0
8. Add 100x cold peptide (unlabeled HA-FRR) to all wells
9. Read plate (I set the plate reader up to scan every minute for 30 minutes then every 10 minutes for 3 hours) I also read the plate once/day for another 3 days until my peptide was competed off.
10. Data were fit to a one phase exponential decay

REFERENCES

Adams, P. D., P. V. Afonine, et al. "PHENIX: a comprehensive Python-based system for macromolecular structure solution." Acta Crystallogr D Biol Crystallogr **66**(Pt 2): 213-21.

Anders, A. K., M. J. Call, et al. "HLA-DM captures partially empty HLA-DR molecules for catalyzed removal of peptide." Nat Immunol.

Andersen, P. S., P. M. Lavoie, et al. (1999). "Role of the T cell receptor alpha chain in stabilizing TCR-superantigen-MHC class II complexes." Immunity **10**(4): 473-83.

Anderson, M. W. and J. Gorski (2003). "Cutting edge: TCR contacts as anchors: effects on affinity and HLA-DM stability." J Immunol **171**(11): 5683-7.

Bakke, O. and B. Dobberstein (1990). "MHC class II-associated invariant chain contains a sorting signal for endosomal compartments." Cell **63**(4): 707-16.

Bandyopadhyay, A., L. Arneson, et al. (2008). "The relative energetic contributions of dominant P1 pocket versus hydrogen bonding interactions to peptide:class II stability: implications for the mechanism of DM function." Mol Immunol **45**(5): 1248-57.

Barker, J. M. (2006). "Clinical review: Type 1 diabetes-associated autoimmunity: natural history, genetic associations, and screening." J Clin Endocrinol Metab **91**(4): 1210-7.

Belmares, M. P., R. Busch, et al. (2003). "Formation of two peptide/MHC II isomers is catalyzed differentially by HLA-DM." Biochemistry **42**(3): 838-47.

Belmares, M. P., R. Busch, et al. (2002). "Structural factors contributing to DM susceptibility of MHC class II/peptide complexes." J Immunol **169**(9): 5109-17.

Berdensen, H. J., Van der Spoel, C.D., et al (1995). "GROMACS: A message-passing parallel molecular dynamics implementation." Comp Phys Comm **91**: 43-56.

Berendsen, H. J. (1984). "Molecular dynamics coupling to an external bath." journal of chemical physics
 81: 3684-90.

Blum, J. S. and P. Cresswell (1988). "Role for intracellular proteases in the processing and transport of class II HLA antigens." Proc Natl Acad Sci U S A **85**(11): 3975-9.

Bolin, D. R., A. L. Swain, et al. (2000). "Peptide and peptide mimetic inhibitors of antigen presentation by HLA-DR class II MHC molecules. Design, structure-activity relationships, and X-ray crystal structures." J Med Chem **43**(11): 2135-48.

Boniface, J. J., D. S. Lyons, et al. (1996). "Evidence for a conformational change in a class II major histocompatibility complex molecule occurring in the same pH range where antigen binding is enhanced." J Exp Med **183**(1): 119-26.

Bouvier, M. and D. C. Wiley (1998). "Structural characterization of a soluble and partially folded class I major histocompatibility heavy chain/beta 2m heterodimer." Nat Struct Biol **5**(5): 377-84.

Brown, J. H., T. Jardetzky, et al. (1988). "A hypothetical model of the foreign antigen binding site of class II histocompatibility molecules." Nature **332**(6167): 845-50.

Brown, J. H., T. S. Jardetzky, et al. (1993). "Three-dimensional structure of the human class II histocompatibility antigen HLA-DR1." Nature **364**(6432): 33-9.

Busch, R., A. Pashine, et al. (2002). "Stabilization of soluble, low-affinity HLA-DM/HLA-DR1 complexes by leucine zippers." J Immunol Methods **263**(1-2): 111-21.

Busch, R., Z. Reich, et al. (1998). "Secondary structure composition and pH-dependent conformational changes of soluble recombinant HLA-DM." J Biol Chem **273**(42): 27557-64.

Busch, R., C. H. Rinderknecht, et al. (2005). "Achieving stability through editing and chaperoning: regulation of MHC class II peptide binding and expression." Immunol Rev **207**: 242-60.

Carven, G. J., S. Chitta, et al. (2004). "Monoclonal antibodies specific for the empty conformation of HLA-DR1 reveal aspects of the conformational change associated with peptide binding." J Biol Chem **279**(16): 16561-70.

Carven, G. J. and L. J. Stern (2005). "Probing the ligand-induced conformational change in HLA-DR1 by selective chemical modification and mass spectrometric mapping." <u>Biochemistry</u> **44**(42): 13625-37.

Chou, C. L. and S. Sadegh-Nasseri (2000). "HLA-DM recognizes the flexible conformation of major histocompatibility complex class II." <u>J Exp Med</u> **192**(12): 1697-706.

Cochran, J. R. and L. J. Stern (2000). "A diverse set of oligomeric class II MHC-peptide complexes for probing T-cell receptor interactions." <u>Chem Biol</u> **7**(9): 683-96.

Cresswell, P. (1994). "Assembly, transport, and function of MHC class II molecules." <u>Annu Rev Immunol</u> **12**: 259-93.

Dai, S., G. A. Murphy, et al. "Crystal structure of HLA-DP2 and implications for chronic beryllium disease." <u>Proc Natl Acad Sci U S A</u> **107**(16): 7425-30.

Davies, M. N., A. Lamikanra, et al. (2008). "Identification of the HLA-DM/HLA-DR interface." <u>Mol Immunol</u> **45**(4): 1063-70.

Denzin, L. K. and P. Cresswell (1995). "HLA-DM induces CLIP dissociation from MHC class II alpha beta dimers and facilitates peptide loading." <u>Cell</u> **82**(1): 155-65.

Denzin, L. K., C. Hammond, et al. (1996). "HLA-DM interactions with intermediates in HLA-DR maturation and a role for HLA-DM in stabilizing empty HLA-DR molecules." <u>J Exp Med</u> **184**(6): 2153-65.

Denzin, L. K., N. F. Robbins, et al. (1994). "Assembly and intracellular transport of HLA-DM and correction of the class II antigen-processing defect in T2 cells." <u>Immunity</u> **1**(7): 595-606.

Doebele, R. C., R. Busch, et al. (2000). "Determination of the HLA-DM interaction site on HLA-DR molecules." <u>Immunity</u> **13**(4): 517-27.

Doebele, R. C., A. Pashine, et al. (2003). "Point mutations in or near the antigen-binding groove of HLA-DR3 implicate class II-associated invariant chain peptide affinity as a constraint on MHC class II polymorphism." <u>J Immunol</u> **170**(9): 4683-92.

Emsley, P. and K. Cowtan (2004). "Coot: model-building tools for molecular graphics." <u>Acta Crystallogr D Biol Crystallogr</u> **60**(Pt 12 Pt 1): 2126-32.

Essmann, u., Perera (1995). "A smooth particle mesh Ewald potential." J Chem Phys **103**: 8577-92.

Fahnestock, M. L., I. Tamir, et al. (1992). "Thermal stability comparison of purified empty and peptide-filled forms of a class I MHC molecule." Science **258**(5088): 1658-62.

Fallang, L. E., S. Roh, et al. (2008). "Complexes of two cohorts of CLIP peptides and HLA-DQ2 of the autoimmune DR3-DQ2 haplotype are poor substrates for HLA-DM." J Immunol **181**(8): 5451-61.

Ferrante, A., M. W. Anderson, et al. (2008). "HLA-DM mediates epitope selection by a "compare-exchange" mechanism when a potential peptide pool is available." PLoS One **3**(11): e3722.

Ferrante, A. and J. Gorski "Cutting edge: HLA-DM-mediated peptide exchange functions normally on MHC class II-peptide complexes that have been weakened by elimination of a conserved hydrogen bond." J Immunol **184**(3): 1153-8.

Frayser, M., A. K. Sato, et al. (1999). "Empty and peptide-loaded class II major histocompatibility complex proteins produced by expression in Escherichia coli and folding in vitro." Protein Expr Purif **15**(1): 105-14.

Fremont, D. H., F. Crawford, et al. (1998). "Crystal structure of mouse H2-M." Immunity **9**(3): 385-93.

Fremont, D. H., W. A. Hendrickson, et al. (1996). "Structures of an MHC class II molecule with covalently bound single peptides." Science **272**(5264): 1001-4.

Fremont, D. H., D. Monnaie, et al. (1998). "Crystal structure of I-Ak in complex with a dominant epitope of lysozyme." Immunity **8**(3): 305-17.

Fu, X. T. and R. W. Karr (1994). "HLA-DR alpha chain residues located on the outer loops are involved in nonpolymorphic and polymorphic antibody-binding epitopes." Hum Immunol **39**(4): 253-60.

Germain, R. N. and L. R. Hendrix (1991). "MHC class II structure, occupancy and surface expression determined by post-endoplasmic reticulum antigen binding." Nature **353**(6340): 134-9.

Glithero, A., J. Tormo, et al. (2006). "The crystal structure of H-2D(b) complexed with a partial peptide epitope suggests a major histocompatibility complex class I assembly intermediate." J Biol Chem **281**(18): 12699-704.

Grotenbreg, G. M., M. J. Nicholson, et al. (2007). "Empty class II major histocompatibility complex created by peptide photolysis establishes the role of DM in peptide association." J Biol Chem **282**(29): 21425-36.

Gunther, S., A. Schlundt, et al. "Bidirectional binding of invariant chain peptides to an MHC class II molecule." Proc Natl Acad Sci U S A **107**(51): 22219-24.

Gupta, S., S. Hopner, et al. (2008). "Anchor side chains of short peptide fragments trigger ligand-exchange of class II MHC molecules." PLoS ONE **3**(3): e1814.

Hansen, T. H., L. Lybarger, et al. (2005). "Recognition of open conformers of classical MHC by chaperones and monoclonal antibodies." Immunol Rev **207**: 100-11.

Henderson, K. N., J. A. Tye-Din, et al. (2007). "A structural and immunological basis for the role of human leukocyte antigen DQ8 in celiac disease." Immunity **27**(1): 23-34.

Hess, B., Bekker, et al (1997). "GEM, lincs: A linear constraint solver for molecular dynamics." J Comp Chem **18**: 1463-72.

Humphrey, W., Dalke, A. (1996). "VMD:visual molecular dynamics." J Mol Graph **14**: 33-8, 27-8.

Jardetzky, T. S., J. H. Brown, et al. (1996). "Crystallographic analysis of endogenous peptides associated with HLA-DR1 suggests a common, polyproline II-like conformation for bound peptides." Proc Natl Acad Sci U S A **93**(2): 734-8.

Jardetzky, T. S., J. C. Gorga, et al. (1990). "Peptide binding to HLA-DR1: a peptide with most residues substituted to alanine retains MHC binding." EMBO J **9**(6): 1797-803.

Jensen, P. E. (1990). "Regulation of antigen presentation by acidic pH." J Exp Med **171**(5): 1779-84.

Joshi, R. V., J. A. Zarutskie, et al. (2000). "A three-step kinetic mechanism for peptide binding to MHC class II proteins." Biochemistry **39**(13): 3751-62.

Kasson, P. M., J. D. Rabinowitz, et al. (2000). "Kinetics of peptide binding to the class II MHC protein I-Ek." Biochemistry **39**(5): 1048-58.

Kaufman, J. F., C. Auffray, et al. (1984). "The class II molecules of the human and murine major histocompatibility complex." <u>Cell</u> **36**(1): 1-13.

Kim, C. Y., H. Quarsten, et al. (2004). "Structural basis for HLA-DQ2-mediated presentation of gluten epitopes in celiac disease." <u>Proc Natl Acad Sci U S A</u> **101**(12): 4175-9.

Kony, D. B., P. H. Hunenberger, et al. (2007). "Molecular dynamics simulations of the native and partially folded states of ubiquitin: Influence of methanol cosolvent, pH, and temperature on the protein structure and dynamics." <u>Protein Sci</u> **16**(6): 1101-18.

Kropshofer, H., S. O. Arndt, et al. (1997). "HLA-DM acts as a molecular chaperone and rescues empty HLA-DR molecules at lysosomal pH." <u>Immunity</u> **6**(3): 293-302.

Kropshofer, H., A. B. Vogt, et al. (1996). "Editing of the HLA-DR-peptide repertoire by HLA-DM." <u>EMBO J</u> **15**(22): 6144-54.

Laberge, M. and T. Yonetani (2008). "Molecular dynamics simulations of hemoglobin A in different states and bound to DPG: effector-linked perturbation of tertiary conformations and HbA concerted dynamics." <u>Biophys J</u> **94**(7): 2737-51.

Lamb, C. A. and P. Cresswell (1992). "Assembly and transport properties of invariant chain trimers and HLA-DR-invariant chain complexes." <u>J Immunol</u> **148**(11): 3478-82.

Lee, J. M., C. M. Kay, et al. (1992). "Conformational changes in mouse MHC class II proteins at acidic pH." <u>Int Immunol</u> **4**(8): 889-97.

Lee, K. H., K. W. Wucherpfennig, et al. (2001). "Structure of a human insulin peptide-HLA-DQ8 complex and susceptibility to type 1 diabetes." <u>Nat Immunol</u> **2**(6): 501-7.

Lindner, R. and E. R. Unanue (1996). "Distinct antigen MHC class II complexes generated by separate processing pathways." <u>EMBO J</u> **15**(24): 6910-20.

Lovitch, S. B. and E. R. Unanue (2005). "Conformational isomers of a peptide-class II major histocompatibility complex." <u>Immunol Rev</u> **207**: 293-313.

Machamer, C. E. and P. Cresswell (1982). "Biosynthesis and glycosylation of the invariant chain associated with HLA-DR antigens." J Immunol **129**(6): 2564-9.

Marcsisin, S. R. and J. R. Engen "Hydrogen exchange mass spectrometry: what is it and what can it tell us?" Anal Bioanal Chem **397**(3): 967-72.

McCoy, A. J., R. W. Grosse-Kunstleve, et al. (2007). "Phaser crystallographic software." J Appl Crystallogr **40**(Pt 4): 658-674.

McFarland, B. J. and C. Beeson (2002). "Binding interactions between peptides and proteins of the class II major histocompatibility complex." Med Res Rev **22**(2): 168-203.

McFarland, B. J., C. Beeson, et al. (1999). "Cutting edge: a single, essential hydrogen bond controls the stability of peptide-MHC class II complexes." J Immunol **163**(7): 3567-71.

McFarland, B. J., J. F. Katz, et al. (2001). "Energetic asymmetry among hydrogen bonds in MHC class II*peptide complexes." Proc Natl Acad Sci U S A **98**(16): 9231-6.

Mikesh, L. M., B. Ueberheide, et al. (2006). "The utility of ETD mass spectrometry in proteomic analysis." Biochim Biophys Acta **1764**(12): 1811-22.

Morris, P., J. Shaman, et al. (1994). "An essential role for HLA-DM in antigen presentation by class II major histocompatibility molecules." Nature **368**(6471): 551-4.

Morton, P. A., M. L. Zacheis, et al. (1995). "Delivery of nascent MHC class II-invariant chain complexes to lysosomal compartments and proteolysis of invariant chain by cysteine proteases precedes peptide binding in B-lymphoblastoid cells." J Immunol **154**(1): 137-50.

Mosyak, L., D. M. Zaller, et al. (1998). "The structure of HLA-DM, the peptide exchange catalyst that loads antigen onto class II MHC molecules during antigen presentation." Immunity **9**(3): 377-83.

Nabavi, N., G. J. Freeman, et al. (1992). "Signalling through the MHC class II cytoplasmic domain is required for antigen presentation and induces B7 expression." Nature **360**(6401): 266-8.

Narayan, K., C. L. Chou, et al. (2007). "HLA-DM targets the hydrogen bond between the histidine at position beta81 and peptide to dissociate HLA-DR-peptide complexes." Nat Immunol **8**(1): 92-100.

Narayan, K., K. W. Su, et al. (2009). "HLA-DM mediates peptide exchange by interacting transiently and repeatedly with HLA-DR1." Mol Immunol **46**(15): 3157-62.

Natarajan, S. K., M. Assadi, et al. (1999). "Stable peptide binding to MHC class II molecule is rapid and is determined by a receptive conformation shaped by prior association with low affinity peptides." J Immunol **162**(7): 4030-6.

Natarajan, S. K., L. J. Stern, et al. (1999). "Sodium dodecyl sulfate stability of HLA-DR1 complexes correlates with burial of hydrophobic residues in pocket 1." J Immunol **162**(6): 3463-70.

Newton-Nash, D. K. and D. D. Eckels (1993). "Differential effect of polymorphism at HLA-DR1 beta-chain positions 85 and 86 on binding and recognition of DR1-restricted antigenic peptides." J Immunol **150**(5): 1813-21.

Nicholson, M. J., B. Moradi, et al. (2006). "Small molecules that enhance the catalytic efficiency of HLA-DM." J Immunol **176**(7): 4208-20.

Nojima, H., M. Takeda-Shitaka, et al. (2002). "Dynamic characteristics of a peptide-binding groove of human HLA-A2 class I MHC molecules: normal mode analysis of the antigen peptide-class I MHC complex." Chem Pharm Bull (Tokyo) **50**(9): 1209-14.

Nojima, H., M. Takeda-Shitaka, et al. (2003). "Dynamic flexibility of a peptide-binding groove of human HLA-DR1 class II MHC molecules: normal mode analysis of the antigen peptide-class II MHC complex." Chem Pharm Bull (Tokyo) **51**(8): 923-8.

Painter, C. A., A. Cruz, et al. (2008). "Model for the peptide-free conformation of class II MHC proteins." PLoS One **3**(6): e2403.

Pashine, A., R. Busch, et al. (2003). "Interaction of HLA-DR with an acidic face of HLA-DM disrupts sequence-dependent interactions with peptides." Immunity **19**(2): 183-92.

Pierre, P., L. K. Denzin, et al. (1996). "HLA-DM is localized to conventional and unconventional MHC class II-containing endocytic compartments." Immunity **4**(3): 229-39.

Rabanal, F., M. D. Ludevid, et al. (1993). "CD of proline-rich polypeptides: application to the study of the repetitive domain of maize glutelin-2." Biopolymers **33**(7): 1019-28.

Rabinowitz, J. D., M. Vrljic, et al. (1998). "Formation of a highly peptide-receptive state of class II MHC." Immunity **9**(5): 699-709.

Reich, Z., J. D. Altman, et al. (1997). "Stability of empty and peptide-loaded class II major histocompatibility complex molecules at neutral and endosomal pH: comparison to class I proteins." Proc Natl Acad Sci U S A **94**(6): 2495-500.

Riberdy, J. M., J. R. Newcomb, et al. (1992). "HLA-DR molecules from an antigen-processing mutant cell line are associated with invariant chain peptides." Nature **360**(6403): 474-7.

Richeldi, L., R. Sorrentino, et al. (1993). "HLA-DPB1 glutamate 69: a genetic marker of beryllium disease." Science **262**(5131): 242-4.

Robinson, J., M. J. Waller, et al. (2009). "The IMGT/HLA database." Nucleic Acids Res **37**(Database issue): D1013-7.

Roche, P. A. and P. Cresswell (1990). "Invariant chain association with HLA-DR molecules inhibits immunogenic peptide binding." Nature **345**(6276): 615-8.

Roche, P. A., M. S. Marks, et al. (1991). "Formation of a nine-subunit complex by HLA class II glycoproteins and the invariant chain." Nature **354**(6352): 392-4.

Rotzschke, O., K. Falk, et al. (1999). "Conformational variants of class II MHC/peptide complexes induced by N- and C-terminal extensions of minimal peptide epitopes." Proc Natl Acad Sci U S A **96**(13): 7445-50.

Rotzschke, O., J. M. Lau, et al. (2002). "A pH-sensitive histidine residue as control element for ligand release from HLA-DR molecules." Proc Natl Acad Sci U S A **99**(26): 16946-50.

Runnels, H. A., J. C. Moore, et al. (1996). "A structural transition in class II major histocompatibility complex proteins at mildly acidic pH." J Exp Med **183**(1): 127-36.

Sadegh-Nasseri, S. and R. N. Germain (1991). "A role for peptide in determining MHC class II structure." Nature **353**(6340): 167-70.

Sadegh-Nasseri, S., S. Natarajan, et al. "Conformational heterogeneity of MHC class II induced upon binding to different peptides is a key regulator in antigen presentation and epitope selection." Immunol Res **47**(1-3): 56-64.

Sadegh-Nasseri, S., L. J. Stern, et al. (1994). "MHC class II function preserved by low-affinity peptide interactions preceding stable binding." Nature **370**(6491): 647-50.

Sato, A. K., J. A. Zarutskie, et al. (2000). "Determinants of the peptide-induced conformational change in the human class II major histocompatibility complex protein HLA-DR1." J Biol Chem **275**(3): 2165-73.

Schmitt, L., J. J. Boniface, et al. (1999). "Conformational isomers of a class II MHC-peptide complex in solution." J Mol Biol **286**(1): 207-18.

Schneider, T. R. (2000). "Objective comparison of protein structures: error-scaled difference distance matrices." Acta Crystallogr D Biol Crystallogr **56**(Pt 6): 714-21.

Scott, C. A., P. A. Peterson, et al. (1998). "Crystal structures of two I-Ad-peptide complexes reveal that high affinity can be achieved without large anchor residues." Immunity **8**(3): 319-29.

Sherman, M. A., D. A. Weber, et al. (1995). "DM enhances peptide binding to class II MHC by release of invariant chain-derived peptide." Immunity **3**(2): 197-205.

Siebold, C., B. E. Hansen, et al. (2004). "Crystal structure of HLA-DQ0602 that protects against type 1 diabetes and confers strong susceptibility to narcolepsy." Proc Natl Acad Sci U S A **101**(7): 1999-2004.

Sieker, F., S. Springer, et al. (2007). "Comparative molecular dynamics analysis of tapasin-dependent and -independent MHC class I alleles." Protein Sci **16**(2): 299-308.

Sloan, V. S., P. Cameron, et al. (1995). "Mediation by HLA-DM of dissociation of peptides from HLA-DR." Nature **375**(6534): 802-6.

Stern, L. J., J. H. Brown, et al. (1994). "Crystal structure of the human class II MHC protein HLA-DR1 complexed with an influenza virus peptide." Nature **368**(6468): 215-21.

Stern, L. J. and D. C. Wiley (1992). "The human class II MHC protein HLA-DR1 assembles as empty alpha beta heterodimers in the absence of antigenic peptide." Cell **68**(3): 465-77.

Stratikos, E., L. Mosyak, et al. (2002). "Identification of the lateral interaction surfaces of human histocompatibility leukocyte antigen (HLA)-DM with HLA-DR1 by formation of tethered complexes that present enhanced HLA-DM catalysis." J Exp Med **196**(2): 173-83.

Stratikos, E., D. C. Wiley, et al. (2004). "Enhanced catalytic action of HLA-DM on the exchange of peptides lacking backbone hydrogen bonds between their N-terminal region and the MHC class II alpha-chain." J Immunol **172**(2): 1109-17.

Sundberg, E. J., P. S. Andersen, et al. (2003). "Structural, energetic, and functional analysis of a protein-protein interface at distinct stages of affinity maturation." Structure **11**(9): 1151-61.

Sundberg, E. J., L. Deng, et al. (2007). "TCR recognition of peptide/MHC class II complexes and superantigens." Semin Immunol **19**(4): 262-71.

Taneja, V. and C. S. David "Role of HLA class II genes in susceptibility/resistance to inflammatory arthritis: studies with humanized mice." Immunol Rev **233**(1): 62-78.

Tobita, T., M. Oda, et al. (2003). "A role for the P1 anchor residue in the thermal stability of MHC class II molecule I-Ab." Immunol Lett **85**(1): 47-52.

Trombetta, E. S. and I. Mellman (2005). "Cell biology of antigen processing in vitro and in vivo." Annu Rev Immunol **23**: 975-1028.

Tsutsui, Y. and P. L. Wintrode (2007). "Hydrogen/deuterium exchange-mass spectrometry: a powerful tool for probing protein structure, dynamics and interactions." Curr Med Chem **14**(22): 2344-58.

Ullrich, H. J., K. Doring, et al. (1997). "Interaction between HLA-DM and HLA-DR involves regions that undergo conformational changes at lysosomal pH." Proc Natl Acad Sci U S A **94**(24): 13163-8.

Verreck, F. A., C. A. Fargeas, et al. (2001). "Conformational alterations during biosynthesis of HLA-DR3 molecules controlled by invariant chain and HLA-DM." Eur J Immunol **31**(4): 1029-36.

Villa, E., A. Balaeff, et al. (2005). "Structural dynamics of the lac repressor-DNA complex revealed by a multiscale simulation." Proc Natl Acad Sci U S A **102**(19): 6783-8.

Vogt, A. B., H. Kropshofer, et al. (1997). "How HLA-DM affects the peptide repertoire bound to HLA-DR molecules." Hum Immunol **54**(2): 170-9.

Vogt, A. B., H. Kropshofer, et al. (1996). "Kinetic analysis of peptide loading onto HLA-DR molecules mediated by HLA-DM." Proc Natl Acad Sci U S A **93**(18): 9724-9.

vogt, A. B., G. Moldenhauer, et al. (1997). "HLA-DM stabilizes empty HLA-DR molecules in a chaperone-like fashion." Immunol Lett **57**(1-3): 209-11.

Weber, D. A., C. T. Dao, et al. (2001). "Transmembrane domain-mediated colocalization of HLA-DM and HLA-DR is required for optimal HLA-DM catalytic activity." J Immunol **167**(9): 5167-74.

Weber, D. A., B. D. Evavold, et al. (1996). "Enhanced dissociation of HLA-DR-bound peptides in the presence of HLA-DM." Science **274**(5287): 618-20.

Yaneva, R., S. Springer, et al. (2009). "Flexibility of the MHC class II peptide binding cleft in the bound, partially filled, and empty states: a molecular dynamics simulation study." Biopolymers **91**(1): 14-27.

Zacharias, M. and S. Springer (2004). "Conformational flexibility of the MHC class I alpha1-alpha2 domain in peptide bound and free states: a molecular dynamics simulation study." Biophys J **87**(4): 2203-14.

Zarutskie, J. A., R. Busch, et al. (2001). "The kinetic basis of peptide exchange catalysis by HLA-DM." Proc Natl Acad Sci U S A **98**(22): 12450-5.

Zarutskie, J. A., A. K. Sato, et al. (1999). "A conformational change in the human major histocompatibility complex protein HLA-DR1 induced by peptide binding." Biochemistry **38**(18): 5878-87.

Zavala-Ruiz, Z., I. Strug, et al. (2004). "A polymorphic pocket at the P10 position contributes to peptide binding specificity in class II MHC proteins." Chem Biol **11**(10): 1395-402.

Zavala-Ruiz, Z., I. Strug, et al. (2004). "A hairpin turn in a class II MHC-bound peptide orients residues outside the binding groove for T cell recognition." Proc Natl Acad Sci U S A **101**(36): 13279-84.

Zehl, M., K. D. Rand, et al. (2008). "Electron transfer dissociation facilitates the measurement of deuterium incorporation into selectively labeled peptides with single residue resolution." J Am Chem Soc **130**(51): 17453-9.

Zheng, W., B. R. Brooks, et al. (2007). "Allosteric transitions in the chaperonin GroEL are captured by a dominant normal mode that is most robust to sequence variations." Biophys J **93**(7): 2289-99.

Zhou, Z., K. A. Callaway, et al. (2009). "Cutting edge: HLA-DM functions through a mechanism that does not require specific conserved hydrogen bonds in class II MHC-peptide complexes." J Immunol **183**(7): 4187-91.

Zhu, Y., A. Y. Rudensky, et al. (2003). "Crystal structure of MHC class II I-Ab in complex with a human CLIP peptide: prediction of an I-Ab peptide-binding motif." J Mol Biol **326**(4): 1157-74.